UNIVERSITÄT BAYREUTH

Master Thesis – Environmental Sciences

Spatio-Temporal Change of Snow Cover in the Pamirs

by
Thomas Senftl

Supervised by Prof. Dr. Cyrus Samimi
Research Group of Climatology
Faculty of Biology, Chemistry & Earth Sciences
University of Bayreuth

Bayreuth, September 2019

1. Referee: Prof. Dr. Cyrus Samimi
2. Referee: Prof. Dr. Michael Hauhs

Abstract

Snow cover is an important indicator of climate change and a central component of the hydrological cycle in Central Asia. The Pamir Mountains are a key region regarding Central Asia's fresh water resources. This study aims to examine changes of snow cover extent (SCE) and duration (SCD) within the Pamirs from 2001 to 2018 to better resolve small-scale differences within the region. The analysis was conducted based on the daily snow cover product of the Moderate Resolution Imaging Spectroradiometer (MODIS). To remove cloud cover, areas with over 60 % gaps were excluded and a simple temporal gap filling was applied. Data accuracy was assessed with Landsat 5 (TM) images on two days with different snow conditions. Validation results demonstrate that MODIS generally mapped snow cover with a reasonable accuracy. Nonetheless, MODIS slightly overestimated and considerably underestimated snow cover in certain conditions. The snow cover analysis results demonstrate that snow cover in the Pamirs has decreased. Although the decrease was not significant for the Pamirs as a whole, significant snow cover reductions were found especially in the Eastern Pamirs. Strong reductions in mean annual SCE of -2.0 to -5.4 % per year were found in the Eastern Pamirs in winter. In contrast, significant positive trends were marginal across the Pamirs throughout all seasons. While no direct assessment of potential causes for the snow cover changes was conducted, results indicate that a decrease in precipitation might be the decisive factor for the observed reductions in the Eastern Pamirs.

Zusammenfassung

Schneebedeckung ist ein wichtiger Indikator für den Klimawandel und ein zentraler Bestandteil des Wasserkreislaufs in Zentralasien. Das Pamir-Gebirge ist eine Schlüsselregion hinsichtlich der Süßwasserressourcen Zentralasiens. Die vorliegende Studie zielt darauf ab, Veränderungen der Schneedeckenausdehnung (SCE) und -dauer (SCD) innerhalb des Pamir-Gebirges von 2001 bis 2018 zu untersuchen, um kleinräumige Unterschiede innerhalb der Region besser aufzulösen. Die Analyse wurde auf der Grundlage des täglichen Schneedeckenprodukts des Moderate Resolution Imaging Spectroradiometer (MODIS) durchgeführt. Um Wolkenbedeckung zu entfernen, wurden Bereiche mit über 60 % Datenlücken ausgeschlossen und ein einfaches zeitliches Lückenfüllen durchgeführt. Die Genauigkeit der Daten wurde mit Landsat 5 (TM) Bildern an zwei Tagen mit unterschiedlichen Schneeverhältnissen bewertet. Die Ergebnisse der Validierung zeigen, dass MODIS die Schneebedeckung generell mit angemessener Genauigkeit abbildete. Nichtsdestotrotz hat MODIS die Schneebedeckung unter bestimmten Bedingungen leicht überschätzt und auch deutlich unterschätzt. Die Ergebnisse der Analyse der Schneebedeckung zeigen, dass die Schneebedeckung im Pamir zurückgegangen ist. Obwohl der Rückgang für den Pamir als Ganzes nicht signifikant war, wurden signifikante Verminderungen der Schneebedeckung insbesondere im Ost-Pamir festgestellt. Starke Verringerungen der mittleren jährlichen Schneebedeckung von $-2{,}0$ bis $-5{,}4$ % pro Jahr wurden im Ost-Pamir im Winter gefunden. Signifikant positive Trends waren im Gegensatz dazu im Pamir über alle Jahreszeiten unbedeutend. Obwohl keine direkte Bewertung von möglichen Ursachen für die Veränderung der Schneebedeckung durchgeführt wurde, deuten die Ergebnisse darauf hin, dass ein Rückgang des Niederschlags der entscheidende Faktor für die beobachteten Verringerungen im Ost-Pamir sein könnte.

Contents

List of Figures

List of Tables

List of Abbreviations

acc.	Accuracy
ANOVA	Analysis of variance
a.s.l.	Above sea level
AVHRR	Advanced Very High Resolution Radiometer
CCD	Cloud cover duration
CCE	Cloud cover extent
e.g.	For example
FSC	Fractional snow cover
GCOS	Global Observing System for Climate
IPCC	Intergovernmental Panel on Climate Change
MK	Mann-Kendall trend test
MODIS	Moderate Resolution Imaging Spectroradiometer
NASA	National Aeronautics and Space Administration
NDSI	Normalized Difference Snow Index
NDVI	Normalized Difference Vegetation Index
NSIDC	National Snow and Ice Data Center
rcl.	Reclassified
SC	Snow cover (only referring to SCE & SCD)
SCD	Snow cover duration
SCE	Snow cover extent
SD	Snow depth
SEB	Surface energy balance
SRB	Surface radiation balance
SWE	Snow water equivalent
SWIR	Shortwave infrared
TM	Thematic Mapper
USGS	U.S. Geological Survey
VIS	Visible spectrum
WMO	World Meteorological Organization

1 Introduction

1.1 Relevance

As a part of the cryosphere, snow is an important component of the Earth's climate system (Vaughan et al., 2013). The cryosphere is often referred to as the "natural thermometer" of the Earth's climate (Vaughan et al., 2013). The fifth IPCC Assessment Report illustrated that there is a general decline in all components of the cryosphere because of rising temperatures (Vaughan et al., 2013). However, the cryosphere is not only influenced by the climate, it is also a crucial factor influencing the climate through strong albedo feedbacks (Flanner et al., 2011; Groisman et al., 1994) and other weaker feedbacks like carbon release due to permafrost thaw (Stieglitz et al., 2003).

Snow cover is particularly important, because it responds very quickly to climate change (Brown and Mote, 2009; Cubasch et al., 2013; Hall and Qu, 2006; Lemke et al., 2007) and is often a crucial component in the hydrological cycle (Barnett et al., 2005; Li et al., 2017; Verbunt et al., 2003). The fifth IPCC Assessment Report therefore described northern hemispheric snow cover extent as a "key indicator of climate change" (Vaughan et al., 2013).

The Pamirs are a high mountain area in Central Asia. As highlighted by the IPCC special report in 2018, high mountain regions like the Pamirs are regarded as "climate change hotspots", due to their hydrological importance and their particularly vulnerable ecosystems (Hoegh-Guldberg et al., 2018). One of the major rivers of Central Asia, the Amu Darya river, originates from the Pamirs, making the Pamirs a key region regarding Central Asia's fresh water resources (Glantz, 2005). As a crucial water resource for countries within the Amu Darya Basin, the river has also been a source of conflict between the countries (Glantz, 2005; Lioubimtseva and Henebry, 2009). Changes in the Pamirs' cryosphere, which feeds the Amu Darya, are thus important to observe (Glantz, 2005). In addition, snow cover changes in the Pamirs are also important for the local communities' livelihoods, since the predominant occupations in the Pamirs are farming and livestock production (Breu and Hurni, 2003; Kassam et al., 2018). Changes in the snow covered area, for instance, have implications on the herders'

seasonal use of pastures (Kassam et al., 2018).

Recent studies researching cryosphere changes in the Pamirs indicate that the response of the cryosphere to climate change might be regionally differentiated (Knoche et al., 2017; Zhou et al., 2017). To better resolve small-scale changes of the cryosphere within the Pamirs, a detailed analysis of the spatio-temporal snow cover variability in the Pamirs was conducted. For this purpose, this study examined changes of snow cover extent (SCE) and snow cover duration (SCD) over the past 18 years.

1.2 Theoretical Background

1.2.1 Snow characteristics

Snow formation. Snow is a part of the cryosphere, which describes all parts of the Earth where water is in a frozen state (Barry and Gan, 2011). The cryosphere includes snow cover, sea ice, lake ice, river ice, glaciers and ice sheets, and frozen ground (IPCC, 2013). Snow is precipitation in form of ice crystals, which are formed in clouds with saturated air below 0 °C (Barry and Gan, 2011; Dong, 2018). The nature of a crystal mainly depends on the temperature and saturation vapor pressure during its formation (Barry and Gan, 2011). Because of the countless combinations there is an enormous amount of different snowflakes (Magono and Chung, 1966). In case atmospheric and ground temperatures are sufficiently low, a snowfall event can create a snow cover.

Snow metamorphism and dependencies. As soon as the snow falls on the ground, it starts undergoing changes in its physical properties (Barry and Gan, 2011; Goodison et al., 1999). Time- and temperature-dependent processes like compaction, settling, freeze-thaw cycles and water vapor diffusion alter the snow's density, thermal conductivity and albedo (Barry and Gan, 2011; Goodison et al., 1999). This process is called snow metamorphism (Goodison et al., 1999). The aging of snow consequently introduces heterogeneity in the snow cover properties. Hence, various classifications schemes for snow cover exist (Sturm et al., 1995).

Whether a freshly developed snow cover will last only for a short time or will cover the ground for a longer period can depend on a variety of factors. The two most important factors usually are atmospheric temperature and precipitation (Brown and Mote, 2009; Déry and Brown, 2007; Li et al., 2018; Scherrer and Appenzeller, 2006; Vaughan et al., 2013). The extent that is covered by snow on the northern hemisphere is strongly anticorrelated with atmospheric temperature, especially in spring (Brown and Robinson, 2011; Déry and Brown, 2007; Karl et al., 1993; Lemke et al., 2007). In general, atmospheric temperature affects a

snow cover in two ways: First, atmospheric temperature affects snow formation by determining whether precipitation occurs as snow or rain (Brown and Mote, 2009; Lemke et al., 2007). Second, it substantially determines snowmelt (Brown and Mote, 2009; Lemke et al., 2007). Precipitation primarily has a positive effect on the duration of a snow cover (Brown and Mote, 2009). In form of snowfall precipitation consequentially increases the persistence of a snow cover (Brown and Mote, 2009). Rainfall, however, has a slight negative effect by transferring heat to the snow cover (Wever et al., 2014). Besides temperature and precipitation, the persistence of a snow cover also depends on the surface energy balance (SEB), since snow still absorbs some shortwave radiation and much longwave radiation (Zhang, 2005). Other factors that can be very important particularly in mountain areas like the Pamirs, are wind and complex topography. During so-called "rain-on-snow" events, for instance, high winds together with warm air temperatures and high humidity considerably enhance snowmelt (Berris and Harr, 1987; Marks et al., 1998; Wever et al., 2014). Another example is the redistribution of snow by wind (Pomeroy et al., 1997; Wayand et al., 2018; Winstral and Marks, 2002). Complex topography can be a major factor, since it does not only influence the redistribution of snow, but also influences other factors like precipitation, temperature or radiation (Elder et al., 1991; Goodison et al., 1999; Wayand et al., 2018). Some further factors that influence snow cover persistence are avalanches (Elder et al., 1991), vegetation (Berris and Harr, 1987; Pomeroy et al., 1998) and pollution (Clarke and Noone, 1985; Doherty et al., 2010). Thus, due to the various influences, not only the snow cover properties, but also the snow cover extent can be very heterogenic.

Snow metrics. To address the often present heterogeneity, different metrics of snow have been defined for studying snow cover. The IPCC (2013) defined five different metrics of snow: snow cover extent (SCE), the seasonal sum of daily snowfall, snow depth (SD), snow cover duration (SCD) and the snow water equivalent (SWE) (Vaughan et al., 2013). In this context, snow cover extent is defined as the area that a snow cover takes up, snow cover duration is described as the number of days, on which the snow is exceeding a certain threshold depth, and the snow water equivalent is defined as the depth of water that would result when a certain mass of snow would melt completely (Vaughan et al., 2013). Each of these metrics has its own importance and the metrics to choose for a study usually depend on the exact research question or the data availability. SCE and SCD, for instance, are of particular importance for studies researching the SEB (e.g. Flanner et al., 2011). On the other hand, SD and SWE are valuable metrics for evaluating effects of snow cover on the hydrological cycle (e.g. Elder et al., 1991). Likewise, not only the effects of the different metrics differ, but also their

dependencies. Whereas SCE and SCD, for instance, are strongly influenced by the atmospheric temperatures at the start and end of the snow season, SD and SWE are more sensitive to the number of snowfall events (Brown and Mote, 2009).

Properties of snow. Snow has unique radiative and thermal properties. These properties lead to a snow cover considerably altering the surface radiation balance (SRB) and consequently the SEB (Goodison et al., 1999; Zhang, 2005).

One major reason for the importance of snow are its radiative properties. Snow has very high reflective properties in the visible spectrum (VIS) combined with low reflective properties in the shortwave infrared (SWIR) (Riggs et al., 2016; Zhang, 2005). In addition, snow has a high emissivity (Zhang, 2005). The superlative reflective properties in the VIS lead to the snow's high albedo (Fig. 1.1). The albedo of an object or a surface indicates the fraction of solar radiation that is reflected by it (IPCC, 2013). In remote sensing products the snow's high albedo is often used to identify snow cover (Tedesco, 2015). However, depending on the condition of the snow, its albedo can vary (Fig. 1.1) (Doherty et al., 2010; Warren, 1982; Wendler and Kelley, 1988). If the snow is fresh, its albedo can exceed 90 % under certain conditions (Wendler and Kelley, 1988). Conversely, in case the snow is old and/or dirty its albedo is reduced significantly (Doherty et al., 2010).

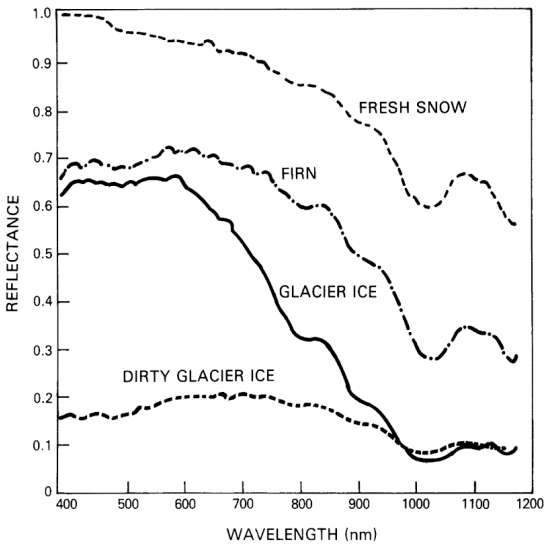

Figure 1.1: Reflectance of different ice surfaces (Hall and Martinec, 1985. Adapted from Qunzhu et al., 1984)

Another important property of snow cover is its low thermal conductivity. The low thermal conductivity is a result of the large fraction of air within a snow cover (Zhang, 2005). In a sense, a snow cover acts as a thermal insulator:

it can strongly inhibit heat exchange between the atmosphere and the ground (Goodison et al., 1999; Stieglitz et al., 2003). On the one hand a snow cover's low thermal conductivity can reduce ground cooling due to heat loss from the surface to the atmosphere, while on the other hand it can also reduce ground warming due to heat transfer from the atmosphere to the surface (Zhang, 2005). Hence, snow cover is crucial for the ground thermal regime and consequently the active layer and permafrost (Goodison et al., 1999; Zhang, 2005).

Influence of snow on the surface energy balance. The presence of a snow cover usually strongly alters the surface energy balance (SEB) (Goodison et al., 1999). The way in which a snow cover alters the SEB is depending on various factors like the initial surface or snow metamorphism, and is thus very specific (Zhang, 2005). Typically, the snow's high albedo directly affects the surface radiation balance (SRB) by increasing the reflected fraction of the incoming shortwave radiation (Wendler and Kelley, 1988). Conversely, the snow's high absorptivity increases the amount of absorbed longwave radiation, while the high emissivity increases the outgoing longwave radiation (Zhang, 2005). In addition, the extremely low thermal conductivity of snow cover can significantly dampen the ground heat flux (Zhang, 2005). Furthermore, snowmelt also affects the latent heat flux (Goodison et al., 1999; Zhang, 2005).

Importance of snow. The area frequently covered by snow is vast (Barry and Gan, 2011; Groisman et al., 1994; Lemke et al., 2007). Due to its ability to store and release water, its low thermal conductivity and its high albedo and other properties a snow cover can be important for various scientific fields. Snow is an important component in climate research (Hantel and Maurer, 2011; Scherrer and Appenzeller, 2006; Vaughan et al., 2013) and often a crucial component in the hydrological cycle (Barnett et al., 2005; Li et al., 2017; Verbunt et al., 2003). Apart from ecological impacts, changes in snow cover can also have a serious economic impact (Burakowski and Magnusson, 2012; James et al., 2014; Sturm et al., 2017).

Snow cover is an important factor to consider in regard of climate change, since the SEB is a major determinant for atmospheric temperatures (Goodison et al., 1999). Not only can changes in SCE influence atmospheric temperatures, a snow cover itself is also very sensitive to temperature changes (Brown and Mote, 2009). This leads to the so-called "snow-albedo feedback" (Qu and Hall, 2013) or more generally "ice-albedo feedback"(IPCC, 2013): warmer temperatures lead to a reduction in surface albedo due to snow metamorphism or snow cover shrinkage, which in turn leads to an amplified warming (Barry and Gan, 2011; Goodison et al., 1999; Qu and Hall, 2013; Vaughan et al., 2013). In contrast, cooler

temperatures would have an opposite effect (Barry and Gan, 2011). Although the interaction of snow cover with temperature is complicated by other processes like atmospheric circulation (Cohen and Rind, 1991), the snow-albedo feedback is considered an important climate feedback mechanism (Cubasch et al., 2013; Flanner et al., 2011; Groisman et al., 1994). Thus, the sensitivity of snow to temperature and precipitation changes makes SCE and SCD important indicators of climate change.

Furthermore, snow is an important source for fresh water (Barnett et al., 2005). The ability to store and release water makes snow a crucial component in the hydrological cycle (Barnett et al., 2005; Goodison et al., 1999; Li et al., 2017; Verbunt et al., 2003). In many regions and especially mountainous regions like the Pamirs, water resources for irrigation, drinking water or energy production depend on snowmelt (Barnett et al., 2005; Li et al., 2017; Vaughan et al., 2013). With regard to the expected reductions in snow cover in context of climate change, such regions are likely to face an increasing risk of water scarcity (Barnett et al., 2005). Moreover, the release of water from snowmelt can also cause floods during rain-on-snow events or more generally due to changes in the seasonal stream-flow patterns (Hamlet and Lettenmaier, 2007; Marks et al., 1998).

1.2.2 Remote sensing of snow

Technique. Remote sensing techniques for snow take advantage of the snow's unique radiative properties (Sect. 1.2.1). Sensors used in remote sensing for snow detection can generally be divided in two kinds: optical sensors and microwave sensors, whereby microwave sensors can be further divided in active (AM) and passive (PM) microwave sensors (Dong, 2018).

Both AM and PM have the major advantage that measurements are not restricted by clouds (as long as there is no precipitation) or nighttime conditions, since they are independent of the solar radiation (Foster et al., 2005). However, the interaction of snow with microwave radiation is complex and other factors like vegetation further complicate an accurate detection (Dong, 2018; Foster et al., 2005). Furthermore, PM is only available in low spatial resolution, since the microwave signal emitted from the Earth's surface is only weak (Dong, 2018). Therefore, the Global Observing System for Climate (GCOS) describes current PM data as inadequate for snow detection in complex terrain (WMO, 2011). Although AM can have high spatial resolution, it can only detect wet snow (König et al., 2001).

Optical sensors, on the other hand, depend on the reflective part of the spectrum and are therefore limited to daytime and cloud free conditions (Dong, 2018). Clouds, especially, are problematic, since they not only block observations,

but can also lead to misclassifications (Dong, 2018; Hall and Riggs, 2007; Riggs et al., 2016). While water clouds can be differentiated reasonably well from snow, confusion of snow and ice clouds is common (Dong, 2018). Apart from that, also cloud or terrain shadow can lead to false classifications (Hall and Riggs, 2007; Riggs et al., 2016; Sorman et al., 2007). Nonetheless, optical sensors have the major advantage that they typically offer a high spatial resolution and are available for comparatively long time periods (Dong, 2018).

One commonly used technique for snow detection with optical sensors is the Normalized Difference Snow Index (NDSI) (Hall and Riggs, 2011). Analog to the Normalized Difference Vegetation Index (NDVI) (Tucker, 1979), the NDSI is a technique based on the ratio of reflectances (Hall and Riggs, 2011). By comparing the reflectance in the VIS and SWIR, the NDSI can reliably detect snow cover (Hall and Riggs, 2011). Other detection techniques are traditional supervised multispectral classifications, spectral-mixture modeling and neural-network analyses (Hall et al., 2001; Rittger et al., 2013).

Advantages & limitations. Remote sensing of snow excels in providing data for a large spatial extent and space-filling observations while at the same time providing consistent data (Dong, 2018; Sturm, 2015). In addition, the cost and work effort for end users of satellite products is usually comparatively low (Sturm, 2015). Conversely, costs for satellite missions are high (Sturm, 2015).

Limitations of remote sensing of snow are the indirect retrieval of snow data by algorithms, the lack of the ability to measure all snow parameters, cloud cover obstructions and cloud-snow confusion, concealed snow cover due to canopy/vegetation and in some cases a limited spatial resolution (Dong, 2018; Sturm, 2015). Moreover, due to the large spatial extent that remote sensing usually provides, snow variations in small basins can be unnoticed (Sturm, 2015). Thus, under certain conditions the application of remote sensing techniques for snow detection, and the accuracy of the remote sensing measurements can be problematic (Sturm, 2015). Therefore, a validation is usually necessary to assess the accuracy of an applied remote sensing product.

Alternatives. Alternatives to remote sensing products for snow cover data are generally field measurements or snow distribution models (Dong, 2018; Sturm, 2015).

Snow distribution models are often used for avalanche forecasting or climate studies (Sturm, 2015). Their main advantage is that they enable future prediction of snow conditions (Dong, 2018). However, the underlying physics are still not entirely understood and such models require knowledge of boundary conditions that are rarely known (Sturm, 2015).

Another option to obtain snow cover data are field measurements. While field measurements provide the most direct approach to measure snow cover and usually yield good results, they are often only representative for a very small area (Sturm, 2015). Moreover, for a better spatial coverage of field measurements, the necessary working effort raises rapidly (Sturm, 2015).

1.3 Study Area

The Pamirs are a mountain area in Central Asia, that primarily lies within Tajikistan, but there are also parts in the neighboring countries Kyrgyzstan, Afghanistan, Pakistan and China. In figure 1.2, the study area (70.4–75.7° E, 36.3–39.9° N) is illustrated with a topographic map.

The study area can be divided in three parts: the Eastern and Western Pamirs – where the division roughly follows the 73° longitude line – as well as the Alai in the very north (Breu and Hurni, 2003). As reflected in figure 1.2, the Pamirs are a high mountain region: more than 90 % of the study area lie above 2500 m a.s.l..

The Eastern Pamirs, including Murghab and Tashkurgan, are characterized by cold and dry conditions (Miehe et al., 2001). The surrounding mountain systems shield the Eastern Pamirs from moist winds from the Indian and Atlantic Oceans, and thus create the desert like conditions (Breu and Hurni, 2003). The continental climate leads to relatively cold summers and severe winters (Breu and Hurni, 2003). While, precipitation in the Eastern Pamirs primarily occurs during summer (Breu and Hurni, 2003; Miehe et al., 2001), precipitation is typically so little, that summers in Murgab and Tashkurgan are generally arid (Miehe et al., 2001). Climatic conditions in the Eastern Pamirs can be summarized as a "cold high-mountain desert" (Vanselow et al., 2012).

The Western Pamirs, including Khorog, Savnob and Ishkashim, are characterized by more humid and comparatively mild conditions (Breu and Hurni, 2003). In contrast to the Eastern Pamirs, precipitation is considerably higher, and typically minimal in summer leading to arid summers (Breu and Hurni, 2003; Miehe et al., 2001).

The Alai mountain range and valley in the north of the study area, including Sary-Mogol and Sary Tash, are characterized by cold and humid conditions (Miehe et al., 2001). In the Alai, precipitation is substantially higher than in the Eastern Pamirs (Miehe et al., 2001). Temperatures recorded in Sary Tash are, however, similar to the temperatures in Murgab (Miehe et al., 2001).

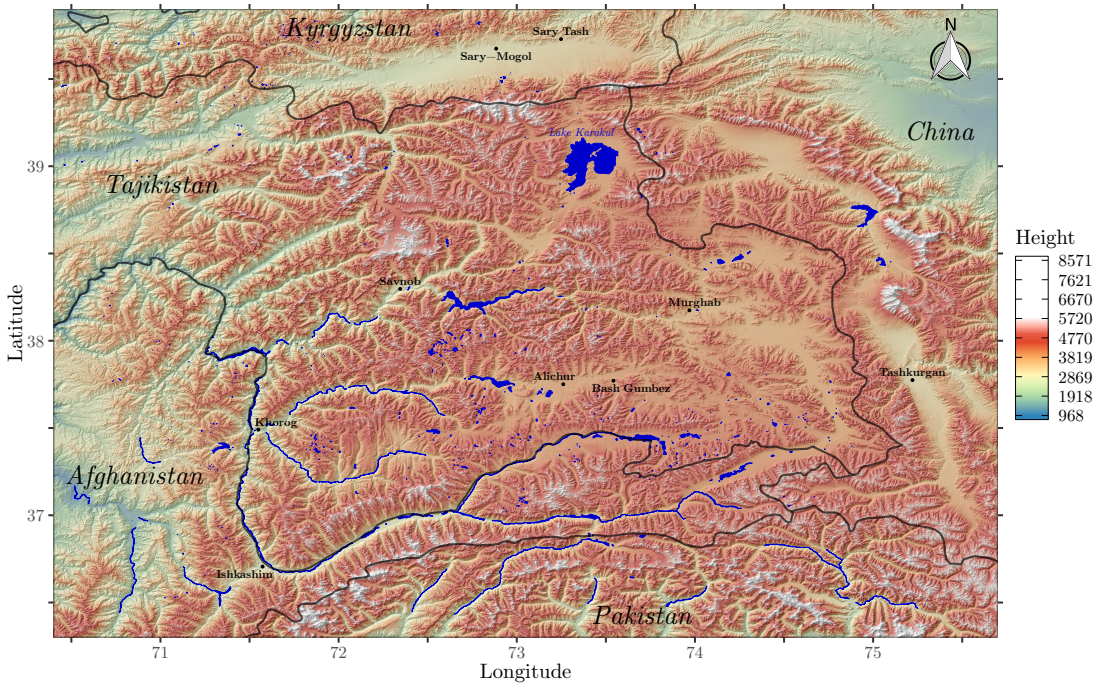

Figure 1.2: Topographic map of the study area. The map is based on the digital surface model of the Advanced Land Observing Satellite (ALOS) provided by the Japan Aerospace Exploration Agency (JAXA) (JAXA, n.d.).

1.4 Current State of Research

Global changes. The fifth IPCC Assessment Report (2013) elucidated that there is a general decline in all components of the cryosphere (Vaughan et al., 2013). Mass budgets of glaciers and ice sheets around the world are negative (Gardner et al., 2013). Furthermore, most snow metrics, including the SCE and SCD, have been decreasing: northern hemispheric SCE has been decreasing over the past 30 years (Derksen and Brown, 2012; Kunkel et al., 2016; Mudryk et al., 2017), especially in spring (Derksen and Brown, 2012; Hernández-Henríquez et al., 2015). Likewise, the SCD has been declining, with the strongest decline in spring, which is related to the reduction in spring SCE (Klein et al., 2016; Peng et al., 2013; Shi et al., 2013). Moreover, research also indicates negative trends in the SWE (Brown, 2000; Kunkel et al., 2016).

However, the response of snow cover metrics to climate change is complex. While atmospheric temperature seems to be the dominant factor influencing snow cover, the dependence of snow cover on precipitation and other factors complicates the response (Brown and Mote, 2009; Brown and Robinson, 2011; Lemke et al., 2007). At high latitudes and elevations, for instance, snow cover could increase, when higher precipitation offsets the shortening of the accumulation season (Brown and Mote, 2009). Hence, regional trends can differ from global trends.

Changes in the Pamirs. Studies researching climate change in the Pamirs indicate that air temperatures and precipitation have been increasing (Chevallier et al., 2014; Finaev et al., 2016; Knoche et al., 2017; Yao et al., 2012), while trends in glacier mass budgets were mostly balanced or increasing except for the Southern Pamirs (Gardelle et al., 2013; Knoche et al., 2017; Yao et al., 2012).

In the Pamirs, average air temperatures have been increasing since the second half of the 20th century (Chevallier et al., 2014; Finaev et al., 2016; Knoche et al., 2017). Warming was especially pronounced in fall and winter seasons (Finaev et al., 2016), while least warming occurred in summer (Finaev et al., 2016; Knoche et al., 2017).

Furthermore, studies indicate that also average precipitation in the Pamirs has increased since the second half of the 20th century (Finaev et al., 2016; Yao et al., 2012). However, according to Finaev et al. (2016) changes in precipitation were heterogeneous, with increases in high mountain areas and decreases in most other areas. In addition, Finaev et al. (2016) found a continuous increase in winter precipitation from 1981 to 2010. The study from Yao et al. (2012) indicated an increase in precipitation in the Eastern Pamirs.

Studies on glacier mass balances in the Pamirs primarily indicate balanced or increasing trends. However, they also indicate that trends differ depending on the region. Yao et al. (2012) and Gardelle et al. (2013) found increasing or balanced glacier mass budgets in the Eastern Pamirs and Western Pamirs respectively. Gardelle et al. (2013) therefore proposed renaming the "Karakoram anomaly" to the "Pamir-Karakoram anomaly", because of the contradiction to the glacier retreat on the global scale. While Knoche et al. (2017) also found increasing trends in the Northern Pamirs, they found decreasing trends in the Southern Pamirs.

Snow cover changes in the Pamirs. Recent studies indicate a decrease in snow cover in the Pamirs, with a shift towards earlier snow melt in spring (Dietz et al., 2014; Finaev et al., 2016; Li et al., 2018; Zhou et al., 2013, 2017).

Zhou et al. (2013) used a 8-day AVHRR data set from 1986 to 2008, which was corrected with the 8-day MODIS snow cover product, to analyze snow cover in the Amu Darya Basin in Central Asia. They detected significant decreasing trends of SCD in the Southern, Eastern and Western Pamirs as well as in the Alai (Zhou et al., 2013). In each case, the trend was accompanied with a shift towards earlier snow melt (Zhou et al., 2013).

Dietz et al. (2014) conducted an analysis on snow cover changes in Central Asia with a combination of AVHRR and MODIS remote sensing data. By combining both sensors they were able to form a continuous data set from 1986 to 2014 (Dietz et al., 2014). While they found no significant trend for the overall SCD

of Central Asia, their results indicated a trend towards earlier snow melt in the Pamirs (Dietz et al., 2014).

Finaev et al. (2016) used Landsat images to calculate the SCE. During the period from 1970 to 2008/09 they found that the mean annual SCE has decreased by 2.5 % across the Pamirs (Finaev et al., 2016).

In a later study, Zhou et al. (2017) used the 8-day AVHRR data set from 1986 to 2008 to conduct a more detailed analysis of the snow cover in Central Asia. They found significant decreases of SCD on mountains in the Pamirs (Zhou et al., 2017). On the other hand, they also found increasing trends in SCD in mid-elevation areas in the Alai and Western Pamirs (Zhou et al., 2017). Both increasing and decreasing trends were related to shifts in the snow cover melt date (Zhou et al., 2017).

In the most recent study, Li et al. (2018) examined the snow cover variability over the Tibetan Plateau during 2001 to 2014 with the 8-day MODIS snow cover product. They found strong negative trends of 1.5 to 3.62 % SCE per year within the Pamirs (Li et al., 2018). The decline in SCE was especially pronounced during December to April (Li et al., 2018).

Expectations & Projections. Long term climate projections predict a widespread decline of SCE, especially in spring (Brown and Mote, 2009; Brutel-Vuilmet et al., 2013). Changes in SWE are expected as well, they depend, however, on the balance between precipitation and temperature changes, which can differ regionally (Collins et al., 2013). Implications of climate change on snow cover in mountain areas like the Pamirs are expected to be a rise of the snow line and changes in SCD and SWE (Beniston, 2003). In addition, a general decline in snow cover and an asymmetrical shortening of the snow season with a stronger shortening at the end of winter are expected (Magnusson et al., 2010). Furthermore, research indicates, that changes of snow metrics are strongest in areas where the temperature is close to the melting point for longer periods of the snow season (Brown and Mote, 2009; Steger et al., 2013). In contrast, continental regions with dry and cold conditions like the Eastern Pamirs showed lower temperature sensitivity in climate projections (Brown and Mote, 2009). Projections for these drier climates tended to be more mixed with increases in maximum SWE and decreases in SCD (Brown and Mote, 2009).

1.5 Research Questions

The complex response of snow cover to climate change in high mountain areas together with the not clear-cut cryosphere changes in the Pamirs call for a more

detailed analysis of snow cover changes in the study area. Therefore the spatio-temporal snow cover variability in the Pamirs was analyzed as a meaningful next step to better resolve small-scale changes of the cryosphere within this region. For this purpose, snow cover changes over the past 18 years were analyzed by using the reliable Moderate Resolution Imaging Spectroradiometer (MODIS) remote sensing data products. Two research questions have been formulated:

Has the snow cover extent (SCE) changed significantly over the past 18 years?

The snow cover extent (SCE) represents the area that is covered by snow (Vaughan et al., 2013). Hence, the SCE yields information about the spatial expansiveness and the quantity of snow.

Finaev et al. (2016) and Li et al. (2018) found that the SCE has decreased in the Pamirs. There are, however, no small-scale results available to assess differences within the Pamirs. By means of this research question overall and regional changes of the SCE in the Pamirs were analyzed, to assess the trend in SCE of the last two decades and visualize differences within the study area.

Has the snow cover duration (SCD) changed significantly over the past 18 years?

In this study, the snow cover duration (SCD) was defined as the number of days during a certain time period, on which a certain area was covered by a considerable amount of snow (Sect. 2.3.1). Contrary to the SCE, the SCD additionally contains information about time related changes like the duration of the snow season. Furthermore, the combination of SCE and SCD allows to discern areas with short (long) but high (low) snow coverage.

Previous studies primarily indicate a decreasing trend in SCD in the Pamirs, and a shift towards earlier snow melt in spring (Dietz et al., 2014; Zhou et al., 2013, 2017). However, the results from Zhou et al. (2017) also indicate a positive trend in SCD in certain areas. By means of this research question the overall and regional changes of the SCD were analyzed, to assess the trend in SCD of the last two decades, visualize regional differences in SCD trends and assess the potential shift towards earlier snow melt in spring.

2 Methods

2.1 Data

2.1.1 Optical remote sensing data

In this study, the remoteness and large spatial extent of the study area, together with the need for a high temporal resolution and a consistent availability over a long time period, led to the choice of remote sensing data. Furthermore, remote sensing is suitable for SCE detection as indicated by the agreement between different remote sensing products (Roesch, 2006).

An optical sensor was chosen, because of the in the introduction mentioned advantages compared to microwave remote sensing (Sect. 1.2.2). Table 2.1 gives an overview of the available data sets of optical sensors for snow detection.

Table 2.1: Overview of optical remote sensing sensors used for snow detection (adapted from Dong, 2018). Satellites of data sets, which have been used in this study, are indicated in bold.

Satellite	Sensors	Spatial Resolution [m]	Temporal Resolution [d]	Launch time
Landsat 1-3	MSS	79	18	1972
Landsat 4-5	MSS/TM	30/120	16	1982
Landsat 7	ETM+/PAN	15/30/60	16	1999
Landsat 8	OLI/TIRS	15/30/100	16	2013
Terra	MODIS	250/463*/1000	1	1999
Aqua	MODIS	250/463*/1000	1	2002
NOAA	AVHRR	1090	1	1978
SPOT 1-3	XS/PAN	10/20	26	1986
SPOT 4/5	XS/PAN	2.5/5/10/20	26	1998
SPOT 6/7	XS/PAN	1.5/6	26	2012
IKONOS	XS/PAN	1/4	3	1999
ERS-2	ASTER-2	1000	2-3	1995
Worldview 2	XS/PAN	0.46/1.84	1	2009
Worldview 3	XS/PAN/SWIR	0.31/1.24/3.70	< 1	2014
Quickbird	XS/PAN	0.65/2.62	1-3.5	2001
Envisat	AATSR/MERIS	1000/300	2-3	2002

* Nominal 500 m resolution, true spatial resolution is approximately 463 m (Román et al., 2004)

2.1.2 MODIS-Terra snow cover product (MOD10A1)

Out of the, in table 2.1 listed, choices the MODIS-Terra snow cover product was chosen for the snow cover analysis.

For this study, high temporal and spatial resolution along with a long, consistent recording period were required. The Global Observing System for Climate (GCOS) recommends a daily temporal resolution and 100 m spatial resolution for snow cover extent (SCE) studies in complex terrain (WMO, 2011). The long recording period was required for a meaningful trend analysis. To adequately meet these requirements, the daily MODIS snow cover product (MOD10A1) was chosen. MOD10A1 offers a decent compromise between a high temporal and spatial resolution, while still providing a long recording period (Tab. 2.1). Furthermore, various studies confirm that the MODIS snow cover products are suitable for snow detection in mountain areas (Crawford, 2015; Gascoin et al., 2015; Jain et al., 2008; Sorman et al., 2007). An additional advantage of MODIS would have been, that the sensor operates on two satellites: Terra and Aqua (Riggs et al., 2016). This is can be utilized to improve the data availability (Gafurov and Bárdossy, 2009; Wang and Xie, 2009). In this study, however, only MODIS-Terra was used due to technical issues that prevented the acquisition of MODIS-Aqua data.

With the MODIS snow cover product series, the NASA already offers a set of preprocessed products, which use the NDSI to specify the snow signal (Riggs et al., 2016). The level-3 product MOD10A1 is a gridded product that contains the "best" NDSI observations out of the available swaths for every day (Riggs et al., 2016). An alternative would have been MOD10A1F, which was newly introduced in collection 6 of the MODIS snow products (Riggs et al., 2016). MOD10A1F represents a cloud-gap-filled data set that was created with a temporal gap filling algorithm (Hall et al., 2010; Riggs et al., 2016). However, since MOD10A1F was not yet available through the NASA's National Snow and Ice Data Center (NSIDC) at the time of this study and information on cloud cover would not have been included, MOD10A1 was selected.

The selection of MODIS comes with the general disadvantages of optical sensors mentioned in the introduction (Sect. 1.2.2). The most relevant disadvantages for this study are problems related to cloud cover, since the Pamirs are a high mountain area with frequent cloud cover.

2.1.3 Landsat 5 (TM)

Landsat 5 Thematic Mapper (TM) images were chosen as reference data for the validation of MODIS.

Landsat images offer a high spatial resolution of 30 m (TM), and are frequently

used to validate the MODIS snow cover products (Crawford, 2015; Dietz et al., 2014; Gascoin et al., 2015). For the validation reference data, images with a high spatial resolution are required to ensure an accurate detection of snow cover. While the temporal resolution of Landsat images is too low for the use in the actual snow cover analysis, it is sufficient for validation purposes.

Apart from Landsat 5, also Landsat 7 and 8 operated within the analyzed time period. For the validation, days in spring 2008 and 2009 were chosen (Sect. 2.2). Therefore, only Landsat 5 and 7 images were possible options, since Landsat 8 started operating in 2013 (Tab. 2.1). Landsat 5 images were then preferred over Landsat 7, because the images in Landsat 7 contain artifacts since 2003. After cloud cover conditions were considered, two images of Landsat 5 (TM) were chosen.

2.2 Validation with Landsat 5 (TM)

2.2.1 Landsat processing

Validation area & date. Only a part of the study area was validated with Landsat images due to its large spatial extent. The validation area was selected based on the results of the snow cover analysis (Sect. 3.2.1). For the chosen area two days with different snow conditions were selected. The exact dates were selected based on snow conditions, the availability of Landsat 5 images and cloud coverage conditions (Sect. 3.2.1). The Landsat images on the chosen days were then used as reference data for the later validation of the gap filled MODIS data set, which underlies the snow cover analysis.

The reason for selecting two images with different snow conditions was, that in this way the accuracy of the applied MODIS data set could be verified under different conditions. Furthermore, images from spring of consecutive years were chosen, since spring offered different snow conditions, while at the same time having less cloud cover than winter. Another advantage of using images from the same season in consecutive years was, that differences in other factors, like illumination conditions, were reduced.

Acquisition. The freely available level-2 Landsat 5 (TM) images were acquired using the Earth Explorer client from the U.S. Geological Survey (USGS).

The level-2 product was chosen, since level-3 products, which would have been already classified, were only available for a part of the U.S. and Alaska. In addition to the basic terrain corrections of the level-1 product, the level-2 product has been further processed with radiometric calibration and atmospheric correction algorithms (USGS, n.d.).

NDSI calculation. First, the acquired Landsat images had to be adjusted with the respective scale factor and grid cells, with values outside the valid range, had to be removed. Next, the NDSI was calculated using equation (2.1) as specified for Landsat TM in MODIS's algorithm theoretical basis document (Hall et al., 2001). Subsequently, negative NDSI values were set to 0, to obtain the same NDSI scale as in the MODIS snow cover products and to ensure that negative NDSI values would not interfere with the later aggregation of grid cells.

$$\text{NDSI} = \frac{\text{TM Band 2} - \text{TM Band 5}}{\text{TM Band 2} + \text{TM Band 5}} \tag{2.1}$$

Although it slightly complicates the interpretation of the validation results, it was chosen not to validate the FSC, but rather the NDSI out of three reasons: First, equation 2.2, which was used to derive the FSC from MODIS's NDSI observations, does only apply to MODIS. The equation was derived by comparing NDSI observations of MODIS with FSC calculations based on Landsat (Salomonson and Appel, 2004, 2006). Second, other approaches for obtaining a FSC Landsat image would have introduced more uncertainty. Third, the validation of the NDSI offers a better assessment of the accuracy of the data set, since the NDSI contains more information than the FSC.

1st cut, reprojection & 2nd cut. Next, the images were cut slightly to reduce memory strain while at the same time still leaving a large enough image to be able to later remove edge effects with a second cutting step. For this, the spatial extent of the image was trimmed from the original extent to 73.25–74.95° E, 37.00–38.10° N.

Afterwards, the images were reprojected form the UTM projection, in which they were originally delivered, to the sinusoidal projection, which MODIS uses. Such a reprojection requires a resampling of the grid cells (Jensen, 2005). In this study a bilinear interpolation method was chosen for calculating the new cell values. This method derives the values of the new grid cells by calculating the distance based weighted average of the four nearest cells (Jensen, 2005). Since the NDSI is cardinal scaled rather than ordinal scaled, the bilinear interpolation yields more accurate values for the new grid cells. It was decided to reproject the Landsat images rather than MODIS, because the resampling errors might be smaller for the Landsat images with their higher spatial resolution.

Following the reprojection, the Landsat images were trimmed to the validation area extent (73.35–74.85° E, 37.10–38.00° N). This second cut ensured that edge effects created from the reprojection were removed.

Aggregation & resampling. Next, the high resolution Landsat images were aggregated and then resampled to obtain the exact same spatial resolution as the MODIS images.

An aggregation mask of 15×15 cells was used. The new value of an aggregated grid cell was computed by averaging all grid cells in the aggregation mask. When there were NA ("not available") values present in the aggregation, the entire new cell was set to NA. This was done to not further reduce the accuracy of the Landsat images. After the described aggregation, the spatial resolution of the aggregated Landsat images was 450×450 m. A resampling step was therefore necessary to reach MODIS's spatial resolution of approximately 463.3 m. The aggregated Landsat images were resampled to the exact spatial resolution of MODIS by using once more a bilinear interpolation.

2.2.2 Validation

The Landsat images were used in three different ways to validate the gap filled MODIS snow cover product. The validation included a *visual assessment* of cell value differences, the comparison of NDSI *distributions* and the calculation of a *confusion matrix* of classified NDSI values.

For the *visual assessment*, the difference in NDSI was calculated for each grid cell and then displayed in a map. This allowed a first general assessment of the accuracy, and an assessment of patterns with positive or negative deviations. Such patterns could then be compared to a topographic map of the validation area to assess a potential interrelation with altitude or terrain.

For the NDSI *distributions*, the distributions of occurring NDSI values in MODIS and Landsat were compared using histograms and density plots. For the density plots, a gaussian kernel was used. The gaussian kernel was preferred over other kernels, because it depicted the distribution better than other alternatives.

Furthermore, a *confusion matrix* was computed after the cell NDSI values had been assigned to six different NDSI classes. The classes start with an NDSI of 0 followed by 0.2 intervals, which were closed on the right. This division was chosen to obtain a reasonable compromise between the resulting accuracies and the number of classes. The class 0 was defined as a single NDSI value, because it contains all grid cells, where no snow signal was detected. The class 0, thus, allows to assess the ability of MODIS to detect snow in conditions with sparse snow cover, for which MODIS tends to have difficulties (Hall and Riggs, 2007).

2.3 Snow Cover Analysis with MOD10A1

2.3.1 MODIS processing

Images of the daily MODIS snow cover product from 2001 to 2018 were processed in several steps to obtain information on snow and cloud cover in the Pamirs.

Theoretically, MODIS images would have been available since February 2000. Nonetheless, only images beginning from 2001 were used, since images before 2001 contained a large amount of gaps.

The decision to use daily images (1.5 million grid cells) over 18 years made it necessary to derive specific processing algorithms, which addressed computation time and memory limits. Therefore, most processing was executed based on a combination of custom functions with *apply* functions. This architecture made it possible to perform cell wise calculations with single function calls, and thus drastically reduced computation time. Memory limitations were addressed by splitting up the study area in multiple small parts.

In the following paragraphs, the successive processing of the downloaded MODIS tiles up to the calculation of the fractional snow cover (FSC), snow cover duration (SCD), cloud cover extent (CCE) and cloud cover duration (CCD) is described. Figure 2.1 outlines the performed MODIS processing procedure.

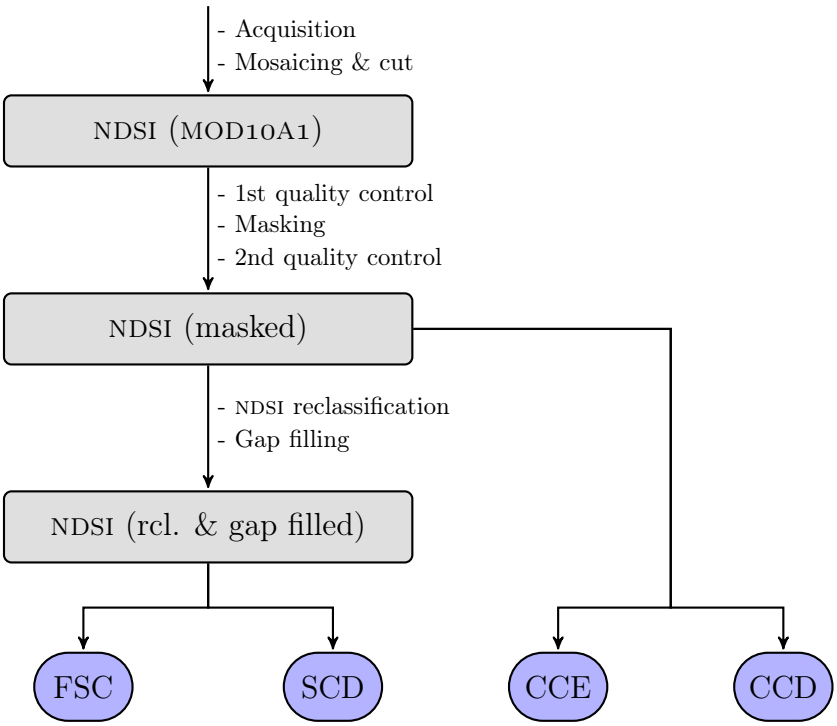

Figure 2.1: Processing of the downloaded MODIS satellite tiles. The figure outlines the different steps involved in the data processing up to the computation of the variables FSC, SCD, CCE and CCD.

Acquisition. The MOD10A1 snow cover product is freely available on the NSIDC homepage. The data is distributed in downloadable tiles of daily temporal resolution. The tiles come with a spatial resolution of approximately 463 m in the sinusoidal projection.

Both, the spatial resolution and the projection, weren't changed, since the highest available spatial resolution was desired and a reprojection would have introduced resampling errors (Lunetta et al., 1991; Slater, 1985). Ramifications of working with the sinusoidal projection were a complicated data processing and the need to later reproject results to geographical coordinates for visualization purposes. To exclude edge effects caused by this reprojection, the displayed extent for *regional* results (Sect. 2.3.2) was slightly trimmed by 0.05°.

Mosaicing & cut. Upon the data acquisition, a mosaicing and subsequent cut was applied. The study area required the combination of three MODIS tiles (h23v04, h23v05, h24v05). For each day the three tiles were first combined, and then trimmed to the study area's geographic extent (70.4–75.7° E, 36.3–39.9° N).

1st quality control, masking & 2nd quality control. A first quality control was conducted, during which missing images and images with differing resolution or extent were extracted. When the respective images could not be obtained in a complete form from the NSIDC homepage, they were noted as gaps (Tab. 2.2).

Next, values outside the study area had to be masked. While raster images exist per definition only as rectangular grids, the shape of the study area in the sinusoidal projection required a non-rectangular shape. This led to the problem that the previously defined rectangular raster included grid cells outside the actual study area. Therefore, cells outside the study area were set to NA by applying a mask. From there on onward, grid cells inside the study area were selected by cell numbers derived from the 10th of August 2001 – a day in a period of days characterized by low cloud cover, with the correct total amount of NA for the outer grid cells and no visible NA cells upon manual inspection.

Following the masking step, a second quality control was conducted. During this second quality control, days that were characterized by an abnormal amount of NA cells (inside the study area) were removed and noted as gaps (Tab. 2.2).

NDSI reclassification & gap filling. To later obtain a data set which only contained NDSI values between 0 and 1, a reclassification was conducted: cell values for "missing data", "no decision", "night", "cloud", "detector saturated" and "fill" were set to NA, and cell values for "inland water" and "ocean" were set to 0 (no snow).

Table 2.2: MODIS gaps for the study area. The table notes all days, for which the tiles were either completely missing or manually removed due to incompleteness or an abnormal amount of NA cells.

Year	Gaps	$\sum$
2001	12-13 Feb‡, 15-30 Jun*, 01-03 Jul*, 09 Aug*, 07 Oct‡, 06 Nov*	24
2002	20-28 Mar*, 15 Apr*	10
2003	01 Feb*, 22 Mar‡, 01 Apr†, 17-24 Dec*	11
2004	19 Feb*	1
2005	22 Sep†, 27 Nov‡	2
2006	21 Jun*, 23 Aug*	2
2008	17 Nov†, 20-23 Dec*	5
2009	09 Sep*	1
2010	06 Mar†, 26 Jun*	2
2014	26 Oct*	1
2016	19-28 Feb*	10
2017	24 Apr*	1

* no tiles of the study area were available
† only part of the study area's tiles were available (differing extent)
‡ images that had a very high number of cells with NA values

Next, a simple temporal gap filling procedure was applied to obtain consistent and (ideally) cloud cover independent results. First, missing days were added as NA. Subsequently, grid cells with time series of more than 60 % NA were excluded from the analysis, because these gaps were considered as not suitable for the chosen gap filling approach. The remaining grid cells with gaps below 60 % were filled by using a simple linear interpolation of the NDSI. Gaps in the very beginning or end of a time series without preceding or subsequent values, were filled by using the closest value that was not NA. Afterwards, leap days in the time series were removed to obtain a consistent time series suited for later trend analyses.

This simple temporal gap filling approach was chosen, since a more elaborate approach would have been beyond the scope of this thesis. Other gap filling techniques besides temporal gap filling include the use of additional sensors, snowline estimation and spatial gap filling using neighboring grid cells (Gafurov and Bárdossy, 2009). The applied approach ensured a complete removal of clouds with reasonable results (Sect. 3.2). Furthermore, some gap filling techniques, like a spatial gap filling that uses neighboring grid cells, could have been problematic considering the study area's complex terrain and the GCOS recommendations for the spatial resolution (WMO, 2011).

FSC, SCD, CCE, CCD computation. The CCE and CCD were calculated from the masked data set by using the cloud flagged cells of the MOD10A1 snow cover product. The calculations of the FSC and SCD were based on the gap filled NDSI data set (Fig. 2.1).

The CCD was computed by first counting the number of days in which a cell was marked as cloud, and then dividing this number by the number of total days of the time period of interest. The CCE was computed by counting the number of cells marked as cloud and then dividing this number by the number of total cells within the study area.

Before the calculation of the FSC and SCD, the NDSI values from the MODIS snow cover product had to be adjusted by a scale factor of 0.01 first, since the original values came as integers only, with a valid range from 0 to 100. The FSC was then calculated by using equation (2.2), which is based on an empirical regression relationship between MODIS-Terra NDSI observations and FSC calculations from Landsat (Salomonson and Appel, 2004, 2006):

$$(-0.01 + 1.45 \times \text{NDSI}) \times 100 \tag{2.2}$$

Subsequently, FSC values smaller than 0 % and greater than 100 % were set to 0 % and 100 % respectively.

The SCD was calculated by counting the number of days, in which the NDSI exceeded a threshold of 0.2, which corresponds to a FSC of 28 % according to equation (2.2). An annual SCD of 100, thus, represents a time series, during which 100 days out of all 365 days had a FSC (NDSI) greater than 28 % (0.2). The NDSI threshold of 0.2 was chosen based on considerations of local terrain and snow heterogeneity in the study area. While it has been common practice for some time to use a NDSI threshold of 0.4 for studies on snow covered area, recent literature recommends a threshold between 0.1 and 0.4 depending on the study area and other factors (Riggs et al., 2015). A higher threshold for the SCD can decrease the error of commission. Low NDSI values can occur even when there is no snow (Riggs et al., 2015). Therefore, a higher threshold can reduce the number of days that were falsely classified as snow covered. However, a higher threshold for the SCD can also increase the error of omission. Thin or sparse snow cover as well as snow in shaded areas can have lower NDSI values (Riggs et al., 2015; Sorman et al., 2007). Thus, in complex terrain or conditions with sparse snow cover, a higher threshold can lead to the omission of days that should have been classified as snow covered. In this study, a threshold of 0.2 was chosen as a reasonable compromise in an area with complex terrain and considerable snow cover heterogeneity.

All calculations were computed annually and seasonally. For the seasonal analysis, the four meteorologic seasons were used: spring (01 Mar → 31 May, 92 days), summer (01 Jun → 31 Aug, 92 days), fall (01 Sep → 30 Nov, 91 days) and winter (01 Dec → 28 Feb, 90 days). Since images from 2001 to 2018 were used, values for winter could only be computed from 2001 to 2017 (with winter 2001

starting in December 2001).

2.3.2 Overall, regional & cell calculations

Calculations were subdivided in three categories: *overall*, *regional* and *cell* calculations. The reasoning behind this subdivision was that each category addresses a different spatio-temporal analysis. Figure 2.2 illustrates all included results of the snow cover analysis together with their respective category and variable.

Overall. The category *overall* refers to calculations regarding the entire study area as a whole. Calculations in this category were intended to assess the conditions of the entire study area rather than spatial differences within the study area.

Calculations belonging to this category were the mean seasonal cycle and trend calculations. For the the mean seasonal cycle the FSC was calculated by averaging the cell FSC values on each day and subsequently averaging the respective day over all years. The CCE of the mean seasonal cycle was calculated as described in the previous section (Sect. 2.3.1) and then averaged over all years. Trend calculations were performed by conducting a trend analysis (Sect. 2.3.3) on the daily and mean FSC time series of the entire study area. Thereby, the daily FSC time series was derived from averaging all cell FSC values on each day, and for the mean FSC an annual/seasonal mean of the study area's FSC was used.

Regional. The category *regional* refers to cell wise calculations of the entire study area. These cell wise calculations allowed to examine spatial differences within the Pamirs. Results of this category could be visualized with maps.

Calculations were mostly analog to calculations in *overall*. The overall mean maps were created by simply averaging the whole time series of each grid cell. Trend calculations were performed in the same way as in *overall* with the difference, that the trend analysis was conducted on each individual cell. For trend maps the slope of the linear trend was displayed for each cell.

Cell. The category *cell* refers to calculations for individual grid cells that were analyzed in more detail. Calculations in this category were performed for grid cells that were situated in regions with noteworthy results or results out of the ordinary, and were, thus, meaningful to inspect.

Overall, results of more than a few cells have been broadly checked, and four cells were inspected in more detail. Nonetheless, only some results of the cell 833289, which lay within a region with noteworthy results, are included in the

results of this thesis. Calculations were performed in the same way as in *regional*, but only on the grid cell of interest.

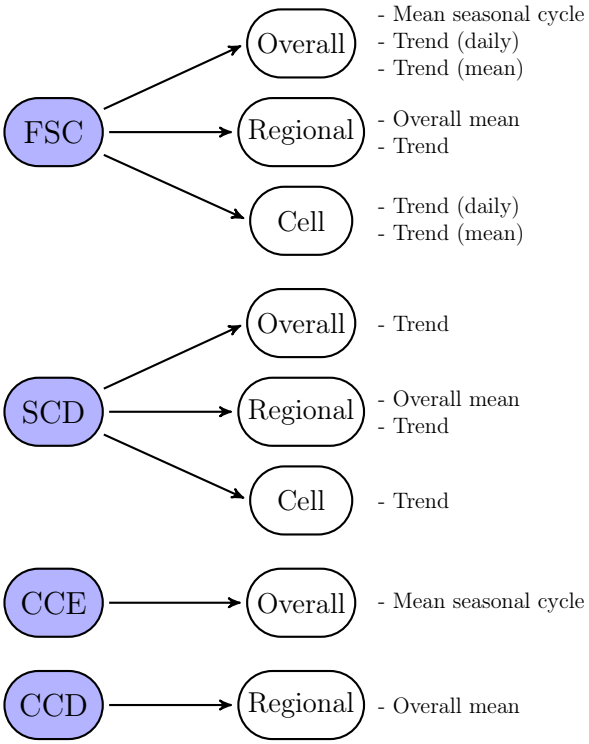

Figure 2.2: Overview of all included results of the snow cover analysis with MODIS. Calculations of the different variables were subdivided in the three categories *overall*, *regional* and *cell*. Each category addresses a different spatial scale.

2.3.3 Trend analysis

A trend analysis was conducted for time series of the entire study area and for time series of all grid cells. The analyzed time period from 2001 to 2018 was examined as a whole; no further temporally subdivided analyses were conducted.

When a seasonal component was present in the time series to be analyzed, like in a daily FSC time series for instance, the time series was decomposed by using an additive model consisting of a seasonal, trend and remainder component. In cases where there was no seasonal component, like for the annual SCD for instance, the time series was simply decomposed by using an additive model consisting of a trend and remainder component.

Moving average. For daily time series, a simple moving average trend was computed by using a symmetric averaging window with a length equal to the frequency of the input time series. Hence, for a time series with daily observations within a whole year (frequency = 365), an averaging window of 365 has been used.

The first value would, thus, be calculated on position 183 as the mean of 1 to 365. This approach was chosen, because then the so calculated moving average was unaffected by seasonality and was a reasonable compromise between sensitivity and noise. Next, the trend component was subtracted from the input time series. Subsequently, the seasonal component was calculated as the average of each time unit over the whole time series. Afterwards, the remainder component was computed as the difference between the input time series and the sum of the seasonal and trend component.

Linear model. A simple linear least squares model was calculated, to obtain an indication of the overall trend (Wilks, 2011). For this, the respective time series was decomposed as in the calculation of the moving average. After the calculation of the seasonal component, a linear model was computed using the original time series subtracted by the seasonal component. Next, the remainder component was computed in the same way as in the moving average.

ANOVA. The analysis of variance (ANOVA) method was used to assess the significance of the linear trend with respect to the null hypothesis of no trend (Wilks, 2011). No ANOVA was conducted when significant autocorrelation was present. Autocorrelation was assessed with the functions specified in Duchon and Hale (2012).

Mann-Kendall trend test. In addition to the linear model combined with the ANOVA test, the Mann-Kendall trend test (MK) was performed to in general test for a non-monotonic trend in the time series (Wilks, 2011). In case of significant autocorrelation, the modified Mann-Kendall trend test (mMK) derived by Hamed and Rao (1998) was used.

2.4 Software

The data acquisition of MODIS, data processing, statistical analyses and validation were all performed using the *R software environment*. Table 2.3 lists all packages, which have been used in the analysis together with their respective field of application. Package dependencies and further packages, which are included in the base installation, are not included in table 2.3. In addition, QGIS was used for the acquisition of data from the OpenStreetMap project. GIMP was used to overlay trend plots with a pattern as indication of significant grid cells. Furthermore, *Blender* was used to create a time lapse video, which illustrates the course of the daily snow cover in the study area for the analyzed time period.

Table 2.3: R packages that were used for this thesis in addition to the packages from the base installation. Package dependencies are not included in the table.

Field of Application	Packages
Data acquisition	MODIS
Processing	ff, plyr, raster, rgdal, RStoolbox, sp
Trend analysis	Kendall, modifiedmk, zoo
Visualization	dichromat, extrafont, ggnewscale, ggplot2, ggpolypath, ggsn, grid, gridExtra, rasterVis, rnaturalearth, shadowtext

3 Results

3.1 Cloud Cover

Cloud cover was generally very high in the Pamirs. On average a grid cell was covered with clouds 49 % of the time. The cloud cover duration (CCD) pattern clearly reflects altitude differences, whereby areas with a high altitude typically had high CCD values. Areas, which had comparatively low CCD values, are mostly valleys in the southwest, east and northeast.

Figure 3.1 illustrates the overall mean CCD in percent for each grid cell of the study area. Cell values ranged from 29 to 88 % CCD. The mean CCD of grid cells within the study area was 49 %. Large parts of the study area had high CCD values (Fig. 3.1). However, there were also areas with comparatively low CCD between 30 and 40 %, mostly in the east and southwest of the study area (Fig. 3.1). When comparing figure 3.1 with the topographic map in figure 1.2 it is apparent, that the observed CCD pattern strongly reflects altitude differences. Areas with high CCD primarily represent regions with major mountain ridges. Differences between the Eastern and Western Pamirs were not apparent.

3.2 Validation

3.2.1 Area and date selection

Validation area. The red inset (73.35–74.85° E, 37.10–38.00° N) in figure 3.2 marks the validation area. This particular region was chosen, because it was characterized by strong snow cover reductions in the snow cover analysis (Sect. 3.3). Additionally, figure 3.2 illustrates the extent of the original Landsat tile (orange inlet) and the processed extent after the first cut (blue inlet).

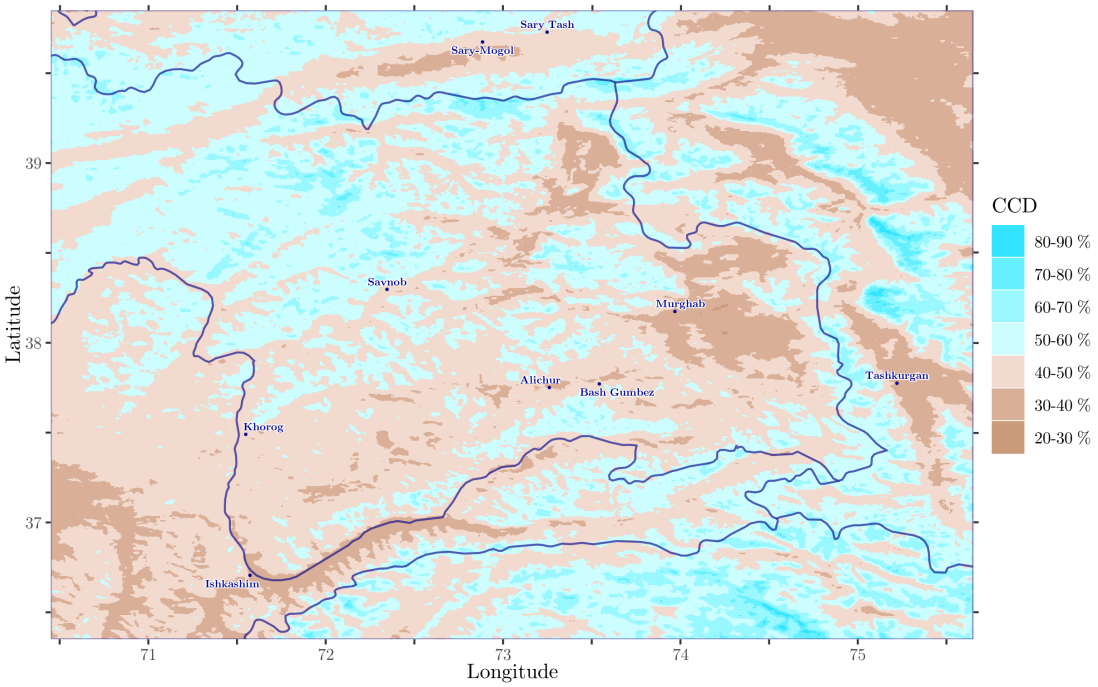

Figure 3.1: Mean cloud cover duration (CCD) in the study area from 2001 to 2018. The colors indicate the percentage of days that have been covered by clouds during 2001 to 2018.

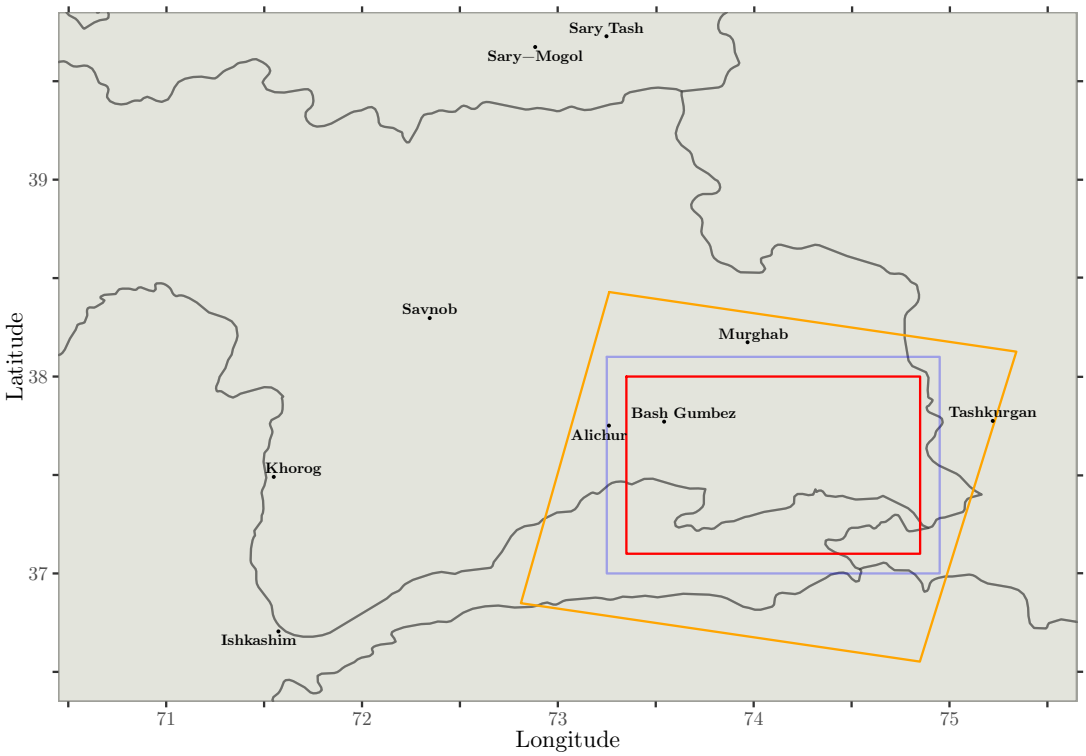

Figure 3.2: Map of the study area with indications for the processed Landsat raster. The orange inlet represents the extent of the original Landsat 5 tile. The blue inlet represents the area after the first cut (Sect. 2.2). The red inlet represents the final validation area.

Validation dates. Two Landsat images were selected, one from the 25th of April 2008 and one from the 11th of March 2009.

The reason to choose images in spring 2008 and 2009 was a difference in snow conditions and other considerations (Sect. 2.2). The snow season 2008 was characterized by comparatively little snow, whereas the snow season 2009 had comparatively much (Sect. 3.3). The exact dates were chosen based on the availability of Landsat 5 images and cloud coverage conditions. Figure 3.3 illustrates the FSC and CCE conditions in spring 2008 and 2009, together with indications for the available Landsat 5 images. MODIS images with the NDSI of the entire study area on both days can be found in the appendix (Fig. A.1, A.2). The 25th of April 2008 and 11th of March were reasonable compromises between different snow conditions at the same season of consecutive years. Furthermore, cloud cover conditions were still acceptable on both days (Fig. 3.3).

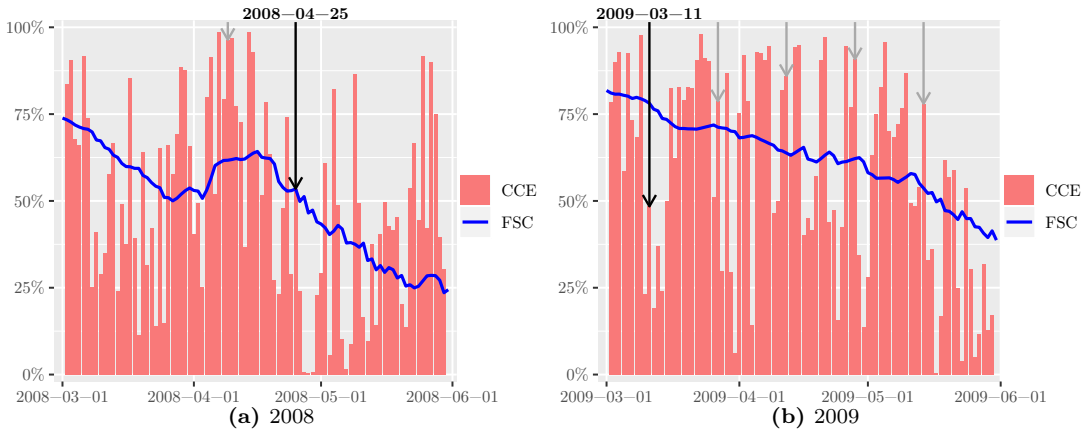

(a) 2008 (b) 2009

Figure 3.3: The selection of the 25th of April 2008 and the 11th of March 2009 as validation dates. The black arrows mark the validation dates. Other available Landsat 5 images, which had not been chosen for the validation, are marked with gray arrows.

3.2.2 Validation on the 25th of April 2008

Visual assessment. MODIS and Landsat showed reasonable agreement in regard of the general NDSI pattern on the 25th of April 2008. However, there were also considerable differences visible between MODIS and Landsat. Results indicate that MODIS overestimated the NDSI in higher altitudes, and underestimated the NDSI in lower altitudes.

Figure 3.4 contrasts the NDSI results of MODIS with the ones from Landsat on the 25th of April 2008. The gap filled MODIS image (Fig. 3.4a) is illustrated together with the high resolution Landsat image (Fig. 3.4b), the aggregated and resampled Landsat image (Fig. 3.4c) and a figure, which indicates the difference in NDSI between MODIS and the aggregated and resampled Landsat image (Fig. 3.4d).

In the gap filled MODIS product, high NDSI were primarily detected on large mountain ridges, while lower NDSI values were detected in more even terrain (Fig. 3.4a). Furthermore, only few NDSI values of medium magnitude were detected, as indicated by the pronounced contrast in figure 3.4a. Despite MODIS's comparatively low resolution there is still a larger lake identifiable in the south of the validation area. However, in contrast to the MODIS image, the high resolution Landsat image contains far more detail (Fig. 3.4b). Mountain ridges are easily identifiable and many lakes and rivers can be identified as well. Since the Landsat image was not gap filled, many NA cells were still present, especially around mountain ridges within the validation area. In the aggregated and resampled Landsat image, a considerable amount of detail was lost (Fig. 3.4c). The notably larger NA areas in figure 3.4c illustrate the aggregation process, during which new grid cells were completely set to NA if one inner cell contained a NA value (Fig. 3.4c).

Figure 3.4d shows the difference between MODIS and the aggregated and resampled Landsat image. While 41 % of all valid grid cells only differed by less than ± 0.05, 44 % of the cells were underestimated (positive classes) and 15 % of the cells were overestimated (negative classes). Therefore, MODIS considerably underestimated and slightly overestimated the snow conditions on the 25th of April 2008. Moreover, Figure 3.4d indicates that MODIS underestimated the NDSI in lower altitudes and overestimated the NDSI in higher altitudes.

NDSI distributions. The analysis of the NDSI distributions of MODIS and Landsat demonstrates that MODIS failed to detect many low NDSI values. In addition, results indicate that MODIS also slightly overestimated high NDSI values.

Figure 3.5 illustrates the distribution of NDSI values for MODIS and Landsat on the 25th April 2008. In MODIS, the vast majority of grid cells had NDSI values close to 0. Also in Landsat the majority of grid cells had NDSI values close to 0. However, the number of grid cells in Landsat with a NDSI of approximately 0 was only between a forth and a third of the number in MODIS. In contrast to MODIS, Landsat detected far more cells with NDSI values of low and medium magnitude. In high NDSI ranges, MODIS slightly overestimated NDSI values. However, the sample size of grid cells with high NDSI values was relatively small on the 25th of April 2008.

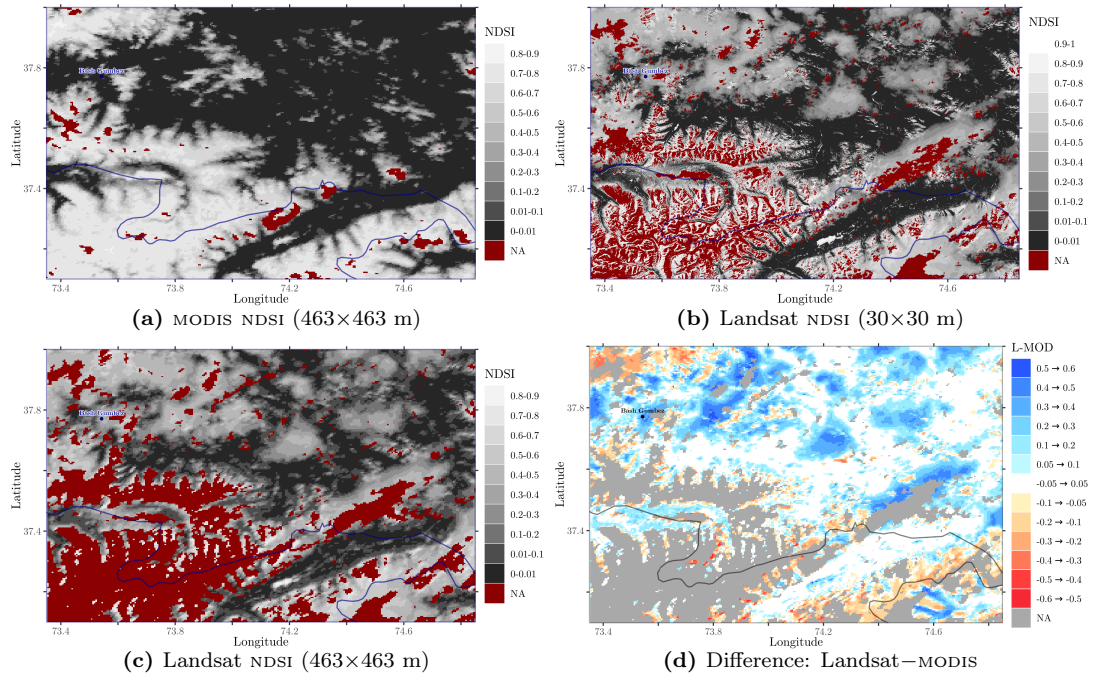

(a) MODIS NDSI (463×463 m) **(b)** Landsat NDSI (30×30 m)

(c) Landsat NDSI (463×463 m) **(d)** Difference: Landsat−MODIS

Figure 3.4: Visual comparison of MODIS and Landsat on the 25th of April 2008. The NDSI of MODIS (a) is illustrated along with the NDSI of the high resolution Landsat image (b) and the aggregated & resampled Landsat image (c). The difference between MODIS and the aggregated & resampled Landsat image is illustrated in (d).

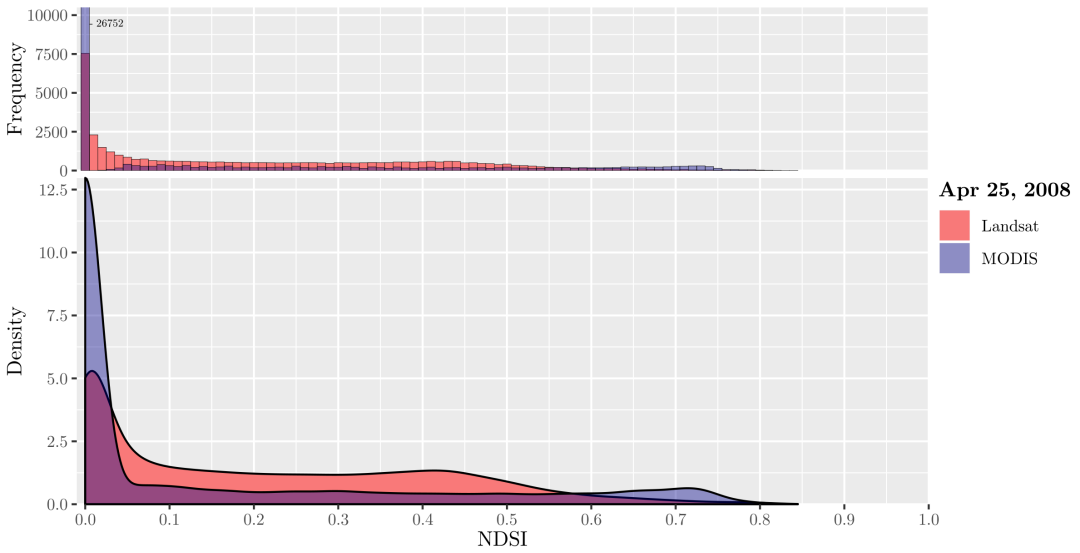

Figure 3.5: NDSI distributions of MODIS and the aggregated & resampled Landsat image on the 25th of April 2008.

Confusion matrix. The confusion matrix confirms that MODIS considerably underestimated low NDSI values. NDSI values up to class 2 (NDSI $= 0.2 \rightarrow 0.4$) were underestimated. The slight overestimation of high NDSI values, as indicated by the NDSI distributions (Fig. 3.5), is not apparent in the confusion matrix. The

overall accuracy of the MODIS image on the 25th of April 2008 with the chosen classification scheme of six classes was relatively low with only 25 %.

Table 3.1 displays the confusion matrix for the validation of MODIS with Landsat. The confusion matrix was created by introducing a classification scheme with six distinct classes and by using the Landsat image as the reference data set. The Landsat image is, thus, regarded as the actual truth. Results of the confusion matrix vary depending on the classification scheme. The here applied scheme with six classes, including a class 0, which solely contains NDSI of 0, led to an overall accuracy of 25 %. In other words, only 25 % of the cells were correctly classified.

The confusion matrix confirms that low NDSI values were underestimated by MODIS. This is indicated by the results of the confusion matrix for class 0 (NDSI = 0) and class 1 (NDSI = $0 \rightarrow 0.2$). MODIS classified 26218 grid cells as class 0, but only 2827 of these grid cells were actually class 0 (with 2898 grid cells in total whose NDSI = 0). Most of the grid cells that MODIS classified as 0 were actually class 1, and a substantial amount of cells were even class 2 or 3. This is reflected in the low user accuracy of 11 % of class 0: only 11 % of the cells that MODIS classified as 0 were actually class 0 (error of commission = 89 %). At the same time the high producer accuracy of 98 % of class 0 – meaning that 98 % of all cells that truly were class 0 were correctly classified as 0 – indicates, that there was no substantial concurrent overestimation of class 0 (error of omission = 2 %). Thus, MODIS considerably overestimated class 0 (NDSI = 0), because it underestimated or rather failed to detect low NDSI values of mainly class 1 and 2. Moreover, MODIS considerably underestimated the NDSI up to class 2, which can be seen by comparing the different rows of the classes 1 and 2 columns from the Landsat reference (Tab. 3.1).

The confusion matrix does not confirm the slight overestimation of high NDSI values, which was observed in the NDSI distributions (Fig. 3.5). Conversely, a slight underestimation is visible: MODIS falsely classified most of the 58 class 5 grid cells as class 4, while only overestimating 32 grid cells with lower NDSI as class 5. However, the small sample size in combination with the chosen classification scheme does not allow for reliable conclusions in this regard.

Table 3.1: Confusion Matrix for the 25th of April 2008. The confusion matrix was created by introducing a classification scheme of six classes: class 0 (NDSI = 0), class 1 (NDSI = 0 → 0.2), class 2 (NDSI = 0.2 → 0.4), class 3 (NDSI = 0.4 → 0.6), class 4 (NDSI = 0.6 → 0.8) and class 5 (NDSI = 0.8 → 1). Individual values within the matrix indicate the number of grid cells with the respective class combination of MODIS and Landsat. Grid cells, which were correctly classified, were assigned to the same class by MODIS and Landsat (e.g. row 0 and column 0).

		Landsat (reference)							
		0	1	2	3	4	5	$\sum$	user acc. [%]
MODIS	0	2827	17036	5086	1269	0	0	26218	11
	1	43	2101	1790	539	8	0	4481	47
	2	25	759	2106	1187	24	0	4101	51
	3	3	150	983	2142	200	2	3480	62
	4	0	23	205	2356	1199	56	3839	31
	5	0	0	0	31	1	0	32	0
	$\sum$	2898	20069	10170	7524	1432	58	42151	
	producer acc. [%]	98	10	21	28	84	0		**25**

3.2.3 Validation on the 11th of March 2009

Visual assessment. On the 11th of March 2009 (high snow cover), the agreement between MODIS and Landsat was much better than on the 25th of April 2008 (sparse snow cover). The majority of grid cells differed by less than ±0.05. Differences between MODIS and Landsat occurred mostly in areas with heterogeneous snow cover, where they could still amount up to ±0.6. Furthermore, on the 11th of March 2009 areas with differing grid cells were far more fragmented than on the 25th of April 2008.

In the same way like for the 25th of April 2008, the MODIS image on the 11th of March 2009 is contrasted with the respective Landsat images in figure 3.6. The 11th of March 2009 was a day with comparatively high snow cover. In contrast to the 25th of April 2008, most grid cells had high NDSI values. In both, MODIS and Landsat, only the northeast of the validation area had low NDSI values (Fig. 3.6). Like before, detail in the high resolution Landsat image is noticeably higher than in the other images, and many NA cells are present in the Landsat images due to cloud cover.

On the 11th of March 2009, 60 % of all grid cells of the validation area differed by less than ±0.05. The agreement between MODIS and Landsat is much better than on the 25th of April 2008. Furthermore, 27 % of all grid cells were underestimated (positive classes) and 12 % of the cells were overestimated (negative classes).

In contrast to the 25th of April 2008, changes between MODIS and Landsat were more fragmented on the 11th of March 2009 (Fig. 3.6d). While on the

25th of April 2008 larger coherent areas with differences are recognizable (Fig. 3.4d), such areas are comparatively small on the 11th of March 2009 (Fig. 3.6d). Furthermore, differences between MODIS and Landsat on the 11th of March 2009 occurred mainly in areas with spatially very heterogeneous snow cover (Fig. 3.6). Nonetheless, grid cell differences could still amount up to ±0.6 (Fig. 3.6d).

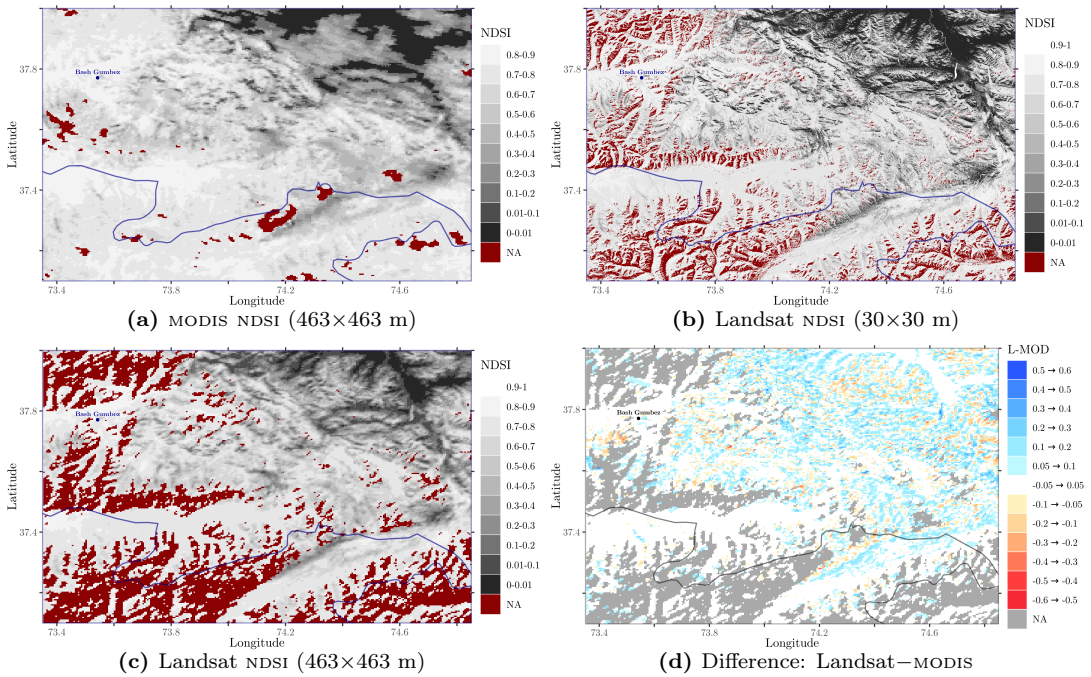

(a) MODIS NDSI (463×463 m) **(b)** Landsat NDSI (30×30 m)

(c) Landsat NDSI (463×463 m) **(d)** Difference: Landsat−MODIS

Figure 3.6: Visual comparison of MODIS and Landsat on the 11th of March 2009. The NDSI of MODIS (a) is illustrated along with the NDSI of the high resolution Landsat image (b) and the aggregated & resampled Landsat image (c). The difference between MODIS and the aggregated & resampled Landsat image is illustrated in (d).

NDSI distributions. The results of the NDSI distributions on the 11th of March 2009 confirm that MODIS underestimated low NDSI values, and slightly overestimated high NDSI values.

Figure 3.7 illustrates the distribution of NDSI values in the validation area for the 11th of March 2009. Similar to the 25th of April 2008, figure 3.7 also indicates that the applied MODIS data set underestimated lower NDSI values, and overestimated high NDSI values. In particular the very low NDSI values were often not detected in MODIS and thus 0. The number of grid cells with NDSI values of medium magnitude were fairly similar in MODIS and Landsat. In the higher NDSI range, MODIS tended to overestimate the NDSI values.

Confusion matrix. The confusion matrix confirms the much better agreement of MODIS and Landsat on the 11th of March 2009 compared to the 25th of April

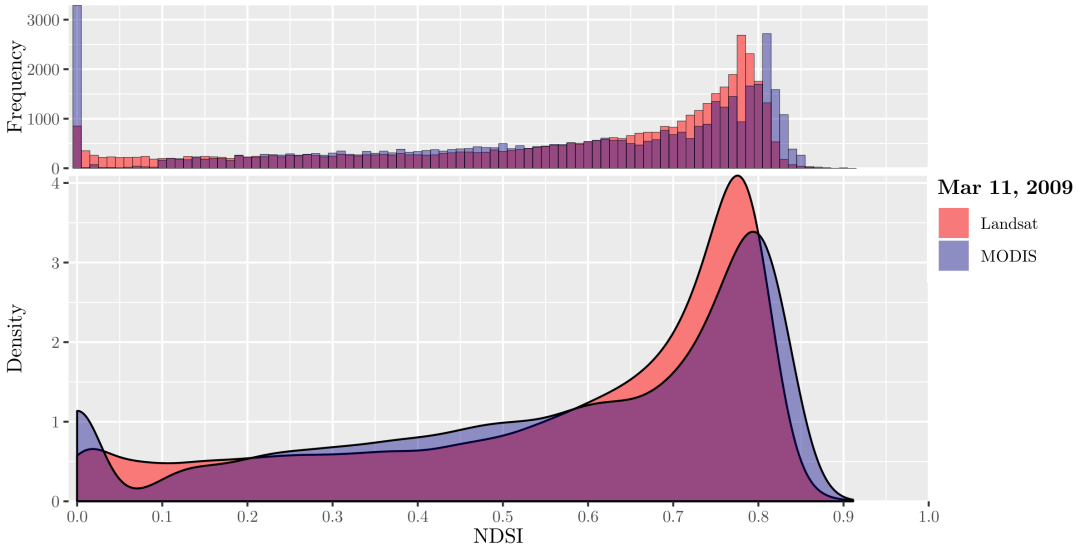

Figure 3.7: NDSI distributions of MODIS and the aggregated & resampled Landsat image on the 11th of March 2009.

2008. The better agreement is reflected in the higher overall accuracy of 65 %. The confusion matrix also confirms the underestimation of low NDSI values and overestimation of high NDSI values in MODIS. In this regard, the underestimation is more apparent than the overestimation.

Table 3.2 displays the confusion matrix for the 11th of March 2009. To create the confusion matrix, the same classification scheme was applied as for the 25th of April 2008. On the 11th of March 2009, MODIS agreed fairly well with the Landsat reference data set. The agreement between MODIS and Landsat is clearly better than on the 25th of April 2008, as reflected by the higher overall accuracy of 65 % (Tab. 3.2).

Similar to 2008, the underestimation of low NDSI values in MODIS is confirmed. The results from class 0 and class 1 both reflect the results of the 25th of April 2008: MODIS overestimated class 0 to the detriment of class 1. Class 0 is characterized by a very low user accuracy of 4 % due to MODIS falsely classifying many class 1 cells as class 0. At the same time the producer accuracy of class 0 is very high (99 %), indicating that there was no substantial overestimation of class 0. On the other hand, the producer accuracy of class 1 is fairly low (24 %) because of the many misclassifications as class 0. Contrarily to the 25th of April 2008, however, the underestimation of low NDSI values is not as apparent as in 2008, since the sample size of grid cells with low NDSI values was smaller. Furthermore, no substantial underestimation of NDSI values in class 2 is indicated on the 11th of March 2009.

The slight overestimation of high NDSI values is, in contrast to 2008, confirmed on the 11th of March 2009. A substantial amount of grid cells, which truly were

class 4, were falsely classified as class 5 in MODIS (Tab. 3.2). In addition, only comparatively few grid cells of class 5 were falsely classified as class 4 or lower (Tab. 3.2). As the net result, class 5 was clearly overestimated. Hence, this illustrates that MODIS overestimated high NDSI values.

Table 3.2: Confusion Matrix for the 11th of March 2009. The confusion matrix was created by introducing a classification scheme of six classes: class 0 (NDSI = 0), class 1 (NDSI = 0 → 0.2), class 2 (NDSI = 0.2 → 0.4), class 3 (NDSI = 0.4 → 0.6), class 4 (NDSI = 0.6 → 0.8) and class 5 (NDSI = 0.8 → 1). Individual values within the matrix indicate the number of grid cells with the respective class combination of MODIS and Landsat. Grid cells, which were correctly classified, were assigned to the same class by MODIS and Landsat (e.g. row 0 and column 0).

		Landsat (reference)							
		0	1	2	3	4	5	$\sum$	user acc. [%]
MODIS	0	146	2958	179	4	0	0	3287	4
	1	1	1236	870	114	3	0	2224	56
	2	0	885	3170	1729	135	1	5920	54
	3	0	63	918	4712	2872	4	8569	55
	4	0	2	51	965	15003	727	16748	90
	5	0	0	0	1	4587	2323	6911	34
	$\sum$	147	5144	5188	7525	22600	3055	43659	
	producer acc. [%]	99	24	61	63	66	76		**61**

3.3 Snow Cover Analysis

The results of the snow cover analysis are structured as follows: the results of the snow cover extent (SCE) analysis are presented first, followed by the results of the snow cover duration (SCD) analysis. In each case, the results were subdivided in *overall*, *regional* and *cell* results, analog to the description in section 2.3.2. *Overall* represents results regarding the entire study area as a whole. *Regional* refers to cell wise results of the whole study area that are illustrated with maps. The category *cell* refers to results of a singular cell that was analyzed in more detail. Within a category, typically an overview of the mean conditions is followed by the results of a trend analysis.

While the snow cover duration (SCD) is directly specified as SCD in days per time period (e.g. days per year: d/y), the results of the snow cover extent (SCE) exclusively use the fractional snow cover (FSC) – the fraction of a certain area that is covered by snow in percent – as a measure for the SCE.

3.3.1 Snow cover extent (SCE)

a. Overall results

Mean seasonal cycle. The study area is characterized by a pronounced seasonal cycle in FSC and CCE. The snow season usually started in September/October and major thaw of snow began in March/April.

Figure 3.8 shows the daily FSC and CCE of the entire study area averaged over the whole period from 2001 to 2018. Thus, figure 3.8 illustrates the mean seasonal cycle of the FSC and CCE for the entire study area. It can be seen that within the Pamirs the snow covered area followed a pronounced seasonal cycle (Fig. 3.8). The mean snow covered area varied from up to 80 % (12th Feb) coverage in winter to only 8 % (23rd Aug) in summer. During the year, the mean FSC varied from 75 % in winter over 58 % in spring and 15 % in summer to 30 % in fall. The overall mean FSC of the study area during the period from 2001 to 2018 was 45 %. The substantial increase in FSC in September/October indicates the beginning of the snow season (Fig. 3.8). Major thaw of snow typically started in March/April, indicated by the noticeably decrease of FSC during these months (Fig: 3.8).

The CCE followed a similar seasonal cycle like the FSC: the maximum CCE lay within February with nearly 84 % (5th Feb) cloud coverage on average, while the minimum CCE lay within September with about 9 % (10th Sep). During the year, the mean CCE varied from 69 % in winter over 56 % in spring and 32 % in summer to 38 % in fall. The overall mean CCE is 49 %. Compared to the FSC, the annual course of the CCE was not as pronounced (Fig. 3.8). This is reflected in the lower standard deviation of the CCE of 17 %, compared to 26 % for the FSC.

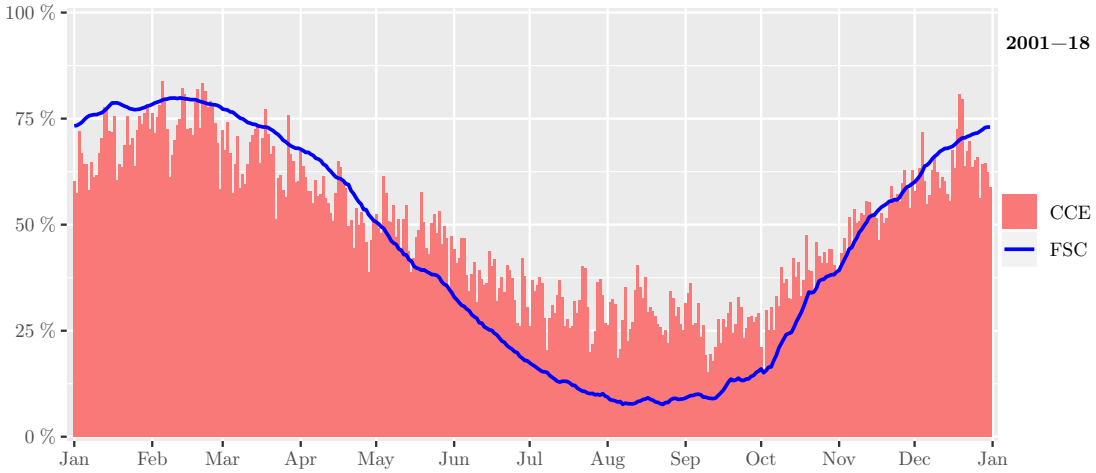

Figure 3.8: Mean seasonal cycle of the FSC and CCE for the study area during 2001 to 2018. The blue line and the red bars indicate the mean daily FSC and CCE.

Trend (daily). The trend analysis of the daily FSC time series from 2001 to 2018 indicates a slight decreasing trend of −0.17 % FSC per year across the Pamirs.

Figure 3.9 illustrates the results of the trend analysis for the daily FSC of the entire study area. The black graph at the top represents the FSC time series. The blue graphs in the middle represent the seasonal and trend components. The red graph at the bottom indicates the remainder of the decomposition with the linear trend component. The linear model indicates a slight negative trend of −0.17 % per year. Over all 18 years, this trend would result in a total decrease of −3.1 % FSC. The moving average (weak blue line) reveals time periods with a high/low snow coverage. Snow seasons with comparatively high snow coverage were 2004/05, 2009/10 and 2011/12, while the snow seasons 2007/08, 2010/11 and 2017/18 had comparably little snow (Fig. 3.9). The only slowly alternating curve of the remainder component indicates that there is still significant autocorrelation present (Fig. 3.9). This is confirmed in figure 3.10a, which illustrates the autocorrelation of the daily FSC without the seasonal component. Due to the present autocorrelation, no reliable statement on the trend significance of the daily trend analysis can be made.

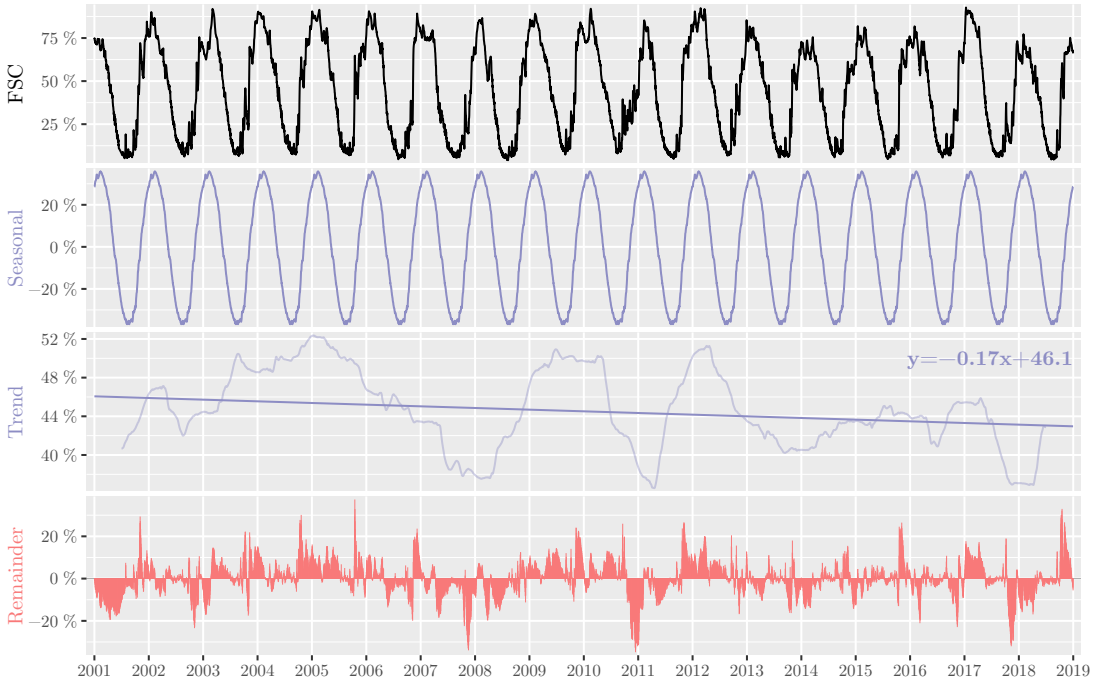

Figure 3.9: Trend analysis of the daily FSC from 2001 to 2018 for the entire study area. The black graph at the top illustrates the original FSC time series. This time series was then decomposed into a seasonal component and a trend component (both blue) as well as a remainder component (red). Both, the decomposition with a linear trend (strong blue line) and the decomposition with a moving average (weak blue line), are indicated. The equation next to the trend graphs belongs to the linear trend and refers to annual time steps. The displayed remainder component represents the residuals of the linear model.

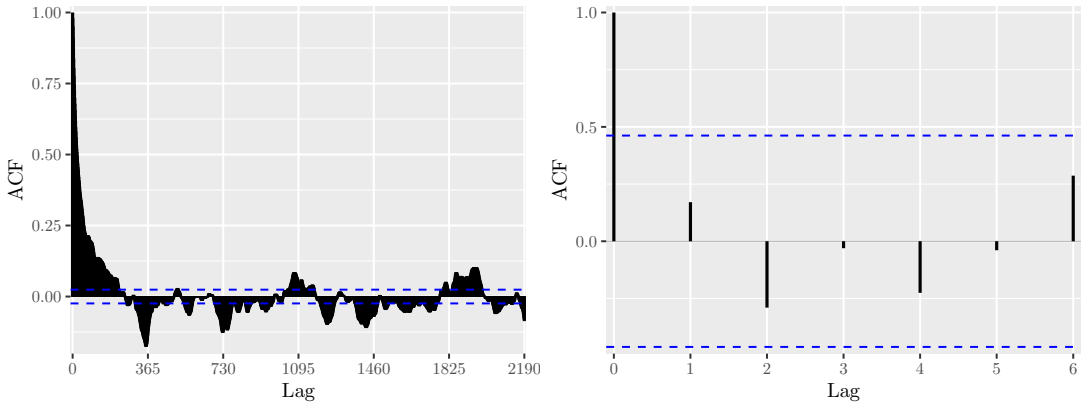

(a) Daily FSC time series **(b)** Mean annual FSC time series

Figure 3.10: Autocorrelation of the daily (a) and mean annual (b) FSC time series from 2001 to 2018. The black bars indicate the autocorrelation of the for the respective lag. The dashed blue line indicate the 95 % confidence interval.

Trend (mean). The slight negative trend in annual FSC for the entire study area was not significant. Negative trends were found in all seasons, with the strongest decrease in winter. The trends for spring, summer and fall were all not significant. The trend in winter, however, was weakly significant.

Figure 3.11 illustrates the trend of the mean annual FSC from 2001 to 2018 for the entire study area. According to the linear trend, the mean annual FSC has decreased by about 3 %. Contrary to the trend analysis of the daily FSC time series, the change between individual years is more apparent. Noteworthy is the year 2007, which had a considerable lower FSC than other years.

In contrast to the trend analysis of the daily FSC, the mean FSC showed no significant autocorrelation (Fig. 3.10b). Therefore, a meaningful assessment of the trend significance was possible. Both, ANOVA (p-value: 0.29) and MK (p-value: 0.44), indicate that the annual trend is not significant.

Figure 3.12 illustrates the seasonal trend analysis. Trends were negative throughout all seasons (Fig. 3.12). The trends in spring, summer and fall were all only minor. In winter, however, a noteworthy trend of -0.67 % per year was detected. This trend would lead to a total decrease of about 11 % FSC from winter 2001/02 to 2017/18. Trends for spring (ANOVA: 0.91, MK: 0.88), summer (ANOVA: 0.84, MK: 0.60) and fall (ANOVA: 0.59, MK: 0.70) were all not significant. The negative trend in winter was weakly significant (ANOVA: 0.059, MK: 0.091).

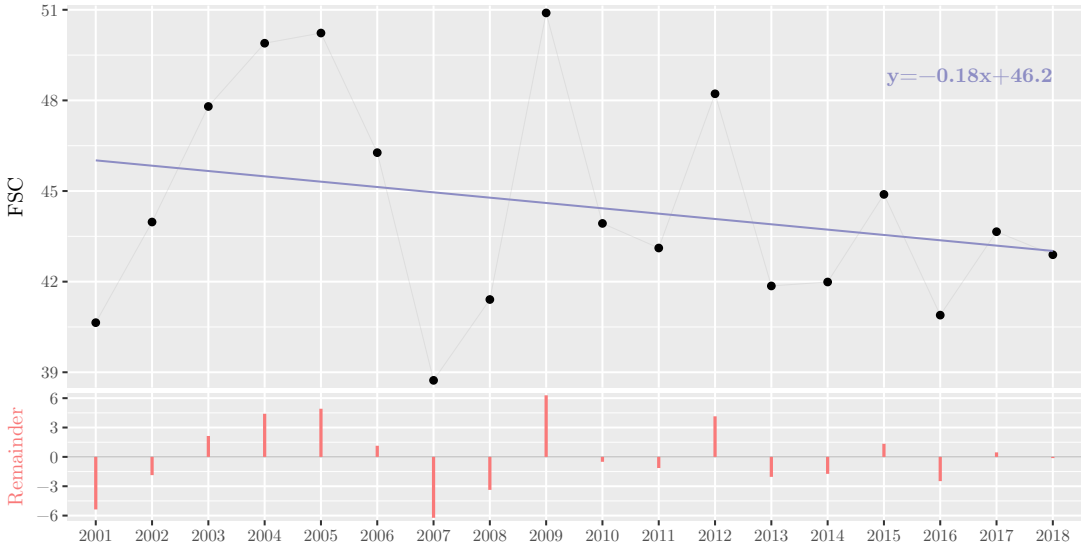

Figure 3.11: Trend analysis of the mean annual FSC for the entire study area. The black dots mark the mean FSC of the respective years. The blue line represents the linear trend. The equation of the linear model is indicated in the upper right corner. The red bars represent the residuals of the linear model.

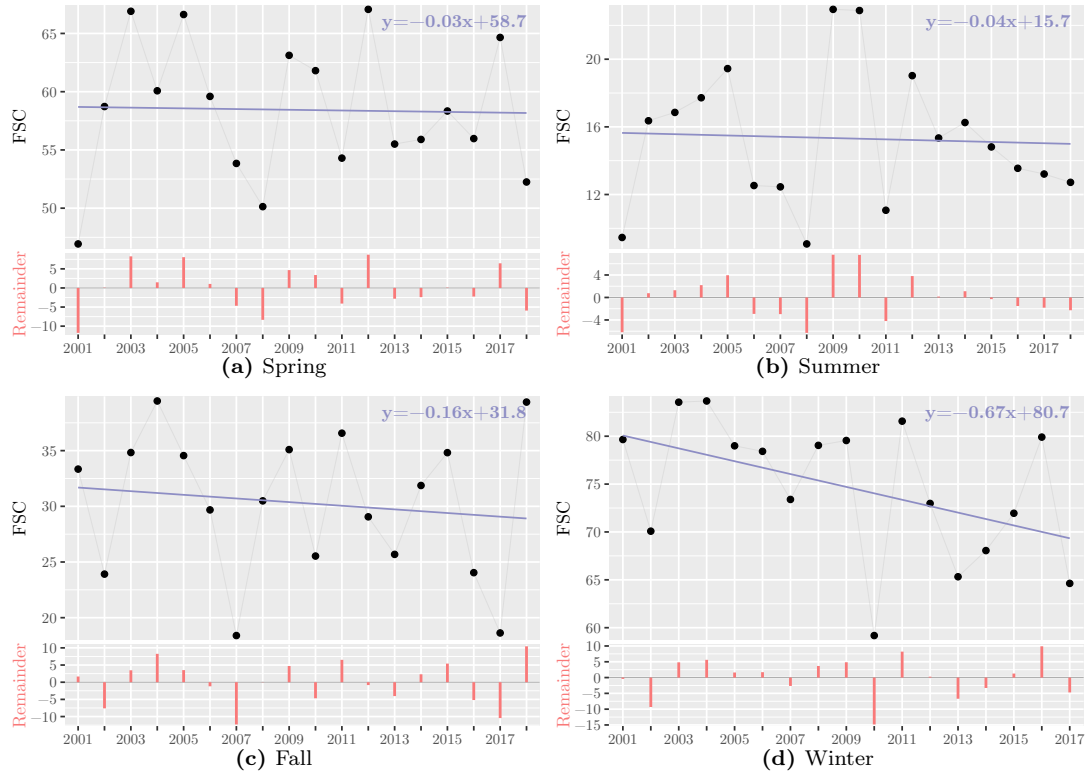

Figure 3.12: Trend analysis of the mean seasonal FSC for the entire study area. The black dots mark the mean FSC of the respective seasons. The blue line represents the linear trend. The equation of the linear model is indicated in the upper right corner. The red bars represent the residuals of the linear model.

b. Regional results

Overall mean. The mean FSC patterns in the Pamirs clearly reflect altitude differences. Furthermore, patterns indicate a difference between higher snow coverage in the Western Pamirs and lower snow coverage in the Eastern Pamirs.

Figure 3.13 displays the overall mean FSC for each grid cell in the study area. The effect of a location's altitude is clearly visible. By comparing figure 3.13 with the topographic map (Fig. 1.2), it is apparent that areas with high FSC values generally represent mountain ridges – this is particularly true for summer (Fig. A.3b). Moreover, large valleys can be identified without much effort (Fig. 3.13). In addition, the figure 3.13 indicates a general decrease in mean FSC from west to east, reflecting the precipitation difference between the Western and Eastern Pamirs. The eastern part of Tajikistan and most of the areas within China, especially, had a noticeable lower mean FSC then most of the rest of the study area. Also noteworthy to mention is that Lake Karakul including its island can be discerned in the northeast of Tajikistan. The lake area had a noticeably higher mean FSC then the surrounding areas. Apart from Lake Karakul, other lakes are difficult to identify.

In the appendix a figure with the seasonal overall mean FSC is included (Fig. A.3). When comparing the different seasons, it is clearly visible that winter had the highest amount of snow cover followed by spring, fall and then summer (Fig. A.3). In summer and fall differences in snow cover were mainly related to differences in altitudes, since most of the snow is located on the mountain ridges (Fig. A.3b). In winter and spring, however, the west-east difference is clearly visible, with higher snow coverage in the west (Fig. A.3). Also interesting is the development of the FSC on Lake Karakul throughout the seasons. In spring, summer and winter, Lake Karakul had a higher mean FSC than its surroundings (Fig. A.3). In fall, however, Lake Karakul had a lower mean FSC than the surrounding areas. In spring, the slightly lower mean FSC in the western part of the lake indicates that Lake Karakul typically thawed from west to east. Furthermore, the mean FSC in winter indicates that the lake typically froze from the east to west.

Trend. The regional trend results indicate a significant negative trend in FSC in the Eastern Pamirs, primarily in southeast Tajikistan. Although the majority of analyzed grid cells in the study area had trends close to 0, more than 80 % of the cells had a negative trend and about 10 % of the cells had a substantial negative trend of more than -0.5 % per year. Only 0.1 % of the grid cells had a substantial positive trend of more than $+0.5$ % per year. The general trend pattern was similar throughout the different seasons except in summer, where

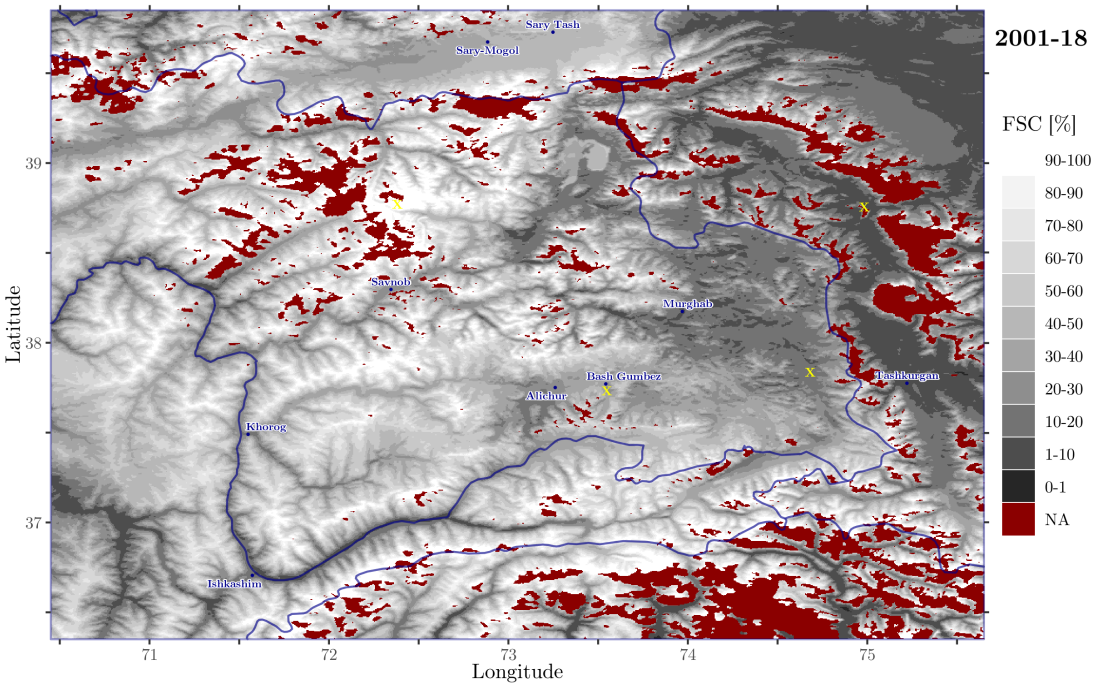

Figure 3.13: Map of the overall mean FSC in the study area from 2001 to 2018. Areas that were left out of the analysis are colored red. State borders and a selection of cities are indicated in blue. The yellow crosses mark individual grid cells that were further investigated.

no substantial trend occurred in the vast majority of the study area. In spring and fall, substantial positive and negative trends were visible, but the majority of the trends was not significant. In winter strong negative trends, especially in the Eastern Pamirs, were visible.

Figure 3.14 displays the results of the regional FSC trend analysis for the whole time period from 2001 to 2018. In the Eastern Pamirs, a large area in the southeast of Tajikistan as well as some areas in China had significant negative trends in the mean FSC (Fig. 3.14). Moreover, significant negative trends were also detected in the Bartang and Shakhdara valleys in the Western Pamirs and in the Alai mountain range. However, the majority of the areas with a significant negative trend lay within southeast Tajikistan and had a change rate of -1.5 to -1 % mean FSC per year (Fig. 3.14). Although 90 % of the grid cells had only trends of less than ± 0.5 % per year (Tab. 3.3), still 81 % of all analyzed cells had a negative trend. Furthermore, while only 0.1 % of the cells had a positive trend of more than $+0.5$ % per year, 10 % of the cells had a negative trend of more than -0.5 % per year, and 1.5 % of the cells had an considerable negative trend of more than -1 % per year (Tab. 3.3). Also noteworthy is the region around 74.98° E and 38.76° N in the Eastern Pamirs, north of Tashkurgan in China. In this region, significant positive trends were detected (Fig. 3.14).

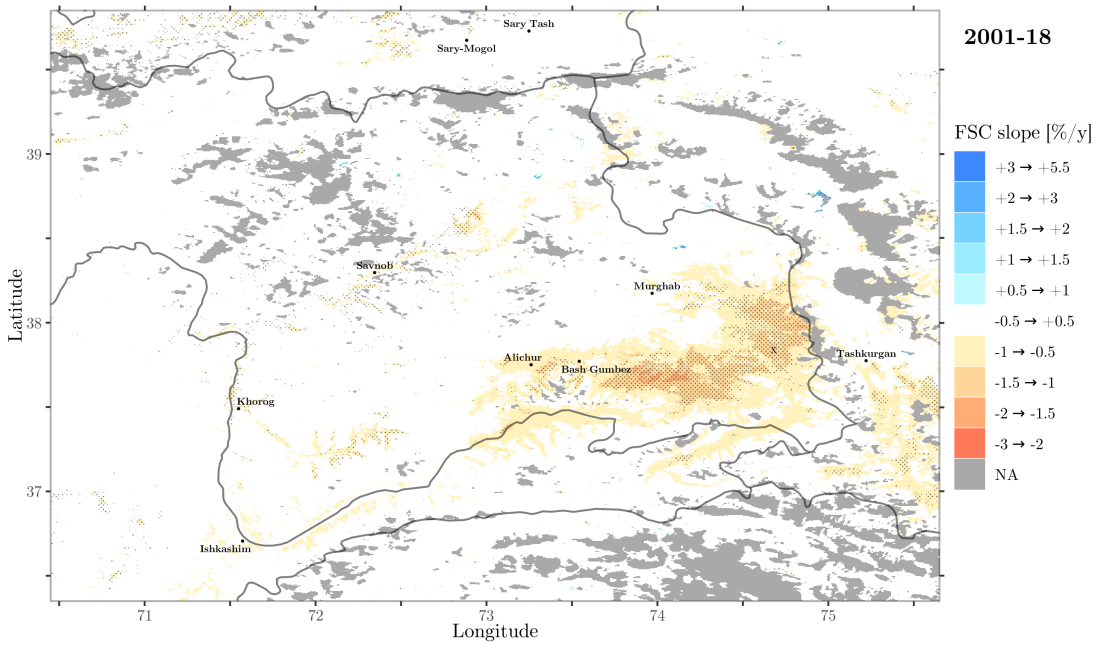

Figure 3.14: Map of the FSC trend from 2001 to 2018 in the study area. Areas that were left out of the analysis are colored gray. The annual change rate is indicated by the slope of the linear trend in colors from blue (positive) to red (negative). White areas were regarded as having no substantial trend. Areas with a significant trend of $p < 0.05$ (based on ANOVA), were marked with a black dot pattern. State borders and a selection of cities are indicated in blue. The individual cell 833289, which was further inspected, is marked with a black cross.

FSC trends for the study area varied depending on the season. In winter, the strongest trends occurred and trends were almost exclusively negative. In spring and fall, still considerable trends were observed and both positive and negative trends occurred. In summer, the vast majority of the study area had no substantial trend. In all seasons, except for spring, the majority of grid cells had a negative trend. Significant trends were almost exclusively negative. However, only in winter large areas had a significant trend. In general, regions with negative trends showed more or less a negative trend throughout all seasons except in summer.

In spring, both regions with negative and positive trends are visible (Fig. 3.15a). The general pattern is similar to the overall trend: the majority of cells had only small trends below ±0.5 %, but there were also considerable negative trends in the Eastern Pamirs, the Alai valley and along some valleys in the Western Pamirs (mainly along the Bartang valley around Savnob, the Gunt river northeast of Khorog and the Shakhdara river southeast of Khorog) (Fig. 3.15a). In contrast to the overall trend, however, there were only very few regions that had a significant trend. Trends in southeast Tajikistan were not significant in spring. An additional slight difference to the overall trend is a more extensive negative trend in the Alai around Sary-Mogol, with a few areas also showing a

significant negative trend. Also noteworthy is that in spring considerably more grid cells had a substantial positive trend than in the overall trend map or in other seasons (Fig. 3.15a, Tab. 3.3).

In summer, the vast majority of the study area had no substantial FSC trend (94 %, s. table 3.3). There were no larger areas with significant trends. In the mid-west of the study area, there were some regions with a substantial negative trend, which were not significant however. Overall, 60 % of all grid cells still had a negative trend in summer.

In fall, there was a significant negative trend in southeast Tajikistan, especially around Alichur and Murghab. In the Alai valley, there was a considerable positive trend, which was not significant. 66 % of the grid cells had a negative trend, and 18 % had a considerable negative trend of more than −0.5 % FSC per year. Similar to spring, the amount of grid cells with a substantial positive trend was considerably higher than in summer and winter (Tab. 3.3).

In winter, large parts of the study area, especially in the Eastern Pamirs, showed a significant negative trend. The main areas with a significant negative trend are the southeast of Tajikistan, the northern Alai, the Eastern Pamirs in China and the Shakhdara and Bartang river valleys. In southeast Tajikistan, there are even regions with a negative trend of more than −3 % mean FSC per year, resulting in a total decrease in mean FSC of more than −51 %.

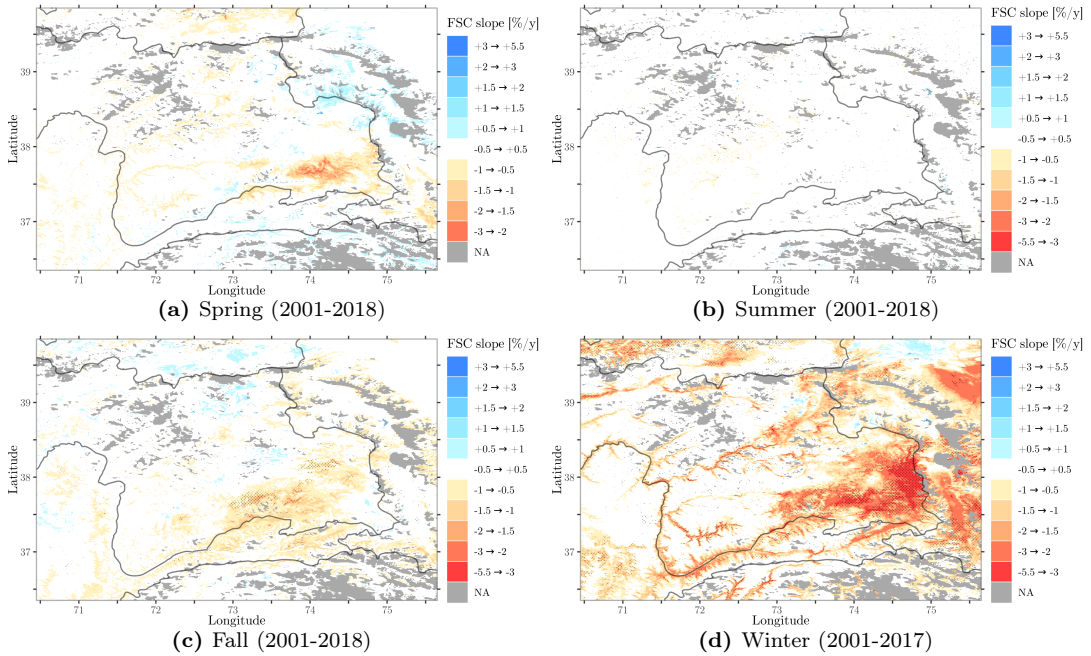

(a) Spring (2001-2018) **(b)** Summer (2001-2018)

(c) Fall (2001-2018) **(d)** Winter (2001-2017)

Figure 3.15: Map of the seasonal FSC trend in the study area. Areas that were left out of the analysis are colored gray. The annual change rate is indicated by the slope of the linear trend in colors from blue (positive) to red (negative). White areas were regarded as having no substantial trend. Areas with a significant trend of $p < 0.05$ (based on ANOVA), were marked with a black dot pattern.

Table 3.3: Grid cell distributions of the different trend classes for the overall and seasonal mean FSC trend maps. In the rows, the proportion of grid cells, which belong to the respective class is listed.

Class [%/y]	Overall [%]	Spring [%]	Summer [%]	Fall [%]	Winter [%]
$+3.0 \rightarrow +5.5$	0.00	0.00	0.00	0.00	0.00
$+2.0 \rightarrow +3.0$	0.00	0.01	0.00	0.00	0.01
$+1.5 \rightarrow +2.0$	0.01	0.01	0.01	0.01	0.01
$+1.0 \rightarrow +1.5$	0.01	0.16	0.02	0.04	0.04
$+0.5 \rightarrow +1.0$	0.06	3.35	0.24	2.20	0.71
$-0.5 \rightarrow +0.5$	90.02	86.89	98.70	80.23	52.70
$-1.0 \rightarrow -0.5$	8.46	7.89	1.02	15.03	18.15
$-1.5 \rightarrow -1.0$	1.36	1.23	0.02	2.34	12.69
$-2.0 \rightarrow -1.5$	0.08	0.38	0.00	0.14	7.98
$-3.0 \rightarrow -2.0$	0.00	0.08	0.00	0.00	6.43
$-5.5 \rightarrow -3.0$	0.00	0.00	0.00	0.00	1.28

c. Cell results

Trend (daily). The daily trend analysis results of grid cell 833289 indicate that high snow conditions in the snow seasons 2003/04 up to 2006/07 in combination with low snow conditions from 2012/13 to 2017/18 were the cause for the strong negative trends in southeast Tajikistan. Furthermore, the closer inspection of the grid cell revealed, that its daily FSC time series was characterized by rapid changes resulting in a spiking character of the time series.

In figure 3.16 the trend analysis for the grid cell 833289 is displayed. This particular grid cell is located in southeast Tajikistan, in a region where a significant negative overall trend was observed (Fig. 3.14). The overall FSC trend for the grid cell was -1.4 % per year, which is fairly high considering this leads to a decrease of -25 % for the whole time period from 2001 to 2018. The moving average of the trend analysis reveals that this strong trend was caused by high snow conditions in the snow seasons 2003/04 to 2006/07 in combination with low snow conditions from 2012/13 to 2017/18. Also noteworthy is the spiking character of the cells' daily FSC time series. In the daily FSC time series it is apparent that changes in FSC occurred rapidly (Fig. 3.16). The cell FSC appears to have peaked after snowfall events with values rapidly raising close to 100 %. Afterwards, FSC values either stayed high or plummeted. In general, snow cover changes happened therefore very swiftly in this grid cell.

Trend (mean). The high snow conditions in the years 2003 to 2006 can be seen in all seasons except for summer. In winter, the trend was very significant and the decisive factor for the overall significance of the trend. The results of the

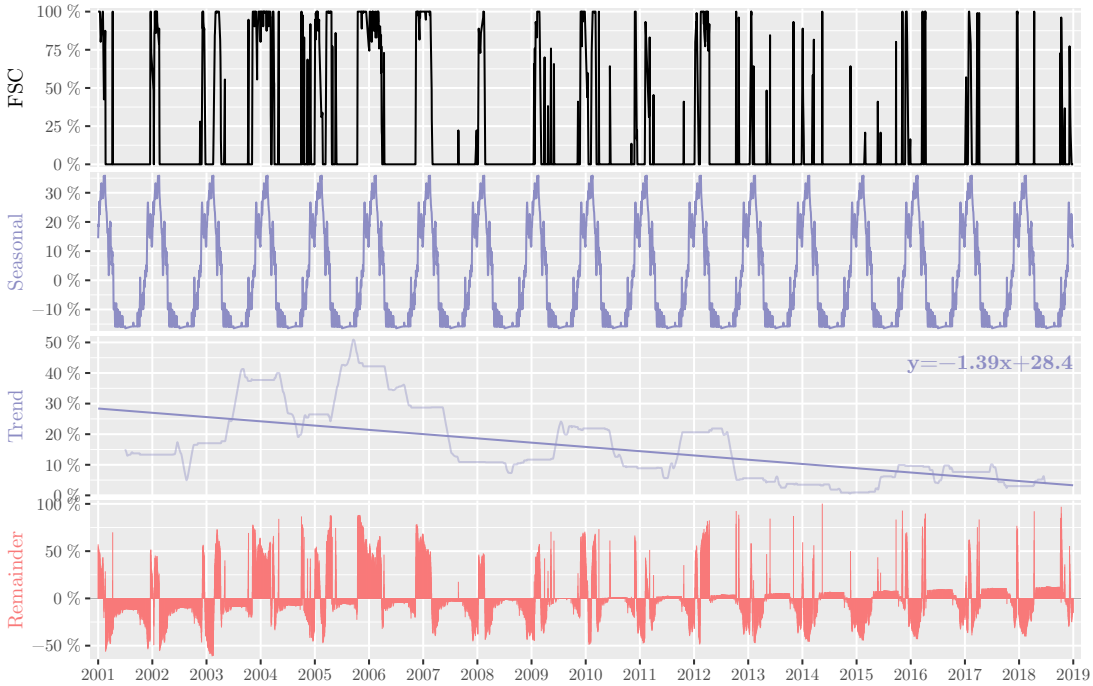

Figure 3.16: Trend analysis of the daily FSC from 2001 to 2018 for the grid cell 833289. The black graph at the top illustrates the cells' original FSC time series. This time series was then decomposed into a seasonal component and a trend component (both blue) as well as a remainder component (red). Both, the decomposition with a linear trend (strong blue line) and the decomposition with a moving average (weak blue line), are indicated. The equation next to the trend graphs belongs to the linear trend and refers to annual time steps. The displayed remainder component represents the residuals of the linear model.

trend analysis of summer indicate that in summer there was no trend detected, because the grid cell typically had no snow during summer.

The results of the trend analysis of the mean FSC of grid cell 833289 confirm the observations from the trend analysis of the cell's daily FSC: The strong negative trend was primarily caused by the years 2003 to 2006, which had high mean FSC values, and the years 2013 to 2018, which had a very low mean FSC values (Fig. 3.17). Autocorrelation for the mean FSC was not significant, and thus the trend significance was assessed. The trend of the mean annual FSC of grid cell 833289 was very significant: both ANOVA (0.003) and MK (0.005) yielded p-values below 0.01.

Results of the grid cell's seasonal trend analysis brought more insight into the results of the regional FSC trend analysis (Fig. 3.15d). While there was no trend in summer, the other seasons all showed a negative trend (Fig. 3.18). In winter, the trend was very significant (ANOVA: 0.003; MK: 0.0008) with an annual change rate of −4.2 %, which results in an overall FSC decrease of −71 % mean FSC in winter. The negative trends in spring (ANOVA: 0.28; MK: 0.79) and fall (ANOVA: 0.16; MK: 0.54) were not significant. Winter was, thus, likely the strongest driver

for the observed overall trend in southeast Tajikistan. In summer, no trend was observed, because of the low snow conditions (Fig. 3.18). At least in the close vicinity of grid cell 833289 there was likely usually no snow during the summer months.

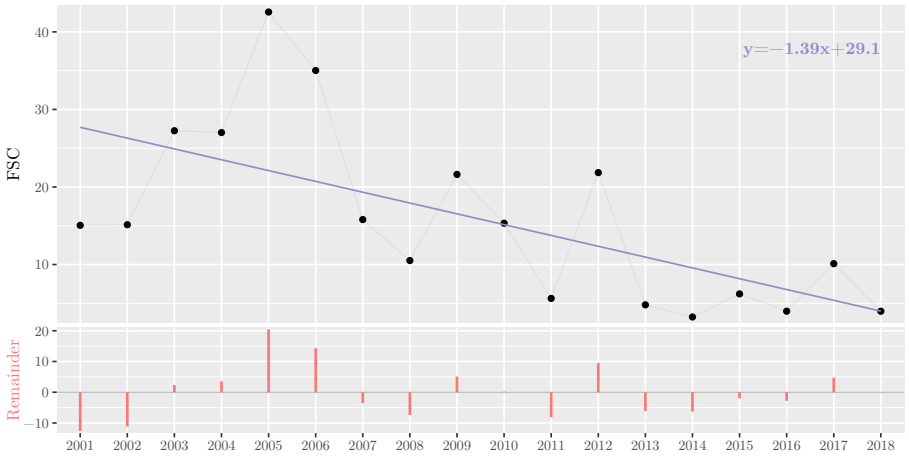

Figure 3.17: Trend analysis of the mean annual FSC from 2001 to 2018 for the drid cell 833289. The black dots mark the cells' mean FSC of the respective years. The blue line represents the linear trend. The equation of the linear model is indicated in the upper right corner. The red bars represent the residuals of the linear model.

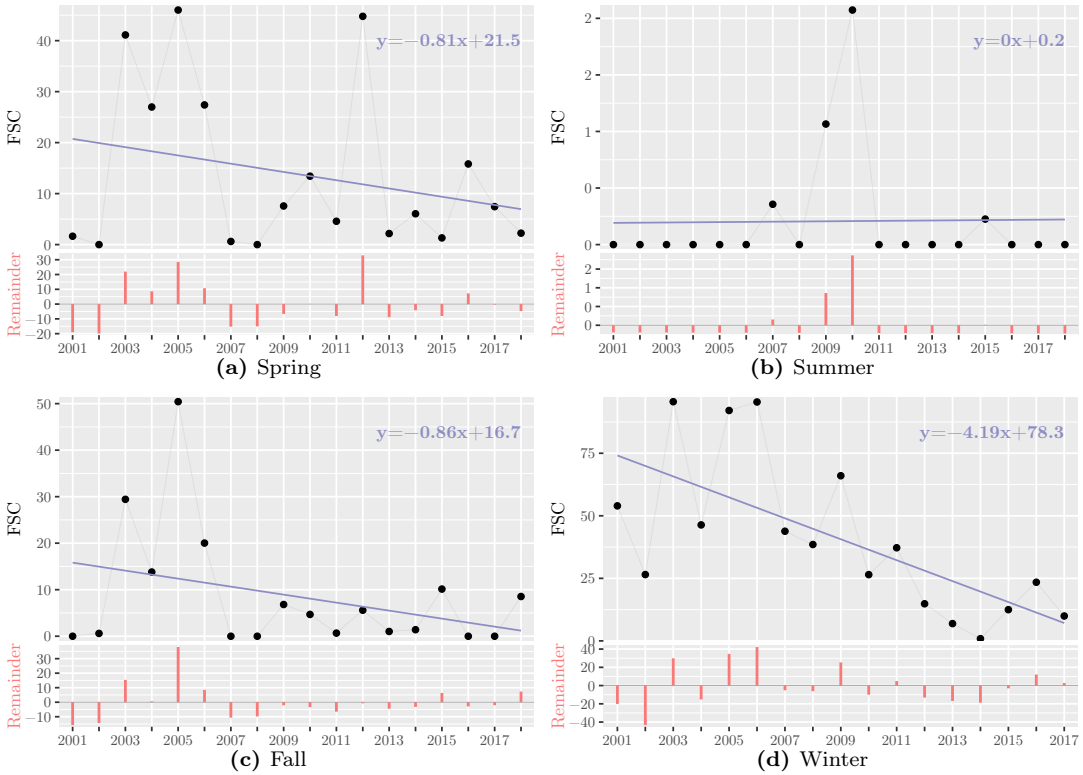

Figure 3.18: Trend analysis of the mean seasonal FSC for the grid cell 833289. The black dots mark the mean FSC of the respective seasons. The blue line represents the linear trend. The equation of the linear model is indicated in the upper right corner.

3.3.2 Snow cover duration (SCD)

a. Overall results

Results of the SCD trend analysis for the entire study area were very similar to the results of the mean FSC. The annual trend in SCD was negative, but not significant. Trends in the different seasons were not significant either, except for winter, which showed a weakly significant negative trend.

The SCD results were very similar to the mean FSC results. Differences between the overall SCD and mean FSC trend maps were only marginal. The respective figures were therefore only appended to this thesis (Fig. A.4, Fig. A.5).

The annual trend of the SCD of the entire study area was -0.66 days per year. The trend was not significant (ANOVA: 0.30; MK: 0.50). The trends of the different seasons were all negative (spring: -0.03 d/y; summer: -0.05 d/y; fall: -0.17 d/y; winter: -0.57 d/y) (Fig. A.5). While spring (ANOVA: 0.90; MK: 0.88), summer (ANOVA: 0.82; MK: 0.60) and fall (ANOVA: 0.56; MK: 0.65) were all not significant, the trend in winter (ANOVA: 0.05; MK: 0.06) was weakly significant.

b. Regional results

Overall mean. The regional results of the mean SCD maps of the study area strongly reflect the mean FSC results. Differences between the annual and seasonal mean SCD patterns and the mean FSC patterns were mainly marginal.

Similar to the overall changes, also the regional results for the overall mean SCD of the study area strongly resemble the mean FSC result (Fig. 3.19). The respective figures for the different seasons can be found in the appendix (Fig. A.6). Results indicate, that the Western Pamirs were generally longer covered with snow than the Eastern Pamirs (Fig. 3.19). In addition, like in for the mean FSC also altitude differences are clearly reflected in the mean SCD (Fig. 3.19). Seasonal results were also more or less equivalent (Fig. A.6). Differences between the mean FSC and the SCD can only be seen in detail. There are, for instance, some differences in the Alai valley, the northeastern part of the study area in China or the eastern part of Tajikistan (Fig. 3.19).

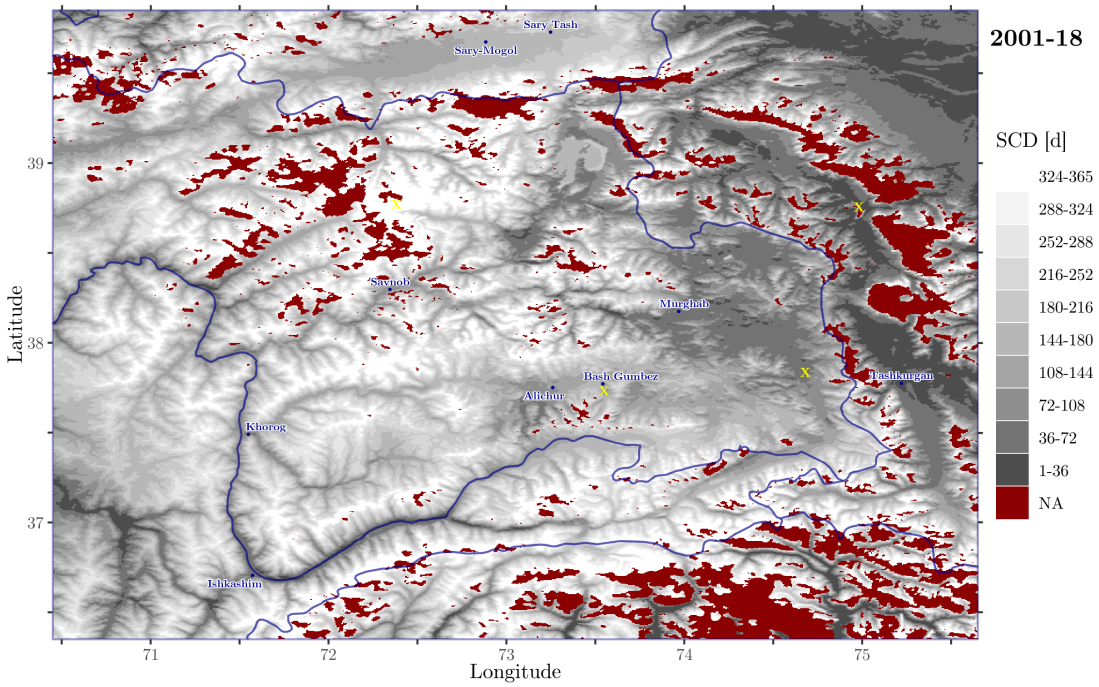

Figure 3.19: Map of the overall mean SCD in the study area. The SCD is displayed in colors from black to white. Areas that were left out of the analysis are colored red. State borders and a selection of cities are indicated in blue.

Trend. Similar to the previous results also the regional trend results strongly reflect the respective mean FSC results. The trend maps show a significant negative trend in SCD in southeast Tajikistan. In spring and fall the majority of the trends was not significant, although substantial trends are visible. In summer, there was no trend in the vast majority of the study area. Contrary, in winter there were strong negative trends, especially in the eastern part of the study area.

Only the trend map for the annual SCD is shown in figure 3.20. The trend results for the seasonal SCD analysis can be found in the appendix (Fig. A.7, Tab. A.1). While the general pattern strongly reflects the annual mean FSC trend map's pattern, the different classes also visualize smaller trends that were not considered substantial in the classification of the mean FSC trend (Fig. 3.20). This resulted in larger areas that indicate considerable trends with a color.

This allows for one noteworthy observation in the Western Pamirs: in spring, negative trends occurred mainly along the valleys as described previously for the mean FSC results (Fig. A.7a). In summer, negative trends "moved up" in altitude and are therefore more or less exclusively on mountain ridges, where there is still snow present during summer (Fig. A.7b).

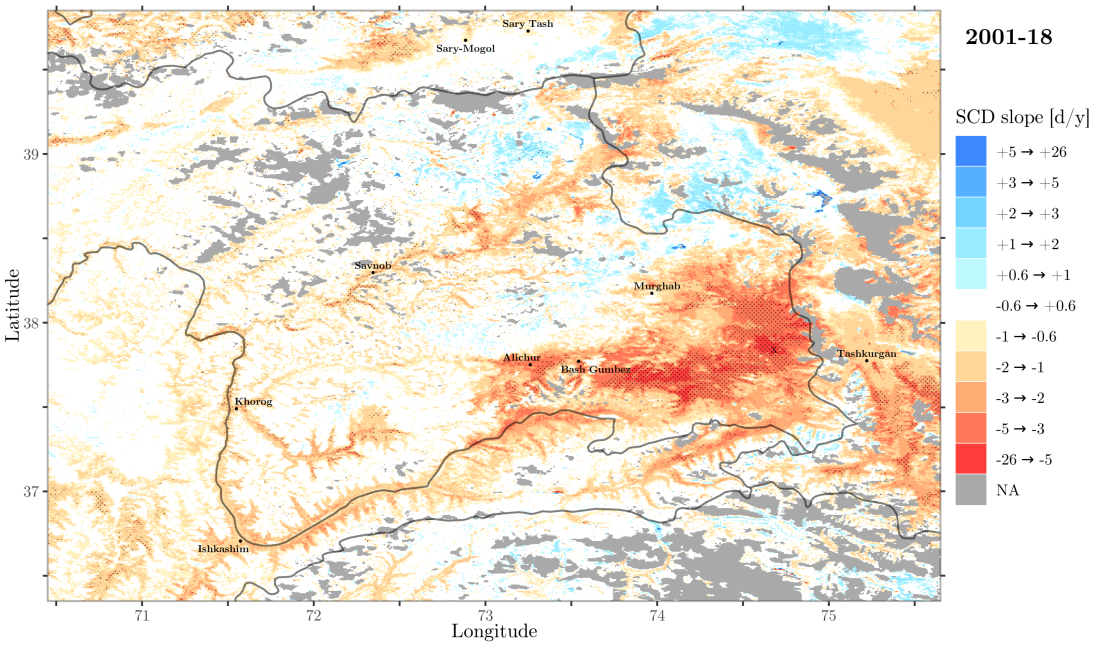

Figure 3.20: Map of the annual SCD trend from 2001 to 2018 in the study area. Areas that were left out of the analysis are colored gray. The annual change rate is indicated by the slope of the linear trend in colors from blue (positive) to red (negative). White areas were regarded as having no substantial trend. Areas with a significant trend of $p < 0.05$ (based on ANOVA), were marked with a black dot pattern. State borders and a selection of cities are indicated in blue. The individual cell 833289, which was further inspected, is marked with a black cross.

c. Cell results

SCD results of the grid cell 833289 were not included since they were almost identical to the mean FSC results. Thus, indicating once more that the mean FSC and SCD in the region were strongly related.

3.4 Summary

The brief analysis of cloud cover patterns show that cloud cover in the study area was very high: on average a cell was covered with clouds nearly half of the time. Furthermore, patterns in CCD clearly reflect altitude differences.

The results of the validation demonstrate that the gap filled MODIS images mapped the general distribution of snow fairly well. Nonetheless, considerable differences were still present on both validation days. While the accuracy of the applied MODIS data set was high on the 11th of March 2009, larger areas with considerable differences were present on the 25th of April 2008. Furthermore, results indicate that the gap filled MODIS data set considerably underestimated low NDSI values, and slightly overestimated high NDSI values.

Results of the snow cover analysis demonstrate that both the SCE and the SCD have generally decreased in the study area from 2001 to 2018. Results of the SCE and SCD analysis were very similar, and mostly even equivalent: differences between the mean FSC and the SCD could only be seen in detail and were mostly marginal. In the subsequent sections, SCE and SCD are, thus, collectively referred to by the acronym SC (snow cover) to enhance readability. It is important to note that the acronym SC does only refer to SCE and SCD and does not include other snow metrics.

Changes in SC over the past 18 years depended on the region and season under consideration. The overall change of the entire study area was negative, but not significant. Seasonal trends of the entire study area were also all negative, but not significant except for winter, which was weakly significant. Changes within the study area were mostly negative. Over 80 % of the grid cells ($\sim$ 80 % of the study area) showed a negative trend in FSC, and fairly large areas, especially in the Eastern Pamirs, showed significant negative trends. In contrast, areas with a significant positive trend were marginal across the Pamirs. As indicated by the results of the entire study area, negative trends within the study area were also dominant in all seasons, and by far strongest in winter, where large areas showed significant negative trends.

4 Discussion

4.1 Validation

4.1.1 Accuracy of MOD10A1

The validation results demonstrate that the applied MODIS snow cover product mapped the general distribution of snow reasonably well. However, especially on the 25th of April 2008 considerable differences between MODIS and Landsat were still present. Furthermore, on both days the respective overall accuracies were fairly low with 25 % in 2008 and 65 % in 2009.

While the overall accuracies do represent the agreement between MODIS and Landsat, the actual numbers have to be treated with care. To be able to assess the accuracy with a confusion matrix, the cardinal scaled NDSI values had to be transferred to an ordinal scale. This was done by simply assigning values to different classes that represent certain NDSI ranges. The overall accuracy can, thus, be altered by applying a different classification scheme with a different number of classes or a different range for individual classes. Furthermore, the overall accuracy only yields information about how many of the cells were correctly classified. In contrast, it does not include information about how severe misclassifications were. Hence, the actual value of the overall accuracy is only limited meaningful in this study. Nonetheless, with the applied classification scheme, the values do still give an idea of how good the performance of the MODIS snow cover product was.

Although the MODIS snow cover product can map snow reasonably well in mountainous terrain, the accuracy is still affected (Crawford, 2015; Hall and Riggs, 2007). Complex atmospheric and illumination conditions can, for instance, introduce considerable differences between images (Crawford, 2015).

In this study, cloud contaminated cells were completely excluded from the validation, so the applied gap filling did not influence the validation results. The main reason for the in part strong deviations between MODIS and Landsat is the observed over-/underestimation of high/low NDSI values in the MODIS data set. In particular the underestimation of low NDSI values did considerably contribute to the very low overall accuracy in spring 2008. Another factor that could affect

validation results is a difference in the recording time of the satellite images on the respective validation dates. The time of recording of MODIS and Landsat can potentially differ by approximately 30-45 min, where changes in NDSI are quite possible in spring (Crawford, 2015). Such short term changes in NDSI could, for instance, be caused by changes in atmospheric or illumination conditions and transient snow fall (Crawford, 2015). Nonetheless, transient snow fall, which has the potential to introduce major disagreement between images, is unlikely to have happened, since days with comparatively low cloud cover had been selected and precipitation in the validation area is generally low. Other factors that cause differences are resampling errors and noise in the data retrival, which can be amplified to extreme NDSI values (Crawford, 2015; Lunetta et al., 1991; Slater, 1985).

In summary, the low overall accuracies are only limited meaningful and should not be overstated. The accuracy should rather be evaluated based on the overall results of the validation, which indicate a reasonable accuracy. While the retrival of snow in mountain areas is complex and various factors can lead to differences between MODIS and Landsat, the observed differences are likely predominantly caused by the over-/underestimation of high/low NDSI values.

4.1.2 Over- & underestimation of NDSI values

The validation results indicate, that the applied MODIS snow cover product substantially underestimated low NDSI values, and also slightly overestimated high NDSI values.

Both, the over- and underestimation of snow in certain conditions, are known problems in MODIS (Crawford, 2015; Hall and Riggs, 2007). MODIS overestimates the FSC in mountain areas, and partly fails to detect snow in conditions with sparse snow coverage (Crawford, 2015; Hall and Riggs, 2007).

The underestimation of low NDSI values was most prominent on the validation day in spring 2008. The 25th of April 2008 was a day with only low snow cover in the validation area. This is illustrated by the large number of cells that belonged to class 1 ($0 < \text{NDSI} \leq 0.2$), which represents snow cover of up to 28 %. On this day MODIS failed to detect low NDSI values in many cases. This substantial underestimation of NDSI values on the 25th of April 2008 led to the considerable performance difference of MODIS on the two validation dates. The detection issues in conditions with sparse snow are likely a result of MODIS's comparatively low spatial resolution, that leads to strongly mixed cell signals. In addition, snow-cloud confusion is also often associated with such conditions in MODIS (Hall and Riggs, 2007).

The overestimation of high NDSI values was most prominent on the second

validation day in spring 2009. In contrast to the first validation day, the 11th of March 2009 was a day with high snow cover in the validation area. On this day, the majority of cells belonged to class 4 ($0.6 < \text{NDSI} \leq 0.8$), which represented snow cover between 86 and 100 %. While MODIS generally performed very well, a slight overestimation of high NDSI values was visible. Crawford (2015) found a very similar overestimation of high NDSI values in mountainous terrain. In the study, Crawford (2015) mentions spatial resolution distortion and differences in solar illumination based on the respective viewing geometry and angle as well as Lambertian scattering and physiographic snow cover variability as possible causes.

In conclusion, the accuracy of the applied MODIS data set is likely considerably lower for conditions with sparse snow cover. Furthermore, a slight systematic overestimation of high NDSI values, like in the study of Crawford (2015), is also likely present throughout the analyzed time period. Possible ramifications for the trend analysis are that negative trends in areas with typically low snow coverage could be intensified, while positive trends in areas with high snow coverage could be concealed. In areas with little snow, like the Eastern Pamirs, negative trends could be intensified, when NDSI values fall within the lower range, where MODIS showed lower detection rates. Nonetheless, the course of the FSC time series of cell 833289 does not support this possibility, since FSC values are mostly either 0 or close to 100 % throughout the whole time series. In other words, a substantial impact on the trend analysis is unlikely.

4.2 Snow Cover Analysis

4.2.1 Decrease of SC (SCE & SCD)

Decline of SC in the Pamirs. SC in the Pamirs has been decreasing from 2001 to 2018. The decreasing trend in snow cover characteristics in the Pamirs, that has been indicated by previous studies, was, thus, confirmed for the past two decades. The decline in mean annual SCE from 2001 to 2018 was more pronounced than Finaev et al. (2016) computed for 1970 to 2008/09, with 3 % compared to 2.5 %. The negative overall trend in SC was, however, not significant.

Since the negative trend in SC was not significant, it is quite possible that the observed negative trend is purely coincidental. One problem is that, the comparatively short time period from 2001 to 2018 and the large study area make it difficult to reliable detect small trends in the SC dynamics. In addition, since the previous studies on cryosphere changes in the Pamirs indicated that there is a spatially differentiated trend, finding a significant overall trend for the entire study area was unlikely. Nonetheless, the negative trend still illustrates

the direction of the change and the general decrease of SC within the Pamirs.

An assessment of potential causes for the decrease of SC in the Pamirs was beyond the scope of this study, and can therefore only be discussed in a speculative manner. The results of Li et al. (2018) show that temperature and precipitation are likely the main determinants for SC changes in the Tibetan Plateau, including the Pamirs.

Increasing air temperatures in the Pamirs are a possible reason for the observed SC decrease, since air temperature is strongly anticorrelated with SCE as has been shown in multiple studies (Brown and Robinson, 2011; Déry and Brown, 2007; Karl et al., 1993; Lemke et al., 2007). Having said this, the strongest decrease of SC was observed in the Eastern Pamirs during winter, where air temperatures are usually well below the melting point. Small temperature increases in winter are, thus, unlikely to be the main driver for the observed SC decrease.

Changes in precipitation could be another explanation, especially since precipitation is typically very important for SC in continental, cold and dry climates like the Eastern Pamirs (Brown and Mote, 2009). Furthermore, the study from Li et al. (2018) indicates that precipitation might be the main driver for SC changes in the Tibetan Plateau. However, the studies from Finaev et al. (2016) and Yao et al. (2012) both indicate that average precipitation across the Pamirs has increased. Moreover, the study from Yao et al. (2012) indicates precipitation increases especially in the Eastern Pamirs and Finaev et al. (2016) found a continuous increase in winter precipitation. Nonetheless, the study from Finaev et al. (2016) also indicates that precipitation changes were heterogeneous, with increases in high mountain areas and decreases in most other areas. Since most of the areas with a significant negative SC trend were located in comparatively even terrain and an increase in precipitation in high mountain areas could have been concealed by a persistent snow cover in these areas, precipitation could quite possibly be the decisive factor for the observed SC decline in the Pamirs.

Besides temperature and precipitation many other factors like changes in wind drift, for instance, could also play a role (Sect. 1.2.1). However, these factors are even more difficult to assess and likely rather important on smaller scales.

Regional differences: SC reductions in the Eastern Pamirs. SC changes within the Pamirs depended on the region under consideration. While changes in the Western Pamirs were mostly minor, significant SC reductions were found in the Eastern Pamirs, especially in southeast Tajikistan. It was, thus, confirmed that changes in snow cover characteristics are not uniform across the Pamirs.

Magnitudes of the significant trends found in the Eastern Pamirs mostly lie within the SCE decreases indicated by Li et al. (2018) of 1.5 to 3.62 % per year. In contrast to Zhou et al. (2017), however, no larger areas with a positive trend

were found.

Areas with a considerable negative trend seem to be mostly situated in comparatively even terrain, whereas considerable trends on mountain ridges appear to be more rare. In addition, areas with a negative trend appear to be primarily regions with comparatively low SC. Interestingly, in certain areas, mostly in the Western Pamirs, a raise of the snow line might be visible, since SC decreases appear to have happened on the hillsides.

These findings further indicate that the observed SC changes in the Pamirs were driven by a combination of factors, which depended on the specific region. The decisive factor for the observed SC decrease in the Eastern Pamirs might have been changes in precipitation. As discussed before, perhaps potential increases of snowfall on mountains were concealed by anyway high SC characteristics, whereas a decline in snowfall events in the respective valleys in the Eastern Pamirs might have been the decisive factor for the observed SC reductions. Hints of a raising snow line in some areas indicate that temperature changes certainly play a role for the snow cover dynamics in the Pamirs. However, temperature might not be the dominant factor for the observed SC decrease from 2001 to 2018.

Seasonal changes: strongest decrease in winter. The strongest decrease in SC in the Pamirs was observed in winter. During winter 2001 to 2017, the negative overall trend across the Pamirs was weakly significant. In contrast, changes during summer were marginal. Furthermore, a shift towards earlier snow melt in spring was not the main determinant for snow cover changes in the Pamirs over the past 18 years.

The finding of strong negative trends across the Pamirs in winter, while in spring almost no significant trends were present, was unexpected. Based on the results of previous studies a strong decline of SC was expected to be present in spring: the general decline in SC was found to be especially pronounced in spring (Derksen and Brown, 2012; Hernández-Henríquez et al., 2015; Klein et al., 2016; Peng et al., 2013), and studies on the Pamirs preponderantly found a shift towards earlier snowmelt in spring (Dietz et al., 2014; Zhou et al., 2013, 2017). Nonetheless, the strong trend in winter still agrees with the results from Li et al. (2018), which indicated a strong decrease during December to April. The only marginal SC changes during summer were to be expected, since during summer there is simply no snow in most of the study area.

As previously discussed, one reason for the observed seasonal differences could be, that precipitation might be the main factor determining SC changes in the Eastern Pamirs. Temperature is usually more important in spring and fall, since air temperatures in the Pamirs are closer to the melting point then (Brown and Mote, 2009; Steger et al., 2013). In contrast, precipitation in winter almost

exclusively happens in form of snowfall events and is thus more important in dry regions with severe winters like the Eastern Pamirs. In addition, low vegetation in the desertlike Eastern Pamirs facilitates wind drift of snow, and thus further increases the dependence of SC persistence on precipitation.

That being said, the weaker trends in spring and fall could also be a result of a lack of snow in the respective areas. The trend patterns in spring and fall still partly reflect the trend patterns found in winter. The results of the grid cell 833289 in the Eastern Pamirs indicate that there just might have been too little snow compared to winter to allow for the detection of a significant trend (Fig. 3.18). This suggests that in certain areas the lack of snow in spring and fall contributed to the fact that the strongest SC changes were found in winter.

The discrepancy to the results of previous studies that indicate a shift towards earlier snow melt in the Pamirs could be a result of the different time period that was examined. Zhou et al. (2013, 2017) analyzed snow cover from 1986 to 2008 and Dietz et al. (2014) analyzed the time period from 1986 to 2014. Also important to consider is, that the snow cover melt date was not directly examined, but rather the change in spring SCD. While changes in spring SCD are closely liked to shifts in the snow cover melt date, a potential shift is still more difficult to detect compared to a direct assessment.

4.2.2 Similarity of SCE and SCD

The SCE and SCD results were extremely similar: SCD results were more or less equivalent to the mean FSC results.

In general, similar results for the two snow metrics were expected, since the SCD and mean SCE both yield information about the amount of snow in the respective area. Furthermore, in previous research SCE changes were found to be closely linked to changes in the duration of the snow season (Brown and Mote, 2009). Nonetheless, it was unexpected that the results with respect to SCD and SCE were basically equivalent.

By comparing both metrics, it was hoped, that areas with low (high) mean FSC and high (low) SCD could be discerned. These areas would have indicated locations that were covered by a long (short) time with little (much) snow. Since the Pamirs are a high mountain area with complex terrain and a high potential for redistribution of snow by strong winds, areas with heterogeneous snow cover that show such differences in SCD and mean SCE were expected. However, differences between both metrics were marginal, thus, implying that the mean SCE is not only linked to the SCD, but can more or less be translated to the SCD. Hence, the SCD – the number of days where there is a substantial amount of snow cover of more than 28 % of the area – is more or less exclusively dependent on the

mean snow covered area in the respective time period.

The results of grid cell 833289 indicate why this was likely the case: the daily FSC time series showed a rapid on- and offset of snow cover, with FSC values being either close to 0 or 100 % with almost no transition period in between. Therefore, nearly every day, on which snow was detected, was also counted as a snow covered day in the SCD: in cell 833289, 1393 out of 6570 days were covered with snow, thereby only 171 days out of the 1393 days had FSC values between 0 and 28 %. Furthermore, over 50 % of the snow covered days had values above 88 % FSC, indicating that changing the threshold for the SCD calculation to 0.3 or 0.4 would not have led to substantially different results. Another factor to consider in this regard is the applied linear gap filling. With a different gap filling approach, the number of days with a FSC between 0 and 28 % would have most likely been even lower.

4.2.3 Spiking character of the FSC cell time series

Individual grid cells showed a rapid on- and offset of snow cover, resulting in a spiking character in their FSC time series (as has been exemplary shown with the results of cell 833289; Fig. 3.16). The lack of moderate FSC values then led to the strong similarity between the SCD and mean SCE. As mentioned previously, this result was not expected.

Besides natural conditions, the over-/underestimation of high/low NDSI values by MODIS is very likely to have contributed to this. The results of the validation with Landsat indicate, that low NDSI values were underestimated by the gap filled MODIS data set, and high NDSI values were slightly overestimated. Both, the underestimation of low values and the overestimation of high values lead to more extreme values, and consequently reinforce the spiking character of the grid cell FSC time series. The underestimation of low NDSI values, in particular, seems to be an important factor in this regard: since MODIS likely failed to detect many low NDSI values, the similarity of the SCD and mean SCE was intensified.

Another factor to consider is the application of the FSC equation. The calculation of the FSC with equation 2.2 contributes to a spiking character of the time series compared to the original NDSI time series. By applying equation 2.2 NDSI values greater than 0.7 are all regarded as 100 % FSC. Information about high NDSI values is, thus, lost and differences within the time series are reduced. However, although this does lead to an amplification of the spiking character compared to the NDSI time series, it is still necessary to obtain information about the FSC, which is considered to be 100 % when a NDSI of 0.7 is detected based on an empirical relationship with Landsat images (Salomonson and Appel, 2004, 2006).

4.2.4 Additional findings

Lake Karakul – potential snow-cloud confusion. Although lake Karakul showed no substantial trend in the snow cover analysis, an interesting development of the snow cover throughout the seasons was found. While the lake had on average higher SC values than its surroundings during spring, summer and winter, it was the other way around in fall.

In spring and winter lake Karakul was typically frozen for more or less the entire season, and thus clearly visible in the SC overall mean maps. Since lake Karakul usually did not start freezing before early December, the SC was lower compared to its surroundings in fall. In summer, however, lake Karakul had, against expectations, a higher SC than its surroundings, although the actual class difference was only one class (e.g. mean FSC: 1-10 % compared to 0-1 %). One reason for this could be, that occasionally the ice layer of lake Karakul had not yet melted by beginning of June. This was indeed the case for the eastern part of lake Karakul in a few years, as could be verified in the time lapse video. However, in the video, another possible explanation could be observed: during summer there seemed to occur sporadic snow-cloud confusion over lake Karakul, where in recurring instances suddenly high NDSI values lit up.

This observation demonstrates the particular problem with cloud cover in optical remote sensing of snow cover. It has to be assumed, that also in other regions with frequent cloud cover, snow-cloud confusion occurred. Nonetheless, because of the stochastic recurrence of the phenomenon it is highly unlikely that it substantially influenced the main results, as can be seen in the mean FSC of lake Karakul in fall and the validation results.

Lake Karakul – east-west differences. Slight differences in the mean FSC within lake Karakul indicated that the eastern part of the lake typically froze earlier and melted later than its western part.

This finding could be verified in the time lapse video. The video also shows that lake Karakul typically froze between early to late December, and thawed between early to late May. The likely cause for the disparity in SC is the difference in depth between the eastern and the western part of the lake. While the eastern part of the lake is fairly shallow ($\sim$ 20 m), the western part is comparatively deep (up to $\sim$ 242 m) (Molchanov, 1929, quoted in Mischke et al., 2010).

Highly positive trend in China north of Tashkurgan. In the SC trend maps, classes with very high SC increases were indicated in the respective legends. These trends occurred in a small area in China north of Tashkurgan around 74.98° E and 38.76° N. To further investigate these extreme SC increases, individual

cells in this area had been inspected manually, and additionally the region was studied in the time lapse video. Both investigations showed that starting in 2012, days with middle to high FSC values increased drastically.

A natural positive trend of the observed magnitude is highly unlikely. Either there have been local disturbances that led to a sudden change in snow cover or measurements in the MODIS snow cover product were not accurate for this particular region.

A closer examination of the data gaps in the MODIS snow cover product indicated that inconsistent measurements in this specific region were potentially the cause. The region is located in an area characterized by a high percentage of gaps. It is in direct vicinity of an excluded area that had more than 60 % gaps. Interestingly, although the region is characterized by a high number of gaps, the area doesn't lie within a region of particularly high cloud cover (Fig. 3.1). Hence, a large portion of this region's gaps were caused by the other MODIS keys "missing data", "no decision", "night", "detector saturated" and "fill". This indicates, that the MODIS sensor might have had difficulties in this particular region and results for this region are likely not accurate.

Another factor that needs to be considered in this regard is the applied gap filling with linear interpolation. An unfavorable distribution of the gaps previous to or after 2012 could theoretically contribute to this discrepancy. Nonetheless, the gap filling alone is highly unlikely to have introduced this trend.

4.3 Limitations

Validation. Within the scope of this thesis a basic validation of the MODIS snow cover product was performed. The complex topography and different climatic conditions within the study area would, however, make a more detailed validation desirable. The validation results illustrate, that in certain situations, the accuracy of the applied MODIS data set can be problematic. A more thorough validation would help to reduce the uncertainty of the snow cover analysis results.

Instead of two days, multiple validation days with differing conditions would be desirable. For this, days from different seasons with different snow, cloud and illumination conditions could be selected. Furthermore, validation results could differ considerably between the different regions within the Pamirs. Therefore, the validation of a larger spatial extent or ideally the entire study area would be desirable. In addition, further data sources with a known high accuracy like field measurements could also be used to improve the reference data.

Snow cover data. Remote sensing in complex terrain is challenging, and requires high spatial and temporal resolution (WMO, 2011). Similarly to improving the validation's reference data, ensuring a high accuracy of the snow data set is also of central importance. The validation results illustrate, that the accuracy of the applied gap filled MODIS-Terra snow data set could still be improved.

A more elaborate gap filling method would likely considerably improve the snow data accuracy. Instead of solely using temporal gap filling, other techniques like Gafurov and Bárdossy (2009) discussed could certainly improve results. Dong and Menzel (2016) and Gao et al. (2010) illustrated that especially the integration of other data sources like field measurements or microwave sensors can considerably increase data accuracy. Furthermore, the applied gap filling should ideally be adapted to respective study area.

Another more simple option would be to use the new MODIS cloud gap filled data set (MOD10A1F), which was introduced in collection 6 of the MODIS snow cover products (Hall et al., 2010; Riggs et al., 2016). Although, a specific gap filling for the study area would be ideal, the cloud free product could still be valuable. While the product was not yet available through the NSIDC at the time of this study, it could be used in future research.

A further possibility would be the use of spectral-unmixing instead of the NDSI for snow detection. While several studies indicate, that the NDSI is sufficient for snow detection in mountainous terrain (Crawford, 2015; Gascoin et al., 2015; Jain et al., 2008; Sorman et al., 2007), a spectral-unmixing approach could perhaps still improve data accuracy in high mountain areas like the Pamirs (Rittger et al., 2013).

Snow cover analysis. In this study a basic trend analysis was conducted to examine overall changes in snow cover within the Pamirs. One limitation of the trend analysis is, that the analyzed time period of 18 years is too short to reliably assess snow cover changes in some areas. The results illustrate that the interannual variability of snow cover in the Pamirs can be quite large, while overall changes in many regions were only slight. The analysis of a longer time period could help to detect smaller changes within the study area. This would be particularly important for studies researching climate change within the Pamirs, since then typically 30 years are needed for reliable statements (WMO, 2019).

Extending the time series in a meaningful way is, however, only possible by making trade-offs. One option would be the integration of the AVHRR data set like in the study from Dietz et al. (2014). However, in this case the integration comes with a considerable loss of spatial resolution, which can be problematic in the Pamirs.

Other limitations. To visualize results, maps with geographic coordinates have been used. Geographic coordinates help to improve readability as compared to the distorted shape of the study area in the sinusoidal projection. However, geographical coordinates have the disadvantage, that areas are distorted. It should therefore be kept in mind, that area sizes in the maps can be misleading. Nonetheless, area distortion in the mid-latitudes is still within acceptable dimensions.

4.4 Implications for future research.

Results demonstrate, that SC changes particularly occurred in the Eastern Pamirs. As a next step, it would be important to assess the cause of the observed snow cover changes to be able to better estimate future changes within the Pamirs.

As indicated by the results of Li et al. (2018), future studies of the snow cover changes in the Pamirs should focus on temperature and precipitation as the main factors for snow cover changes. Furthermore, a long-term analysis that compares changes in snow cover, temperature and precipitation would allow for a more reliable assessment.

For a more complete assessment of the snow cover changes within the Pamirs, the additional analysis of the SWE would be important. The results of Brown and Mote (2009) indicate that in drier climates like the Eastern Pamirs, decreases in SCD are paired with increases in SWE maximum. The results of this thesis and other studies support that such a mixed change occurred in the Pamirs. The SCD in the Pamirs has decreased. At the same time average precipitation in the Eastern Pamirs has increased (Finaev et al., 2016; Yao et al., 2012), although several indicators point to a decrease in precipitation as the plausible reason for the observed SC decline. An increase in SWE in certain areas could partly explain this discrepancy. Snow cover changes in high altitudes, where snow cover is high throughout the year, should therefore additionally be assessed with the SWE.

In addition, further improvement of the base snow data in complex terrain is of central importance to minimize uncertainty in the results. Besides addressing the before mentioned limitations, the integration of additional data sources could greatly improve the accuracy. One meaningful approach to address shortcomings of individual remote sensing sensors is the combination of multiple sensors as suggested by Crawford (2015). Another promising approach would be the combination of remote sensing observations with field measurements and hydrological models like Dong (2018) suggested. In this way advantages of different measurement techniques could be combined.

5 Conclusion

A detailed analysis of snow cover changes in the Pamirs was conducted to better resolve small-scale differences within the region. The daily MODIS snow cover product was used to assess snow cover changes over the past 18 years.

The validation of MODIS with Landsat 5 (TM) demonstrated that the daily MODIS snow cover product mapped snow cover in the Pamirs with reasonable accuracy. Nonetheless, MODIS slightly overestimated high NDSI values and considerably underestimated low NDSI values particularly in conditions with sparse snow cover. A high level of accuracy of the underlying data is of central importance to reduce uncertainty in the study results. To further increase the accuracy, a combination of multiple sensors as suggested by Crawford (2015) would be a possibility. A promising approach to better address shortcomings of remote sensing data would be the combination of remote sensing observations with field measurements and hydrological models like Dong (2018) suggested.

Results of the snow cover analysis demonstrate that the decline of snow covered area in the Pamirs has continued in the 21st century. Results indicate, that snow cover has primarily decreased in the Eastern Pamirs during winter. The study, thus, confirmed that snow cover changes within the Pamirs are not uniform. Interestingly, the shift towards an earlier snow melt in the Pamirs, which has been indicated by previous studies, was not the main factor for the observed snow cover changes. Although the snow cover duration in spring has generally decreased across the Pamirs, negative trends in winter were decisive for the overall trend. Therefore, local communities in the Eastern Pamirs seem to face reductions in winter snow cover rather than a shift of the snow season.

The results of this study helped to better resolve small-scale changes of snow cover in the Pamirs. As a next step, future research needs to assess the drivers for the observed changes. Li et al. (2018) showed that temperature and precipitation are likely the main factors for snow cover changes in the Tibetan Plateau. Results of this thesis indicate that reductions in winter snowfall would be a plausible explanation for the observed snow cover reductions in the Eastern Pamirs. The additional analysis of the snow water equivalent could thereby help to better assess the influence of precipitation on the observed changes.

Appendices

A3.2 Validation

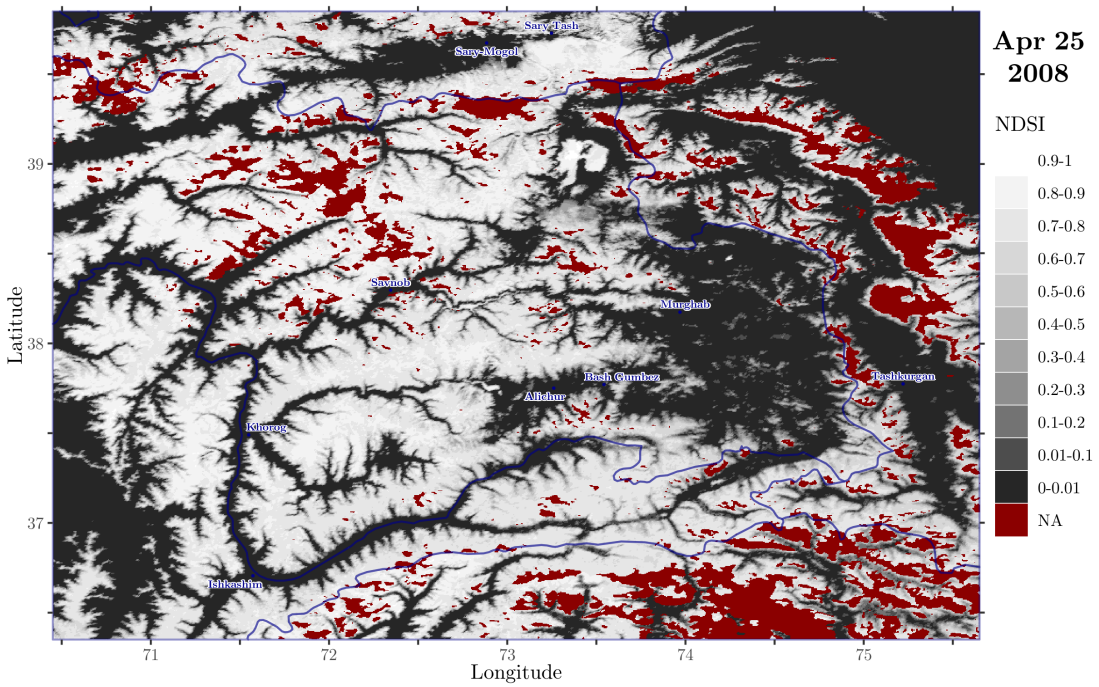

Figure A.1: MODIS NDSI of the entire study area on the 25th of April 2008.

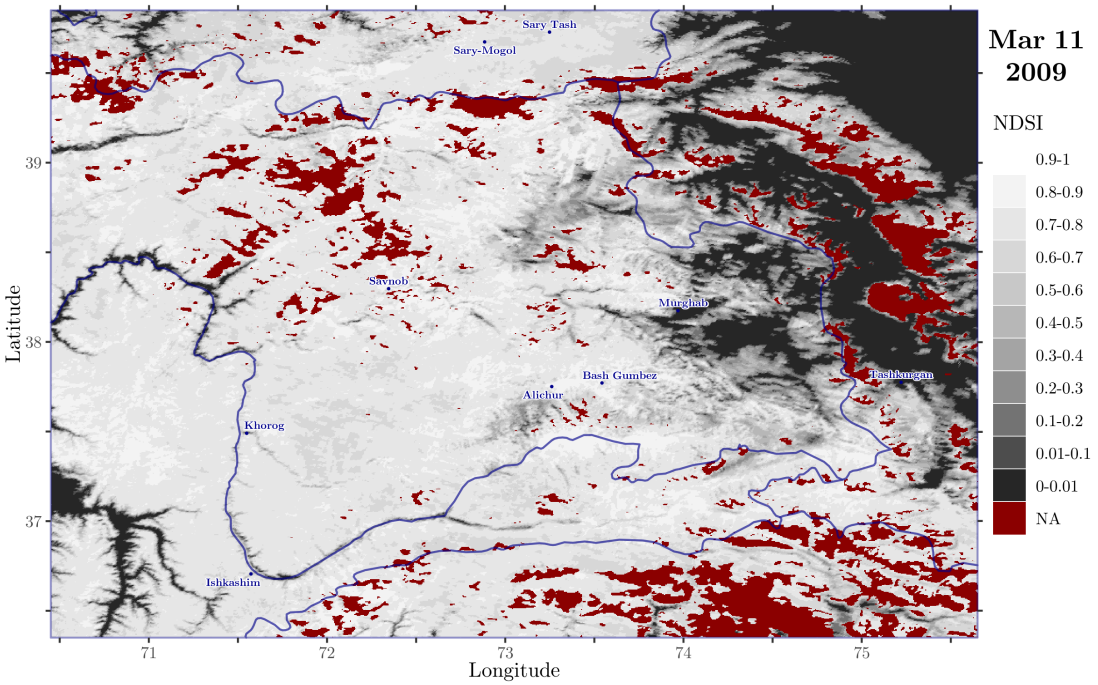

Figure A.2: MODIS NDSI of the entire study area on the 11th of March 2009.

A3.3 Snow Cover Analysis

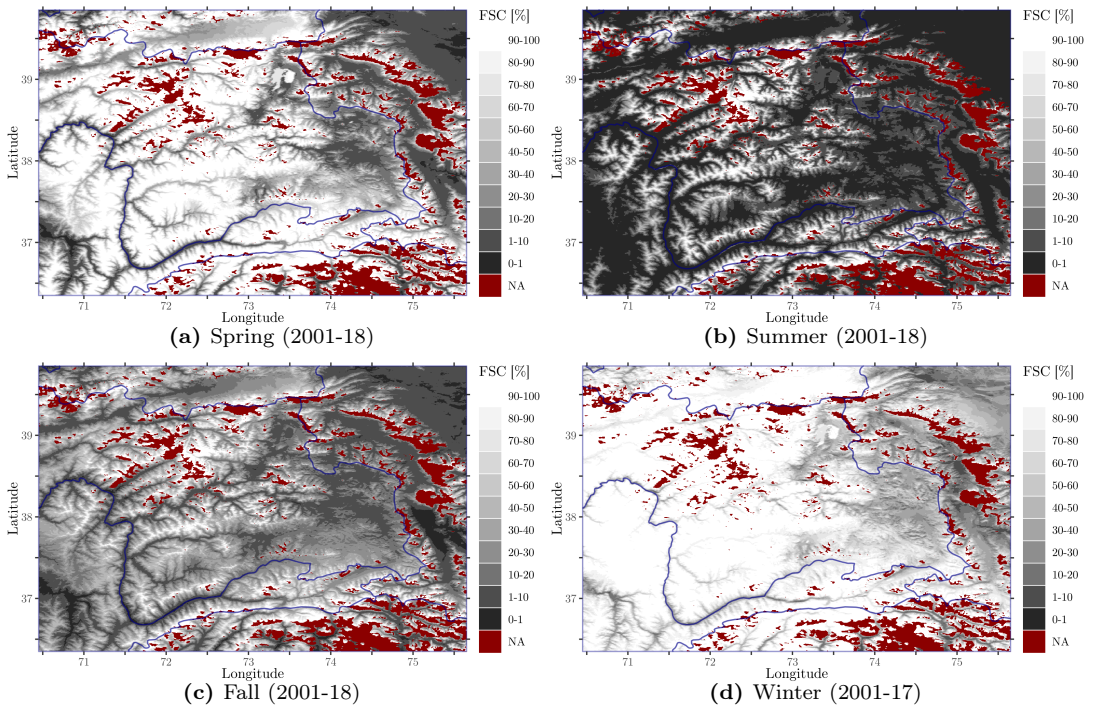

(a) Spring (2001-18)

(b) Summer (2001-18)

(c) Fall (2001-18)

(d) Winter (2001-17)

Figure A.3: Maps for the mean FSC of the different seasons in the study area. Areas that were left out of the analysis are colored red.

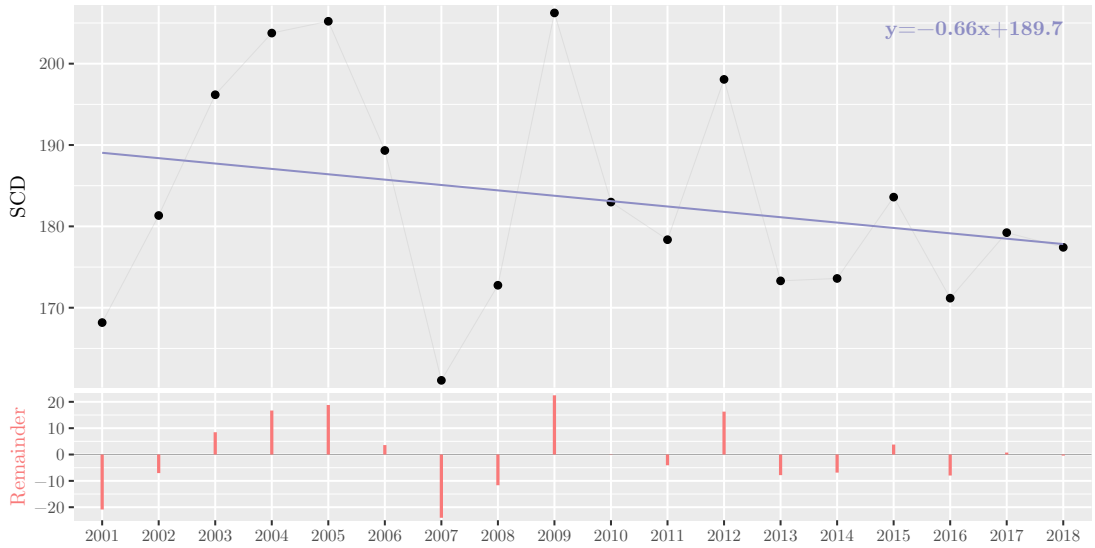

Figure A.4: Trend analysis of the annual SCD for the entire study area from 2001 to 2018. The black dots mark the SCD of the respective years. The blue line represents the linear trend. The equation of the linear model is indicated in the upper right corner. The red bars represent the residuals of the linear model.

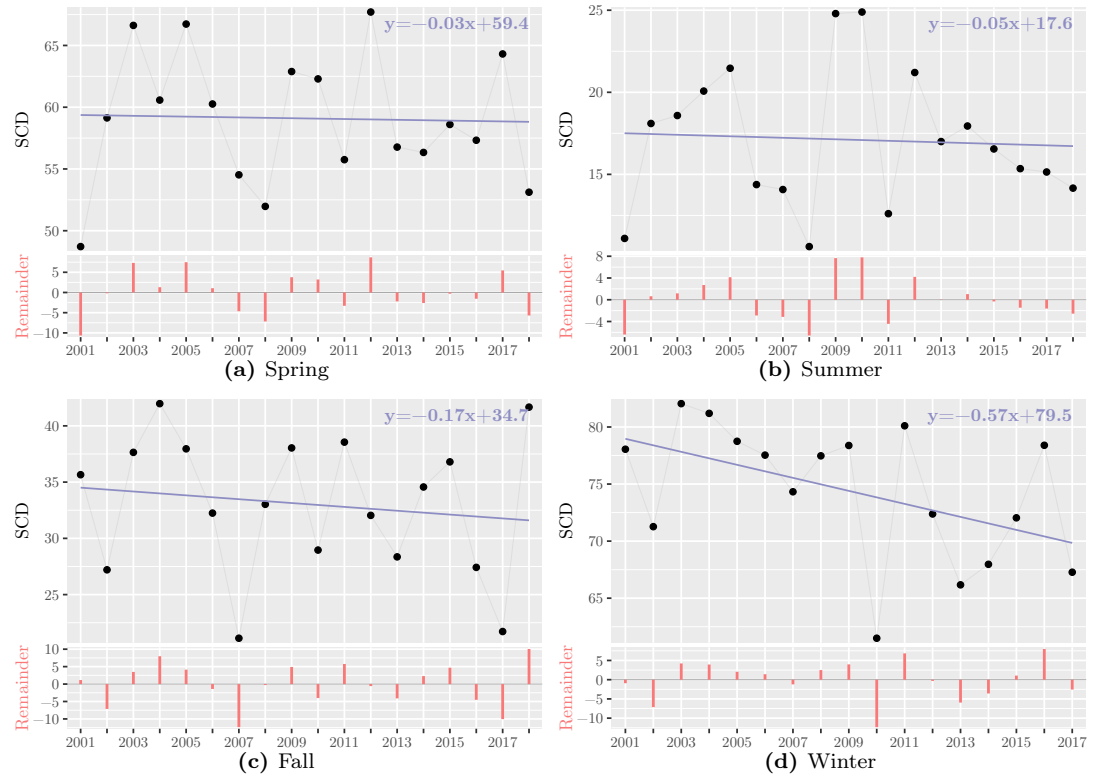

Figure A.5: Trend analysis of the seasonal SCD for the entire study area. The black dots mark the SCD of the respective seasons. The blue line represents the linear trend. The equation of the linear model is indicated in the upper right corner. The red bars represent the residuals of the linear model.

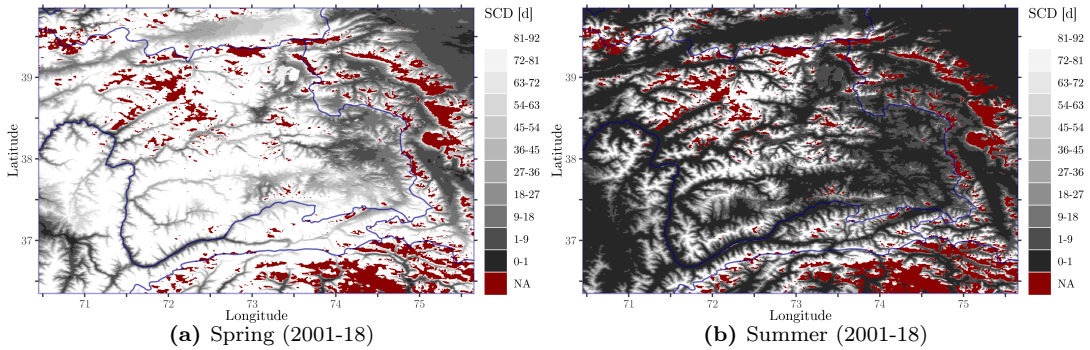

(a) Spring (2001-18) **(b)** Summer (2001-18)

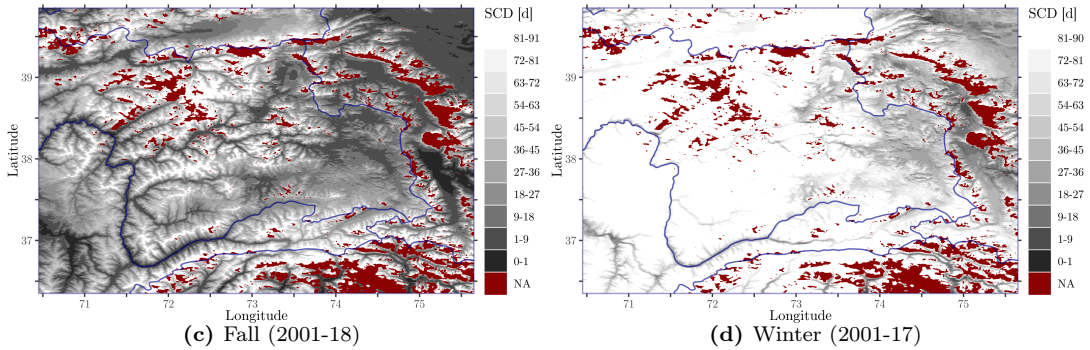

(c) Fall (2001-18) **(d)** Winter (2001-17)

Figure A.6: Maps of the mean SCD of the different seasons in the study area. Areas that were left out of the analysis are colored red.

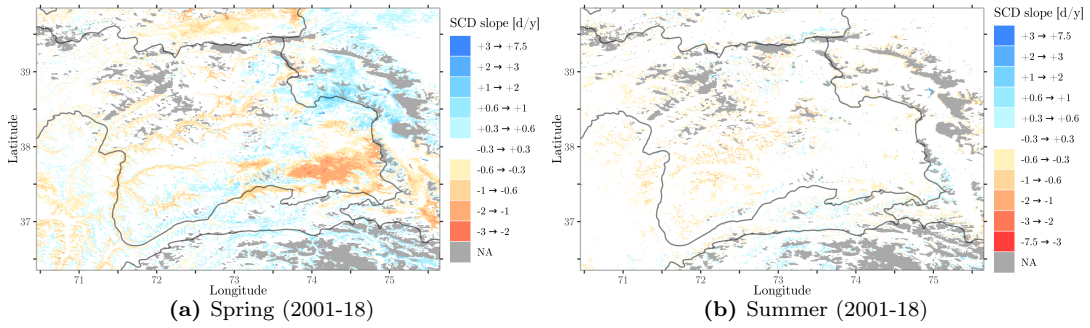

(a) Spring (2001-18) **(b)** Summer (2001-18)

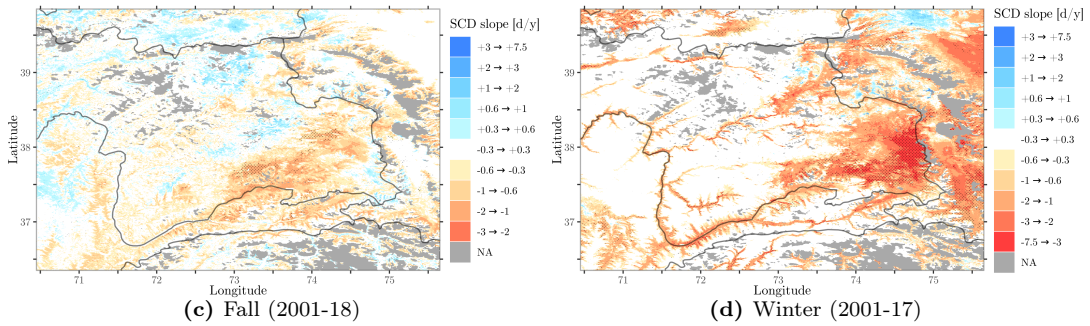

(c) Fall (2001-18) **(d)** Winter (2001-17)

Figure A.7: Map of the seasonal SCD trend in the study area. Areas that were left out of the analysis are colored gray. The annual change rate is indicated by the slope of the linear trend in colors from blue (positive) to red (negative). White areas were regarded as having no substantial trend. Areas with a significant trend of $p < 0.05$ (based on ANOVA), were marked with a black dot pattern.

Table A.1: Grid cell distributions of the different trend classes for the annual and seasonal SCD trend maps. In the rows, the proportion of grid cells, which belong to the respective class is listed.

Annual trend		Seasonal trend				
Class [d/y]	Overall [%]	Class [d/y]	Spring [%]	Summer [%]	Fall [%]	Winter [%]
$+5.0 \rightarrow +26$	0.02	$+3.0 \rightarrow +7.5$	0.01	0.00	0.00	0.01
$+3.0 \rightarrow +5.0$	0.02	$+2.0 \rightarrow +3.0$	0.01	0.01	0.01	0.01
$+2.0 \rightarrow +3.0$	0.06	$+1.0 \rightarrow +2.0$	0.33	0.03	0.14	0.10
$+1.0 \rightarrow +2.0$	1.38	$+0.6 \rightarrow +1.0$	2.07	0.29	1.69	0.49
$+0.6 \rightarrow +1.0$	2.98	$+0.3 \rightarrow +0.6$	10.51	2.23	7.30	0.91
$-0.6 \rightarrow +0.6$	54.24	$-0.3 \rightarrow +0.3$	69.24	89.87	57.87	54.95
$-1.0 \rightarrow -0.6$	14.47	$-0.6 \rightarrow -0.3$	11.06	6.19	19.03	9.63
$-2.0 \rightarrow -1.0$	17.10	$-1.0 \rightarrow -0.6$	5.07	1.26	10.81	9.67
$-3.0 \rightarrow -2.0$	6.24	$-2.0 \rightarrow -1.0$	1.69	0.11	3.16	16.33
$-5.0 \rightarrow -3.0$	3.11	$-3.0 \rightarrow -2.0$	0.02	0.01	0.00	6.70
$-26 \rightarrow -5.0$	0.38	$-7.5 \rightarrow -3.0$	0.00	0.00	0.00	1.19

Bibliography

Barnett, T.P., J.C. Adam, and D.P. Lettenmaier (2005). "Potential impacts of a warming climate on water availability in snow-dominated regions". In: *Nature* 438, pp. 303–309.

Barry, R. and T.Y. Gan (2011). *The Global Cryosphere – Past, Present and Future*. Cambridge, United Kingdom and New York, NY, USA: Cambridge University Press.

Beniston, M. (2003). "Climatic change in mountain regions: a review of possible impacts". In: *Climatic Change* 59, pp. 5–31.

Berris, S.N. and R.D. Harr (1987). "Comparative Snow Accumulation and Melt During Rainfall in Forested and Clear-Cut Plots in the Western Cascades of Oregon". In: *Water Resources Research* 23, pp. 135–142.

Breu, T. and H. Hurni (2003). *The Tajik Pamirs: Challenges of Sustainable Development in an Isolated Mountain Region*. University of Berne: Centre for Development and Environment (CDE).

Brown, R.D. (2000). "Northern Hemisphere Snow Cover Variability and Change, 1915-97". In: *American Meteorological Society* 13, pp. 2339–2355.

Brown, R.D. and P.W. Mote (2009). "The Response of Northern Hemisphere Snow Cover to a Changing Climate". In: *Journal of Climate* 22, pp. 2124–2145.

Brown, R.D. and D.A. Robinson (2011). "Northern Hemisphere spring snow cover variability and change over 1922-2010 including an assessment of uncertainty". In: *The Cryosphere* 5, pp. 219–229.

Brutel-Vuilmet, C., M. Ménégoz, and G. Krinner (2013). "An analysis of present and future seasonal Northern Hemisphere land snow cover simulated by CMIP5 coupled climate models". In: *The Cryosphere* 7, pp. 67–80.

Burakowski, E. and M. Magnusson (2012). *Climate Impacts on the Winter Tourism Economy in the United States*. Natural Resources Defense Council, New York, N. Y.: Prepared for Protect Our Winters (POW) and Natural Resources Defense Council (NRDC).

Chevallier, P., B. Pouyaud, M. Mojaïsky, M. Bolgov, O. Olsson, M. Bauer, and J. Froebrich (2014). "River flow regime and snow cover of the Pamir Alay

(Central Asia) in a changing climate". In: *Hydrological Sciences Journal* 59 (8), pp. 1491–1506.

Clarke, A.D. and K.J. Noone (1985). "Soot in the arctic snowpack: a cause for perturbations in radiative transfer". In: *Atmospheric Environment* 19-12, pp. 2045–2053.

Cohen, J. and D. Rind (1991). "The Effect of Snow Cover on the Climate". In: *Journal of Climate* 4, pp. 689–706.

Collins, M., R. Knutti, J. Arblaster, J.-L. Dufresne, T. Fichefet, P. Friedlingstein, X. Gao, W.J. Gutowski, T. Johns, G. Krinner, M. Shongwe, C. Tebaldi, A.J. Weaver, and M. Wehner (2013). "Long-term Climate Change: Projections, Commitments and Irreversibility". In: *Climate Change 2013: The Physical Science Basis. Contribution of Working Group I to the Fifth Assessment Report of the Intergovernmental Panel on Climate Change*. Ed. by T.F. Stocker, D. Qin, G.-K. Plattner, M. Tignor, S.K. Allen, J. Boschung, A. Nauels, Y. Xia, V. Bex, and P.M. Midgley. Cambridge, United Kingdom and New York, NY, USA: Cambridge University Press.

Crawford, C.J. (2015). "MODIS Terra Collection 6 fractional snow cover validation in mountainous terrain during spring snowmelt using Landsat TM and ETM+". In: *Hydrological Processes* 29, pp. 128–138.

Cubasch, U., D. Wuebbles, D. Chen, M.C. Facchini, D. Frame, N. Mahowald, and J.-G. Winther (2013). "Introduction". In: *Climate Change 2013: The Physical Science Basis. Contribution of Working Group I to the Fifth Assessment Report of the Intergovernmental Panel on Climate Change*. Ed. by T.F. Stocker, D. Qin, G.-K. Plattner, M. Tignor, S.K. Allen, J. Boschung, A. Nauels, Y. Xia, V. Bex, and P.M. Midgley. Cambridge, United Kingdom and New York, NY, USA: Cambridge University Press.

Derksen, C. and R. Brown (2012). "Spring snow cover extent reductions in the 2008-2012 period exceeding climate model projections". In: *Geophys. Res. Lett.* 39, p. L19504.

Déry, S.J. and R.D. Brown (2007). "Recent Northern Hemisphere snow cover extent trends and implications for the snow-albedo feedback". In: *Geophysical Research Letters* 34, pp. 1–6.

Dietz, A.J., C. Conrad, C. Kuenzer, G. Gesell, and S. Dech (2014). "Identifying Changing Snow Cover Characteristics in Central Asia between 1986 and 2014 from Remote Sensing Data". In: *Remote Sensing* 6, pp. 12752–12775.

Doherty, S.J., S.G. Warren, T.C. Grenfell, A.D. Clarke, and R.E. Brandt (2010). "Light-absorbing impurities in Arctic snow". In: *Atmospheric Chemistry and Physics* 10, pp. 11647–11680.

Dong, C. (2018). "Remote sensing, hydrological modeling and in situ observations in snow cover research: A review". In: *Journal of Hydrology* 561, pp. 573–583.

Dong, C. and L. Menzel (2016). "Producing cloud-free MODIS snow cover products with conditional probability interpolation and meteorological data". In: *Remote Sensing of Environment* 186, pp. 439–451.

Duchon, C. and R. Hale (2012). *Time Series Analysis in Meteorology and Climatology – An Introduction*. West Sussex, UK: John Wiley & Sons, Ltd.

Elder, K., J. Dozier, and J. Michaelsen (1991). "Snow Accumulation and Distribution in an Alpine Watershed". In: *Water Resources Research* 27, pp. 1541–1552.

Finaev, A.F., L. Shiyin, B. Weijia, and J. Li (2016). "Climate Change and Water Potential of the Pamir Mountains". In: *Geography. Environment. Sustainability.* 9, pp. 88–105.

Flanner, M.G., K.M. Shell, M. Barlage, D.K. Perovich, and M.A. Tschudi (2011). "Radiative forcing and albedo feedback from the Northern Hemisphere cryosphere between 1979 and 2008". In: *Nature Geoscience* 4, pp. 151–155.

Foster, J.L., C. Sun, J.P. Walker, R. Kelly, A. Chang, J. Dong, and H. Powell (2005). "Quantifying the uncertainty in passive microwave snow water equivalent observations". In: *Remote Sensing of Environment* 94, pp. 187–203.

Gafurov, A. and A. Bárdossy (2009). "Cloud removal methodology from MODIS snow cover product". In: *Hydrology and Earth System Sciences* 13, pp. 1361–1373.

Gao, Y., H. Xie, N. Lu, T. Yao, and T. Liang (2010). "Toward advanced daily cloud-free snow cover and snow water equivalent products from Terra-Aqua MODIS and Aqua AMSR-E measurements". In: *Journal of Hydrology* 385, pp. 23–35.

Gardelle, J., E. Berthier, Y. Arnaud, and A. Kääb (2013). "Region-wide glacier mass balances over the Pamir-Karakoram-Himalaya during 1999-2011". In: *The Cryosphere* 7, pp. 1263–1286.

Gardner, A.S., G. Moholdt, J.G. Cogley, B. Wouters, A.A. Arendt, J. Wahr, E. Berthier, R. Hock, W.T. Pfeffer, G. Kaser, S.R.M. Ligtenberg, T. Bolch, M.J. Sharp, J.O. Hagen, M.R. van den Broeke, and F. Paul (2013). "A Reconciled Estimate of Glacier Contributions to Sea Level Rise: 2003 to 2009". In: *Science* 340, pp. 852–857.

Gascoin, S., O. Hagolle, M. Huc, L. Jarlan, J.-F. Dejoux, C. Szczypta, R. Marti, and R. Sánchez (2015). "A snow cover climatology for the Pyrenees from MODIS snow products". In: *Hydrology and Earth System Sciences* 19, pp. 2337–2351.

Glantz, M.H. (2005). "Water, climate, and development issues in the Amu Darya Basin". In: *Mitigation and Adaptation Strategies for Global Change* 10, pp. 23–50.

Goodison, B.E., R.D. Brown, R.G. Crane, R. Alley, R Bales, D. Barber, R. Barry, C. Bentley, T. Carrol, D. Cline, C.R. Duguay, G.M. Flato, D.K. Hall,

R. Harrington, J. Kargel, H. Kieffer, S. Munro, C. Parkinson, B. Raup, A. Rothrock, and M. Sharp (1999). "Cryospheric Systems". In: *EOS Science Plan*, pp. 261–307.

Groisman, P.Y., T.R. Karl, and R.W. Knight (1994). "Observed Impact of Snow Cover on the Heat Balance and the Rise of Continental Spring Temperatures". In: *Science* 263, pp. 198–200.

Hall, A. and X. Qu (2006). "Using the current seasonal cycle to constrain snow albedo feedback in future climate change". In: *Geophysical Research Letters* 33, pp. 1–4.

Hall, D.K. and J. Martinec (1985). *Remote Sensing of Ice and Snow*. London: Chapman and Hall Ltd.

Hall, D.K., G.A. Riggs, and V.V. Salomonson (2001). "Algorithm Theoretical Basis Document (ATBD) for the MODIS Snow and Sea Ice-Mapping Algorithms". In:

Hall, D.K. and G.A. Riggs (2007). "Accuracy assessment of the MODIS snow products". In: *Hydrological Processes* 21, pp. 1534–1547.

Hall, D.K., G.A. Riggs, J.L. Foster, and S.V. Kumar (2010). "Development and evaluation of a cloud-gap-filled MODIS daily snow-cover product". In: *Remote Sensing of Environment* 114, pp. 496–503.

Hall, D.K. and G.A. Riggs (2011). "Normalized-difference snow index (NDSI)". In: *Encyclopedia of Earth Sciences Series, Encyclopedia of Snow, Ice and Glaciers*.

Hamed, K.H. and A.R. Rao (1998). "A modified Mann-Kendall trend test for autocorrelated data". In: *Journal of Hydrology* 204, pp. 182–196.

Hamlet, A.F. and D.P. Lettenmaier (2007). "Effects of 20th century warming and climate variability on flood risk in the western U.S." In: *Water Resources Research* 43, pp. 1–17.

Hantel, M. and C. Maurer (2011). "The median winter snowline in the Alps". In: *Meteorologische Zeitschrift* 20, pp. 267–276.

Hernández-Henríquez, M.A., S.J. Déry, and C. Derksen (2015). "Polar amplification and elevation-dependence in trends of Northern Hemisphere snow cover extent, 1971-2014". In: *Environ. Res. Lett.* 10, p. 044010.

Hoegh-Guldberg, O., D. Jacob, M. Taylor, M. Bindi, S. Brown, I. Camilloni, A. Diedhiou, R. Djalate, K.L. Ebi, F. Engelbrecht, J. Guiot, Y. Hijioka, S. Mehrotra, A. Payne, S.I. Seneviratne, A. Thomas, R. Warren, and G. Zhou (2018). "Impacts of 1.5°C Global Warming on Natural and Human Systems". In: *Global Warming of 1.5° C. An IPCC Special Report on the impacts of global warming of 1.5° C above pre-industrial levels and related global greenhouse gas emission pathways, in the context of strengthening the global response to the threat of climate change, sustainable development, and efforts to eradicate*

poverty. Ed. by V. Masson-Delmotte, P. Zhai, H.-O. Pörtner, D. Roberts, J. Skea, P.R. Shukla, A. Pirani, W. Moufouma-Okia, C. Péan, R. Pidcock, S. Connors, J.B.R. Matthews, Y. Chen, X. Zhou, M.I. Gomis, E. Lonnoy, T. Maycock, M. Tignor, and T. Waterfield. In Press.

IPCC (2013). "Annex III: Glossary [Planton, S. (ed.)]" In: *Climate Change 2013: The Physical Science Basis. Contribution of Working Group I to the Fifth Assessment Report of the Intergovernmental Panel on Climate Change*. Ed. by T.F. Stocker, D. Qin, G.-K. Plattner, M. Tignor, S.K. Allen, J. Boschung, A. Nauels, Y. Xia, V. Bex, and P.M. Midgley. Cambridge, United Kingdom and New York, NY, USA: Cambridge University Press.

Jain, S.K., A. Goswami, and A.K. Saraf (2008). "Accuracy assessment of MODIS, NOAA and IRS data in snow cover mapping under Himalayan conditions". In: *International Journal of Remote Sensing* 29(20), pp. 5863–5878.

James, T., A. Evans, E. Madly, and C. Kelly (2014). *The Economic Importance of the Colorado River to the Basin Region*. Arizona State University, W.P. Carey School of Business, Tempe.

JAXA (n.d.). *ALOS Global Digital Surface Model (AW3D30)*. `https://www.eorc.jaxa.jp/ALOS/en/aw3d30/`. Accessed: 2019-03-27.

Jensen, J.R. (2005). *Introductory Digital Image Processing – A Remote Sensing Perspective (Third Edition)*. Upper Saddle River, New Jersey, USA: Pearson Prentice Hall.

Karl, T.R., P.Y. Groisman, R.W. Knight, and R.R. Heim JR. (1993). "Recent Variations of Snow Cover and Snowfall in North America and Their Relation to Precipitation and Temperature Variations". In: *Journal of Climate* 6, pp. 1327–1344.

Kassam, K-A.S., M.L. Ruelle, C. Samimi, A. Trabucco, and J. Xu (2018). "Anticipating Climatic Variability: The Potential of Ecological Calendars". In: *Human Ecology* 46, pp. 249–257.

Klein, G., Y. Vitasse, C. Rixen, C. Marty, and M. Rebetez (2016). "Shorter snow cover duration since 1970 in the Swiss Alps due to earlier snowmelt more than to later snow onset". In: *Climatic Change* 139, pp. 637–649.

Knoche, M., R. Merz, M. Lindner, and S.M. Weise (2017). "Bridging Glaciological and Hydrological Trends in the Pamir Mountains, Central Asia". In: *Water* 9, p. 422.

König, M., J-G. Winther, and E. Isaksson (2001). "Measuring snow and glacier ice properties from satellite". In: *Reviews of Geophysics* 39(1), pp. 1–27.

Kunkel, K.E., D.A. Robinson, S. Champion, X. Yin, T. Estilow, and R.M. Frankson (2016). "Trends and Extremes in Northern Hemisphere Snow Characteristics". In: *Curr Clim Change Rep* 2, pp. 65–73.

Lemke, P., J. Ren, R.B. Alley, I. Allison, J. Carrasco, G. Flato, Y. Fujii, G. Kaser, P. Mote, R.H. Thomas, and T. Zhang (2007). "Observations: Changes in Snow, Ice and Frozen Ground". In: *Climate Change 2007: The Physical Science Basis. Contribution of Working Group I to the Fourth Assessment Report of the Intergovernmental Panel on Climate Change*. Ed. by S. Solomon, D. Qin, M. Manning, Z. Chen, M. Marquis, K.B. Averyt, M. Tignor, and H.L. Miller. Cambridge, United Kingdom and New York, NY, USA: Cambridge University Press.

Li, C., F. Su, D. Yang, K. Tong, F. Meng, and B. Kan (2018). "Spatiotemporal variation of snow cover over the Tibetan Plateau based on MODIS snow product, 2001-2014". In: *International Journal of Climatology* 38, pp. 708–728.

Li, D., M.L. Wrzesien, M. Durand, J. Adam, and D.P. Lettenmaier (2017). "How much runoff originates as snow in the western United States, and how will that change in the future?" In: *Geophysical Research Letters* 44, pp. 6163–6172.

Lioubimtseva, E. and G.M. Henebry (2009). "Climate and environmental change in arid Central Asia: Impacts, vulnerability, and adaptations". In: *Journal of Arid Environments* 73, pp. 963–977.

Lunetta, R.S., R.G. Congalton, L.K. Fenstermaker, J.R. Jensen, K.C. McGwire, and L.R. Tinney (1991). "Remote Sensing and Geographic Information System Data Integration: Error Sources and Research Issues". In: *Photogrammetric Engineering & Remote Sensing* 57(6), pp. 677–687.

Magnusson, J., T. Jonas, I. López-Moreno, and M. Lehning (2010). "Snow cover response to climate change in a high alpine and half-glacierized basin in Switzerland". In: *Hydrology Research* 41, pp. 230–240.

Magono, C. and W.L. Chung (1966). "Meteorological Classification of Natural Snow Crystals". In: *Journal of the Faculty of Science, Hokkaido University* 7-2, pp. 321–335.

Marks, D., J. Kimball, D. Tingey, and T. Link (1998). "The sensitivity of snowmelt processes to climate conditions and forest cover during rain-on-snow: a case study of the 1996 Pacific Northwest flood". In: *Hydrological Processes* 12, pp. 1569–1587.

Miehe, G., M. Winiger, J. Böhner, and Z. Yili (2001). "The climatic diagram map of High Asia. Purpose and concepts." In: *Erdkunde* 55(1), pp. 94–97.

Mischke, S., I. Rajabov, N. Mustaeva, C. Zhang, U. Herzschuh, I. Boomer, E.R. Brown, N. Andersen, A. Myrbo, E. Ito, and M.E. Schudack (2010). "Modern hydrology and late Holocene history of Lake Karakul, eastern Pamirs (Tajikistan): A reconnaissance study". In: *Palaeogeography, Palaeoclimatology, Palaeoecology* 289, pp. 10–24.

Molchanov, L.A. (1929). "Lakes of Central Asia". In: *Trudy Sredneaziat. Gos. Univ., Geografiya* 3. Tashkent. (in Russian), pp. 26–31.

Mudryk, L.R., P.J. Kushner, C. Derksen, and C. Thackeray (2017). "Snow cover response to temperature in observational and climate model ensembles". In: *Geophys. Res. Lett.* 44, pp. 919–926.

Peng, S., S. Piao, P. Ciais, P. Friedlingstein, L. Zhou, and T. Wang (2013). "Change in snow phenology and its potential feedback to temperature in the Northern Hemisphere over the last three decades". In: *Environ. Res. Lett.* 8, p. 014008.

Pomeroy, J.W., P. Marsh, and D.M. Gray (1997). "Application of a distributed blowing snow model to the arctic". In: *Hydrological Processes* 11, pp. 1451–1464.

Pomeroy, J.W., D.M. Gray, K.R. Shook, B. Toth, R.L.H. Essery, A. Pietroniro, and N. Hedstrom (1998). "An evaluation of snow accumulation and ablation processes for land surface modelling". In: *Hydrological Processes* 12, pp. 2339–2367.

Qu, X. and A. Hall (2013). "On the persistent spread in snow-albedo feedback". In: *Climate Dynamics* 42, pp. 69–81.

Qunzhu, Z., M. Cao, X. Feng, F. Liang, X. Chen, and W. Sheng (1984). "Study on spectral Reflection characteristics of snow ice and water of northwest China". In: *Science in China Series B-Chemistry, Biological, Agricultural, Medical & Earth Sciences* 27, pp. 647–656.

Riggs, G.A., D.K. Hall, and M.O. Román (2015). *VIIRS Snow Cover Algorithm Theoretical Basis Document (*ATBD*)*. NASA VIIRS project document.

Riggs, G.A., D.K. Hall, and M.O. Román (2016). *MODIS Snow Products Collection 6 User Guide*. NASA VIIRS project document.

Rittger, K., T.H. Painter, and J. Dozier (2013). "Assessment of methods for mapping snow cover from MODIS". In: *Advances in Water Resources* 51, pp. 367–380.

Roesch, A. (2006). "Evaluation of surface albedo and snow cover in AR4 coupled climate models". In: *Journal of Geophysical Research* 111, p. D15111.

Román, M.O., D.K. Hall, and G.A. Riggs (2004). MODIS*/Terra Snow Cover Daily L3 Global 500m SIN Grid, Version 6*. `https://nsidc.org/data/MOD10A1/versions/6?qt-data_set_tabs=3#qt-data_set_tabs`. Accessed: 26-08-2019.

Salomonson, V.V. and I. Appel (2004). "Estimating fractional snow cover from MODIS using the normalized difference snow index". In: *Remote Sensing of Environment* 89, pp. 351–360.

Salomonson, V.V. and I. Appel (2006). "Development of the Aqua MODIS NDSI Fractional Snow Cover Algorithm and Validation Results". In: IEEE *Transactions on Geoscience and Remote Sensing* 44(7), pp. 1747–1756.

Scherrer, S.C. and C. Appenzeller (2006). "Swiss Alpine snow pack variability: major patterns and links to local climate and large-scale flow". In: *Climate Research* 32, pp. 187–199.

Shi, X., S.J. Déry, P.Y. Groisman, and D.P. Lettenmaier (2013). "Relationships between Recent Pan-Arctic Snow Cover and Hydroclimate Trends". In: *Journal of Climate* 26, pp. 2048–2064.

Slater, P.N. (1985). "Radiometric Considerations in Remote Sensing". In: *Proceedings of the* IEEE 73(6), pp. 997–1011.

Sorman, A.Ü., Z. Akyürek, A. Sensoy, A.A. Sorman, and A.E. Tekeli (2007). "Commentary on comparison of MODIS snow cover and albedo products with ground observations over the mountainous terrain of Turkey". In: *Hydrology and Earth System Sciences* 11, pp. 1353–1360.

Steger, C., S. Kotlarski, T. Jonas, and C. Schär (2013). "Alpine snow cover in a changing climate: a regional climate model perspective". In: *Clim. Dyn.* 41, pp. 735–754.

Stieglitz, M., S.J. Déry, V.E. Romanovsky, and T.E. Osterkamp (2003). "The role of snow cover in the warming of arctic permafrost". In: *Geophysical Research Letters* 30, pp. 54.1–54.4.

Sturm, M., J. Holmgren, and G. Liston (1995). "A Seasonal Snow Cover Classification System for Local to Global Applications". In: *Journal of Climate* 8, pp. 1261–1283.

Sturm, M. (2015). "White water: Fifty years of snow research in WRR and the outlook for the future". In: *Water Resources Research* 51, pp. 4948–4965.

Sturm, M., M.A. Goldstein, and C. Parr (2017). "Water and life from snow: A trillion dollar science question". In: *Water Resources Research* 53, pp. 3534–3544.

Tedesco, M. (2015). *Remote Sensing of the Cryosphere*. John Wiley & Sons, Ltd.

Tucker, C.J. (1979). "Red and photographic infrared linear combinations for monitoring vegetation". In: *Remote Sensing of Environment* 8, pp. 127–150.

USGS (n.d.). *USGS EROS Archive – Landsat Archives – Landsat 4-5 TM Level-2 Data Products – Surface Reflectance*. `https://www.usgs.gov/centers/eros/science/usgs-eros-archive-landsat-archives-landsat-4-5-tm-level-2-data-products-surface`. Accessed: 2019-08-30.

Vanselow, K.A., T. Kraudzun, and C. Samimi (2012). "Grazing Practices and Pasture Tenure in the Eastern Pamirs". In: *Mountain Research and Development* 32(3), pp. 324–336.

Vaughan, D.G., J.C. Comiso, I. Allison, J. Carrasco, G. Kaser, R. Kwok, P. Mote, T. Murray, F. Paul, J. Ren, E. Rignot, O. Solomina, K. Steffen, and T. Zhang (2013). "Observations: Cryosphere". In: *Climate Change 2013: The Physical Science Basis. Contribution of Working Group I to the Fifth Assessment Report*

of the Intergovernmental Panel on Climate Change. Ed. by T.F. Stocker, D. Qin, G.-K. Plattner, M. Tignor, S.K. Allen, J. Boschung, A. Nauels, Y. Xia, V. Bex, and P.M. Midgley. Cambridge, United Kingdom and New York, NY, USA: Cambridge University Press.

Verbunt, M., J. Gurtz, K. Jasper, H. Lang, P. Warmerdam, and M. Zappa (2003). "The hydrological role of snow and glaciers in alpine river basins and their distributed modeling". In: *Journal of Hydrology* 282, pp. 36–55.

Wang, X. and H. Xie (2009). "New methods for studying the spatiotemporal variation of snow cover based on combination products of MODIS Terra and Aqua". In: *Journal of Hydrology* 371, pp. 192–200.

Warren, S.G. (1982). "Optical Properties of Snow". In: *Reviews of Geophysics and Space Physics* 20, pp. 67–89.

Wayand, N.E., C.B. Marsh, J.M. Shea, and J.W. Pomeroy (2018). "Globally scalable alpine snow metrics". In: *Remote Sensing of Environment* 213, pp. 61–72.

Wendler, G. and J. Kelley (1988). "On the albedo of snow in Antarctica: a contribution to I.A.G.O." In: *Journal of Glaciology* 34, pp. 19–25.

Wever, N., T. Jonas, C. Fierz, and M. Lehning (2014). "Model simulations of the modulating effect of the snow cover in a rain-on-snow event". In: *Hydrology and Earth System Sciences* 18, pp. 4657–4669.

Wilks, D.S. (2011). *Statistical Methods in the Atmospheric Sciences (Third Edition)*. The Boulevard, Langford Lane, Kidlington, Oxford, UK: Elsevier.

Winstral, A. and D. Marks (2002). "Simulating wind fields and snow redistribution using terrain-based parameters to model snow accumulation and melt over a semi-arid mountain catchment". In: *Hydrological Processes* 16, pp. 3585–3603.

WMO (2011). *GCOS Systematic Observation Requirements for Satellite-Based Data Products for Climate (2011 Update)*. Geneva, Switzerland: World Meteorological Organization, GCOS.

WMO (2019). *WMO Statement on the State of the Global Climate in 2018*. Geneva, Switzerland: World Meteorological Organization.

Yao, T., L. Thompson, W. Yang, W. Yu, Y. Gao, X. Guo, X. Yang, K. Duan, H. Zhao, B. Xu, J. Pu, A. Lu, Y. Xiang, D.B. Kattel, and D. Joswiak (2012). "Different glacier status with atmospheric circulations in Tibetan Plateau and surroundings". In: *Nature climate change* 2, pp. 663–667.

Zhang, T. (2005). "Influence of the seasonal snow cover on the ground thermal regime: An overview". In: *Reviews of Geophysics* 43, pp. 1–23.

Zhou, H., E. Aizen, and V. Aizen (2013). "Deriving long term snow cover extent dataset from AVHRR and MODIS data: Central Asia case study". In: *Remote Sensing of Environment* 136, pp. 146–162.

Zhou, H., E. Aizen, and V. Aizen (2017). “Seasonal snow cover regime and historical change in central Asia from 1986 to 2008”. In: *Global and Planetary Change* 148, pp. 192–216.

Declaration of Authorship

I hereby declare that I have written this master thesis independently and did not use any other sources or aids apart from those indicated. Furthermore, I declare that this thesis has not already been submitted for the obtainment of an academic degree.

Bayreuth, September 2, 2019

Thomas Senftl